DEVELOPMENT OF A PLANT MEMBRANE-ON-CHIP PLATFORM FOR INTERROGATING PROTEIN-MEDIATED METAL TRANSPORT

A Dissertation

Presented to the Faculty of the Graduate School

of Cornell University

In Partial Fulfillment of the Requirements for the Degree of

Doctor of Philosophy

by

Barituziga Banuna

May 2025

DEVELOPMENT OF A PLANT MEMBRANE-ON-CHIP PLATFORM FOR INTERROGATING PROTEIN-MEDIATED METAL TRANSPORT

Barituziga Banuna Ph. D.

Cornell University 2025

Transporter proteins are ubiquitous in nature and play major roles in the uptake, redistribution, and efflux of ions and small molecules required by organisms to maintain homeostasis. Disruptions to transporter function are associated with a variety of diseases and phenotypical abnormalities. In humans, this is evident in the case of diseases such as Menkes and Wilson while in plants, disruption of copper transporters has been associated with phenotypic abnormalities such as reduced growth, fruit yield, and death. The prevalence and association of transporter proteins to many diseases and disorders have highlighted their importance and made them the target of scientific investigation.

Despite the strong interest in these proteins, transporter proteins remain a challenge to study. In plants, access to the plasma membrane is hampered by the presence of the cell wall and transport proteins may also be localized to internal organelles further limiting their accessibility. Membrane proteins contain hydrophobic regions complicating attempts to isolate and study them, as these non-polar moieties must be stabilized to maintain form and function. Traditional methodologies for measuring transporter proteins heavily rely on indirect *in vivo* assays that often require expression in non-native systems, possibly resulting in changes in protein behavior. Direct measurement modalities such as patch-clamp are mainly amenable to certain transporter proteins, such as ion channels, which display electrogenic and fast transport activity. This precludes the measurement of ion transport of many slower or electroneutral transporters such as transport proteins.

To address the demand for characterizing this class of proteins, I developed a biomimetic system capable of the direct translation of transport protein function to measurable output, called, “Plant Membrane-on-Chip” platform. This platform leverages the properties of supported lipid membranes to recapitulate the native membrane environment of the transporter proteins through the inclusion of native membrane materials and retention of orientation and fluidity properties. The crucial addition of a biocompatible electronic chip enables the measurement of transporter function using traditional electrochemical characterization techniques that are label-free, sensitive, and non-destructive. For this dissertation, I demonstrate the use of a Plant Membrane-on-Chip device derived from *Arabidopsis thaliana* plasma membrane material in electrically measuring the function of the copper transporter protein AtCOPT1. Critically, this project highlighted how the use of traditional resistance-based analysis methodologies can be incorporated with new bio-mimics to detect the activity of a non-electrogenic transporter previously thought to be unamenable to direct electrical analyses.

BIOGRAPHICAL SKETCH

Barituziga Banuna was born in Nigeria and grew up in Buffalo, NY where he went to City Honors School. He developed a love of science and engineering in his early years and then completed his Bachelor of Science in Chemical Engineering at the University at Buffalo. He had an early head start into research working on his first research project in high school at Roswell Park Cancer Institute and would have multiple more opportunities in his college years. As an undergrad he worked on research understanding the role on chemical additives on the urolith crystallization under Prof. Marina Tsianou. He also worked under Dr. Mark Allen at the University of Maryland-Baltimore County on the application of bio-tethering to improve lithium-ion battery technology. After receiving his B.S., Barituziga began his PhD in the Chemical and Biomolecular Engineering Department at Cornell University under the study of Prof. Susan Daniel to follow his interest in bioelectronics.

This dissertation is dedicated to my family, friends, teachers and mentors who have supported me through this journey

ACKNOWLEDGEMENTS

First, I would like to acknowledge my committee members: Susan Daniel my advisor, Abraham Stroock, and Olena Vatamaniuk

I want to thank all the people who mentored and trained me throughout this entire degree. Special thanks to Miriam Huerta with whom I collaborated with on this work and provided a wealth of knowledge. Thank you to Ju-Chen Chia who provided a chemical engineer a guiding hand into the world of plants. I'd also like to thank Juliana Carten who taught me so much about cloning for your time and dedication to the training the next generation.

A huge thanks to the members of the Daniel Lab past and present with a special shout out to Tiffany Tang, Alexis Oswalt, Ambika Pachaury, Ferra Pinnock, Zeinab Mohammed, Zachary Manzer, Yu-An Chien, Hui Su, Zhongmou Chao, and Pom Strauss. Thank you to Angela Sem my first undergrad student, you taught me so much about how to be a mentor. I'd also like to thank the members of the Olena lab for their patience and help especially to Tetiana-Olena Zavodna who I could always rely on for good cheer on a rainy day.

I would like to thank Jeff Godowski and all the members of the Rose House team who made Cornell feel like a home as well as my colleagues in the CBE Women's Group and NRT program.

Final thanks go to my friends both in Cornell and out, and my family.

TABLE OF CONTENTS

LIST OF FIGURES

LIST OF TABLES

CHAPTER 1: INTRODUCTION

The cell contains many membranes that serve multiple functions such as cell signaling, response, and compartmentalization. These functional membranes are integral to numerous biological processes and the maintenance of homeostasis of the cell. While most membranes are primarily composed of phospholipids, they are also highly complex and contain a large variety of proteins, sugars, and classes of lipids. Biological membranes play a prominent role in the mediation of the uptake and distribution of micronutrients, ions, and small molecules which is of great scientific interest. Of particular importance is how metal micronutrients are transported due to their critical function in biological processes.

The presence of metal ions in biological organisms is a balancing act. When present in higher amounts, metal ions induce toxicity and abnormalities in many cases through the generation of free radicals.[1] One such metal micronutrient is copper which serves as a cofactor of enzymes involved in respiration, photosynthesis, and oxidative stress management.[1,2] However, despite copper's major biological role much remains to be learned about its cellular uptake, redistribution, and subsequent export. In humans, loss of copper homeostasis is associated with Menkes and Wilson's diseases, while in plants, copper deficiency results in marked phenotypic abnormalities in leaves, roots, and reproductive tissues.[3] A key player in this delicate equilibrium are transport proteins which are present in biological membranes and facilitate the movements of molecules and ions between cellular compartments and the environment. Loss of transporter function is often correlated to phenotypic defects similar to those under metal micronutrient deficiency or toxicity, depending on the role of the transport in question.[1,4,5]

Much of our understanding of copper transporters originates from studies in animals leaving us with clear gaps in our understanding of how these transporters function in plants. This knowledge gap can in part be attributed to the difficulty in studying transmembrane proteins but

also the unique difficulties that present themselves in plant systems. In the following sections, I expand upon these challenges and the unique methods of overcoming them.

1.1 Arabidopsis Metal Ion Transporters

In many eukaryotes, several copper transporters have been identified,[4,6,7] but the primary transporter proteins responsible for high affinity copper transport are believed to be the family of Copper Transport Proteins (CTR) found in humans, animals, and yeast. Similarly, plants possess a homologue to CTR known as COPT (COPper Transporter). In Arabidopsis, six members of the CTR/COPT family have been identified **[Fig 1.1].** Denoted as AtCOPT1/2/3/4/5/6, all have been associated with Cu(I) transport except COPT4 whose function remains unknown.[3,8] Each COPT occupies a functional niche in the plant; AtCOPT1 and AtCOPT2 are highly expressed in the roots where they mediate Cu(I) uptake.[9–11] AtCOPT5 is found throughout the plant as is AtCOPT6 though its primary expression is in vascular tissues.[3] AtCOPT3/5 have been shown to be localized to the internal membrane compartments. AtCOPT5 is believed to facilitate Cu efflux from vacuole storage under copper deficiency and AtCOPT3 is thought to be associated with membranes of the ER, but limited evidence of this is available.[1,12,13]

X-ray crystal structure of the human homologue hCtr1 indicates that it possesses three transmembrane (TM) helices with an extracellular N-termini and cytosolic C-terminal.[14,15] While X-

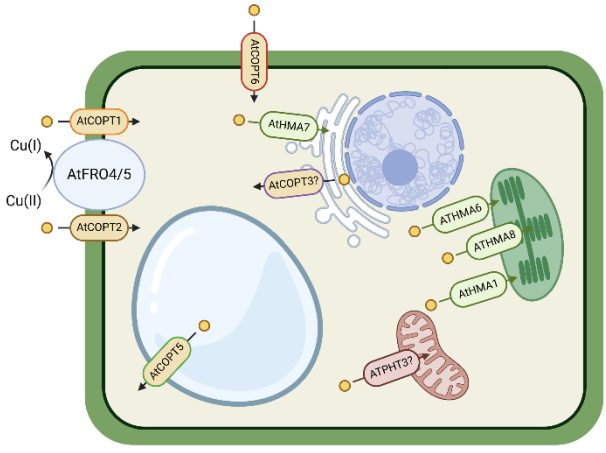

Figure 1.1 Copper Transporter System in Arabidopsis *Depiction of the proposed copper transportation system in an Arabidopsis cell mediated by transporter proteins to achieve copper uptake, efflux and redistribution inter- and extracellularly.*
Figure created with BioRender

ray crystal structures of AtCOPTs have yet to be resolved, protein folding predictions and the highly conserved nature of the CTR/COPT family suggest that AtCOPTs should be structurally similar.[10,16,17] CTR/COPTs have a conserved N terminal motif, MXXXM motif on TM2, GXXXXG motif on TM3, and cysteine rich CXC motif on the c-terminal **[Fig. 1.2].**[8,14,15] The n-terminal Met127 is proposed to be required for Cu(I) acquisition from the extracellular environment, Met260 of the TM2 motif for transport and the C terminal for offloading of Cu(I) to cytosolic copper chaperones.[18,19] Recent work in AtCOPT1 has identified His43 as a residue in the N-terminal domain of essential for copper ligand binding and stabilization.[20] Interestingly, His43 mutants retained activity in yeast but proved unstable in Arabidopsis, once again, highlighting the caveats to exogenous expression. The small number of transmembrane domains in CTR/COPT as compared to many other membrane transporters that have 6-12 or more suggest that CTR/COPT must homo-oligomerize to form a

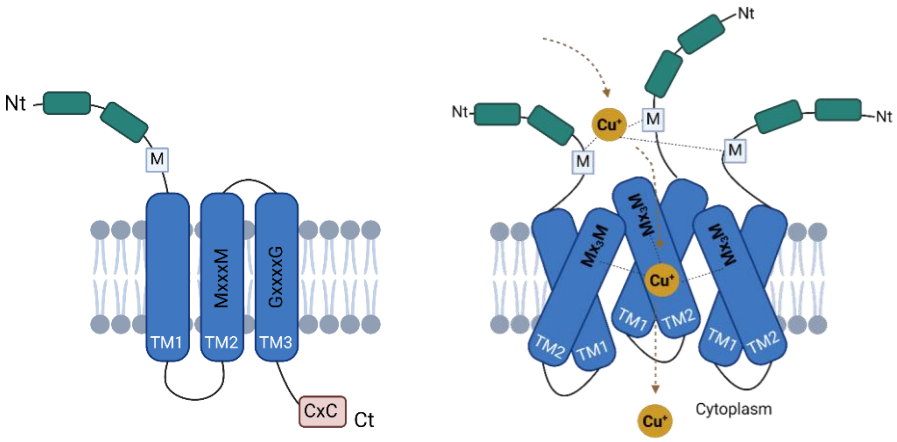

Figure 1.2: Proposed structure of CTR/COPT
(RIGHT) *Structure of CTR/COPT family of Cu transporters. Important features included three transmembrane domains with conserved residues in transmembrane domain 2 (TM2) and transmembrane domain 3 (TM3). Additional features include an extraluminal n-terminal (Nt) with methionine residues and a luminal c-terminal (Ct) with a largely conserved cysteine motif* ***(LEFT)*** *CTR/COPT in the proposed trimer complex for Cu(I) transport with the transmembrane domains forming a transmembrane pore. (TM3 not show for simplicity). Methionine residues in the Nt recruit Cu(I) from the microenvironment where it is then shuttled through the pore by methionine residues in TM2 before reaching the Ct CxC for subsequent transport by copper chaperones*

Figure created with BioRender

functional membrane pore.[14,15] Evidence has also been shown to indicate that they trimerse and can also form heteromers and interact with proteins outside the CTR/COPT family.[21–23] AtCOPT1 is known to interact with AtCOPT6 and two ER localized proteins[9], UBAC2a and UBAC2b, have been reported to interact with AtCOPT1 and promote its accumulation.[24] AtCOPT1/2/6 are believed to be high-affinity (Km ≤ 5μM) Cu(I) specific transporters localized to the plasma membrane and controlled by the Cu homeostasis regulator, SQUAMOSA promotor-binding protein-like 7 (SPL7).[9,10,25] Uptake assays in yeast on CTR/COPT indicate a specificity to monovalent cations, primarily Cu(I) and to a lesser extent Ag(I) with some evidence in CTR showing that some divalent cations like Zn(II) might have an inhibitory effect on CTR/COPT mediated transport, but the mechanism behind this interaction remains to be elucidated.[8,9,26] The reduction of the predominate oxidative state Cu(II) to Cu(I) is thought to be accomplished by several cell surface metalloreductases including FRO4/5 in *A. thaliana* and recent studies in hCTR1 suggest the possibility of reducing biological agents such as ascorbate.[27,28]

1.2 Current Strategies for Plant Functional Studies

In plant cells, the plasma membrane plays a key function in the uptake of specific micronutrients, while other specialized membranes such as the vacuole tonoplast help to maintain homeostasis through the storage and later release of nutrients within the cell. Studying these membranes and the transport proteins that support their functions has proven to be a challenge arising, in part, from physical barriers such as the protective plant cell wall and inaccessibility of inner membrane compartments. Additionally, there is the relative difficulty of genetic manipulation in plants, and the limited availability of tools to directly study these membrane transporters' biophysiological behavior. Patch clamp[29] and cell-based/isolated membrane uptake[8,30] and functional complementation assays are three traditional techniques

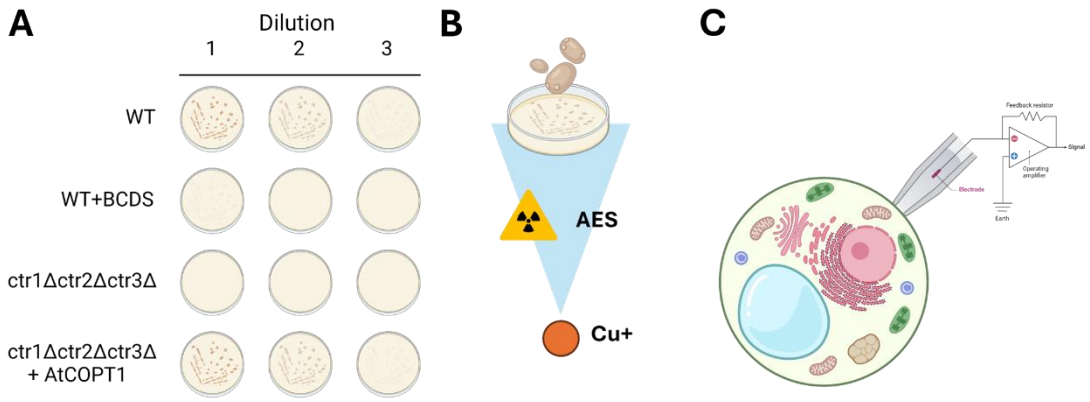

Figure 1.3: Strategies for Plant Functional Studies

(A) *Depiction of a typical yeast functional complementation assay. Yeasts are grown on ethanol/glycerol YPEG non-fermentable medium. Numbers indicate dilutions of starting culture. Copper chelator BCDS eliminates growth of wildtype (WT). Copper uptake incompetent mutant (ctr1Δ ctr2Δ ctr3Δ) fail to grow on YPEG but the growth defect is rescued by addition of AtCOPT1 gene.* ***(B)*** Carton of uptake assay performed with *copper uptake incompetent mutant (ctr1Δ ctr2Δ ctr3Δ) modified to express plant COPT protein. Ion specificity and uptake is measured by radio-tracing or atomic emission spectroscopy related techniques.* ***(C)*** *Simple depiction of a patch-clamp setup on a protoplast. Glass micropipette probe with an electrode with single amplification circuitry establishes a seal with the plant plasma membrane.*

Figure created with BioRender

that attempt to accomplish this **[Fig 1.3]**. While these methods can be useful tools in understanding transporter protein function, due to the limitations of the plant system they are often carried out in non-native cell lines. Patch-clamp studies require sufficiently high depolarization or currents for measurable outputs. In some cases, the protoplast and transporter combination may not provide this, and an alternative is the exogenous expression into patch-clamp friendly cells such as frog oocytes that can provide higher responses. Yeast, primarily *Saccharomyces cerevisiae*, has been a model organism for genetic complementation and uptake due to their speed of growth, ease of genetic manipulation as compared to plants and their homology to plants and other eukaryotes. With limited advancement in techniques, the comprehensive study of inner membrane proteins remains largely inaccessible, and the use of exogenous cell-based assays like yeast complementation is ubiquitous.

1.3 *In-Vivo* Yeast Assays

Yeast cell-based studies have proven to be pivotal towards the discovery of transporters in the model plant species *Arabidopsis thaliana* and generally take the form of complementation or uptake assays. Uptake assays are commonly used in conjunction with functional complementation to provide a quantification of transporter activity. Typically, this is achieved by exposing uptake deficient yeast transformed with a AtCOPT to radiotraceable ^{64}Cu or using Atomic Absorption Spectrophotometry and measuring the Cu accumulation after a set time **[Fig 1.3b]**.[8] The identification of the first putative *A. thaliana* copper transporter COPT1 was described by Kampfenkel et al using functional complementation assays with the *S. cerevisiae* yeast mutant (*ctr1-3*) deficient in high affinity copper uptake.[31] As a result of the mutation, yeast is unable to grow on nonfermentable carbon sources like glycerol under conditions of copper deficiency without transformation with the complementing Arabidopsis COPT1 (AtCOPT1) gene **[Fig 1.3a]**. With this study a COPper Transporters) family have been identified using *S. cerevisiae* CTR (Copper Transporter Protein) uptake deficient mutants (*ctr1Δ ctr2Δ ctr3Δ*).[9] In these mutants, expression of AtCOPT2 and AtCOPT6 were found to rescue growth defect of the mutant phenotype, as did AtCOPT3 and AtCOPT5 to a lesser extent, indicating these proteins function as copper transporters.[4] These seminal works have provided a baseline for our understanding of Arabidopsis copper transporters. However, ectopic expression of proteins poses several problems – alterations to native protein behavior, lack of or mis-coordinated post-translational modifications like glycosylation, and unintended interactions with heterologous systems. This is highlighted by proteins such as AtCOPT4 which failed to transfect in yeast, likely through induced toxicity and has yet to be functionally characterized.[8]

1.4 Patch-clamp

Another tool of interest is the use of electrophysiological techniques like patch-clamp to

understand transporter behavior. Developed initially by Neher and Sakmann in 1976, patch-clamp is increasingly popular in the mammalian space for the study of clinically relevant ion channels but the adoption of patch-clamp to the plant sphere has proven to be much slower and challenging.[32–35] As a simplified explanation, patch-clamp is a technique where membranes are held at either a voltage (voltage-clamp) or current (current-clamp) using a glass micropipette electrode to form a seal with the membrane and the resultant currents or potentials recorded **[Fig 1.3c].** Generally, due to the presence of ion channels and pumps, cells maintain an ion gradient that results in a membrane potential, known as the resting potential, under steady-state conditions. Upon addition of substrates or other initiators, provided the measured protein can induce a sufficiently high electrochemical change to be detected the opening of the transporter results in either a measurable depolarization or hyperpolarization. By evaluating the response, guided inferences can be made as to the kinetics and mechanism of the transport process.

Often proteins are expressed exogenously in African clawed frog *Xenopus laevis* oocytes due to their transfection compatibility, minimize electrical noise, and provide a larger target for probing. However the measurement process remains challenging, and the throughput limited. While frog oocytes are an important model for patch-clamp, concerns have been raised regarding the effects of their exogenous nature particularly in observable differences in IC50 (half-maximal inhibitory concentration) obtained from oocytes vs mammalian cell lines.[36] An alternative to this is the patching of vascular plant protoplasts, however obtaining a sufficient "giga-seal" to minimize noise and provide high-resolution readings is difficult with protoplasts and along with the limitations of genetic manipulation techniques in plants its adoption has been slow.[37] Initial studies in plants and oocytes showed limited success in illuminating the key mechanisms of CTR/COPT-mediated transport and in *A. thaliana* no measurable response was obtained with COPT1, COPT2 and COPT5 under Cu exposure.[17] Based on these factors it is clear that to gain a better understanding of COPT proteins we need new ways to study these

proteins in their native setting.

1.5 A New Platform for Transporter Studies: Supported Lipid Bilayers

Cell membranes are specialized biological membranes composed of amphiphilic phospholipids, structural and functional proteins as well as several other biomolecules, lipids and sugars. These membranes are specialized based on their functional role and localization and perform critical roles in intercellular communication, signal transduction, enzymatic activity, and ion transport.[38–40] Failure of membrane proteins associated with many of these processes often leads to drastic and sometimes lethal effects. Due to the prevalence and ubiquitous nature of these proteins, many tools have been developed to investigate the properties of cell membranes. One such development is the creation of bilayers that retain the double leaflet structure of native membranes and are composed of purified lipids incorporated with extracted and purified proteins.[41–43] This extraction process, often detergent based, risks damaging protein targets and the reconstitution step is difficult, especially with transmembrane proteins that contain hydrophobic regions that render them insoluble.[44,45]

Pioneered by Tamm and McConnell, supported lipid bilayers (SLB) began as simple mono-lipid bilayers that have evolved to allow for the incorporation of many more complex molecules and proteins. These modern SLBs can be created from membrane-derived vesicles and have been used extensively by the Daniel group to study membrane interactions with a variety of biological subjects.[46–48] Generally, there are three major methods for the preparation of SLBs – Langmuir-Blodgett (LB)/Langmuir-Schaefer (LS), solvent-assisted lipid bilayer (SALB), and vesicle fusion. Incorporation of proteins into bilayers with LB/LS and SALB methods is difficult due to the presence of organic solvents so most applications towards the formation of native membrane SLBs have utilized vesicle fusion.[49] To form SLBs with vesicle fusion, vesicles are isolated from membranes that have budded off in either a natural or

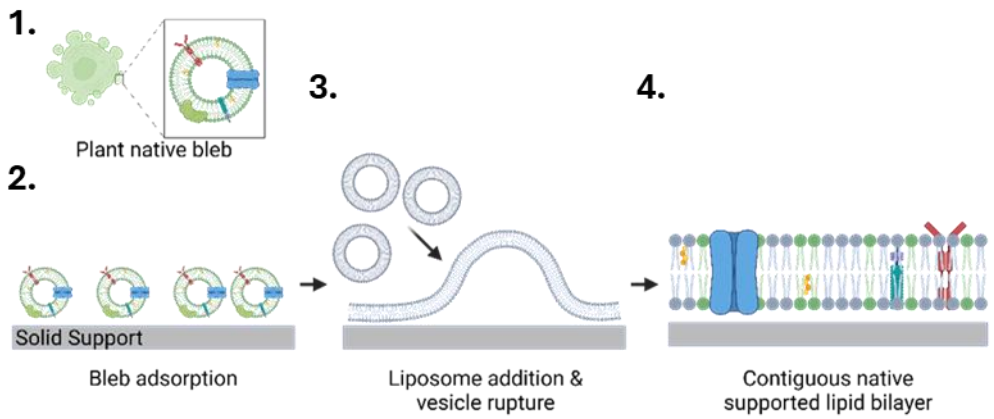

Figure 1.4: Schematic of the formation of plant supported lipid bilayers via vesicle fusion
(1) Microvesicle plant 'bleb' isolated from protoplast (2) Blebs adsorbed onto a surface treated solid support (3) Addition of tailored composition fusogenic liposomes (5) Rupture of liposomes and blebs resulting in formation of a contiguous
Figure created with BioRender

induced process and are then ruptured on a solid support using fusogenic liposomes **[Fig 1.4].** The rupture of vesicles is dominated by electrostatic and van der Waals interactions and as such, this process can be highly dependent on surface chemistries and roughness. As the compositions of vesicles vary, fusogenic liposome charge and composition must be tailored. Commonly used liposomes include 1-Palmitoyl-2-oleoyl-glycero-3-phosphocholine (POPC) and other lipids which vary by head group and number of double bonds. The differences in these properties amongst phospholipids allow for the tunning of liposome charge, curvature, and membrane fluidity. The resultant SLB is around 4 nm in thickness and floats on a 1nm layer of water that confers a level of mobility to membrane proteins. If further mobility is required SLBs can be formed on hydrophilic polymers that act as cushions limiting contact to the solid support.[50–52] The advantage to this approach is that the resulting membranes retain key features of the native biological system such as orientation, constituents, and component diversity along with mobility.[51–53] This provides a platform for study that is a more holistic representation of the native membrane and maintains some of the properties/processes that are present in the living cell. In turn, this platform allows for the possibility to investigate protein transporters without the worry of off-target and unexpected effects of ectopic expression. The

planar nature of SLBs makes them amenable to a range of optical and electrochemical characterization methodologies. Prior work by our lab and others has shown that SLB can be integrated with electrical sensor systems to understand mammalian and bacterial membrane protein's function.[48,54] This provides a tool for the study of membrane proteins *in vitro* while maintaining them in a like-native environment often not possible with patch clamp and yeast assays. By taking advantage of this compatibility, the goal of my thesis work was to create a bio-mimetic platform that retains the basic functions of the plant membrane and to utilize it to study the Arabidopsis family of copper transporters, specifically COPT1.

1.6 Electrochemical Characterization

Electrophysiological characterization of membrane proteins has become increasing popular over time due to its ability to supply easily quantifiable data, simplicity and the direct insight it provides into processes controlled by electrochemical interactions.[55] Generally, these techniques utilize a system of electrodes wherein specific voltages, currents, or resistances are maintained or fluxed and the corresponding response is recorded. Techniques that utilize relatively small voltages are highly desirable as they minimize damage to biological structures. The use of impedance-based sensing techniques such as EIS is amenable with transporters that are slow or electroneutral, unlike traditional patch-clamp. Furthermore, many transporters behave as single file ion channels which have been shown to display ion permeation rate changes with concentration and have saturable velocities making them ideal for models of enzyme kinetics such as Michaelis-Menton.[56,57]

The Daniel group and others have shown the capability of this technique to be expanded to the investigation of SLB through the incorporation of a conductive support material.[48,58,59] Common surfaces compatible with SLBs include metals such as gold or silver, metal oxides like indium-tin oxide (ITO) and organic molecules such as polymers. An

increasingly popular material, the conductive polymer poly(3,4-ethylenedioxythiophene) p-type doped with poly(styrene sulfonate) (PEDOT:PSS) is often used due to its biocompatibility and its volumetric capacitance.[60–62] Additionally, as PEDOT:PSS swells in aqueous solutions, it acts as a support aiding to preserve the integrity and in-plane mobility of membrane proteins.

1.7 Organic Electrochemical Transistors

Organic Electrochemical Transistors (OECT) are an electrophysiology platform that allows for the interrogation of surface materials. OECTs amplify signals and allow for the capture of intrinsic time constants that relate to the permissibility of ion flux through the added surface material and subsequent doping and de-doping of the underlying conjugated polymer, such as PEDOT:PSS.[55,63] Generally, OECTs are composed of a gate, a source, and a drain electrode. The source and drain are interconnected via an organic semiconductor channel material like PEDOT:PSS. In practice, the source and drain electrodes are in contact with the electrolyte, and the voltage at the drain is controlled by the gate electrode resulting in a change in drain current.[60,61,64] The OECT device's configuration enables a variety of electrical characterization

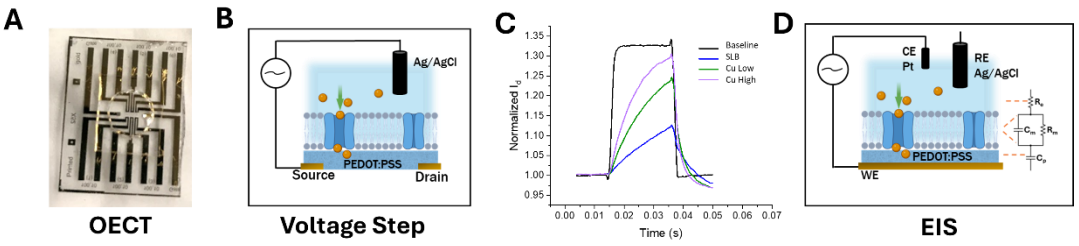

Figure 1.5: Organic Electrochemical Transistor
(A) *Image of an Organic Electrochemical Transistor (OECT) device* ***(B)*** *Depiction of OECT device configured for Voltage Step Analysis experiments* ***(C)*** *Representative drain current response of a single experiment with a Plant-on-Chip OECT device measured using Voltage Step analysis. Plain PEDOT device (black), SLB (blue), and analyte treatment at a low (green) and higher concentration (purple). The upward shift in the curve is indicative of a decrease in time delay as the transporter activates allowing ion flux.* ***(D)*** *Depiction of the OECT device configured for Impedance Spectroscopy (EIS) measurements*

Figure created with BioRender

assays **[Fig 1.5].** A technique used in conjunction with OECTs is potential step chronoamperometry (also known as voltage step analysis) wherein a step voltage is applied at the gate, and the transient current response at the drain and its delay are recorded. This time delay, related to the ion flux and overlaying surfaces admittance, is dependent on the porosity of the SLB and thus allows for detection of the opening of ion channels and transporters. OECTs can also be configured for use in impedance-based measurements by using the entire transistor as the working electrode.

1.8 Electrochemical Impedance Spectroscopy

Impedance based techniques such as electrochemical impedance spectroscopy (EIS) are another powerful technique to study SLBs owing to its non-destructive and sensitive properties. EIS utilizes a system of electrodes wherein a current is passed through at various frequencies (typically 10^0 to 10^6 Hz) and the impedance response is recorded. The impedance is a complex quantity composed of a real and imaginary component and is defined as the inverse of the admittance in an alternating current and so in this system represents the resistance to current flow in an alternating current. The derivation of the electrical model is formulated from the assumption of a dielectric 'slab' with an ionic current arising from ion flux through it, and a capacitive current, originating from the variation over time of ions building up at the slab boundary.[65] The total resultant current is the sum of these two values and is thus simulated by an RC mesh - resistor (for ionic current) and a capacitor (for capacitive current) in parallel. The impedance profile of a material applied in the electrical path can then be regarded as an additional RC meshes in series.

Resistive and capacitive components respond differently to the application of an alternating current with frequency. A pure resistor yields a current, I, of the same frequency, f, and a magnitude described by the equation:

$$\mathbf{V = IR} \quad \mathbf{(1)}$$

However, a capacitor yields a current similarly of same frequency but with an amplitude of $2\pi fC$ out of phase by $-\pi/2$. Therefore, the impedance, Z, for a resistive element is equal to the resistance, and the impedance in a capacitive element is given by:

$$\boldsymbol{Z = \frac{1}{i\omega C}} \quad \mathbf{(2)}$$

where ω is the angular frequency.[65] Hence on a Bode plot of log(|impedance|) vs. log(frequency) the impedance profile from EIS of a resistor element appears as a constant horizontal line of fixed impedance while that of a capacitive element appears as a downward slope as capacitive impedance decreases with increasing frequency.

A bare device composed of a PEDOT:PSS coated gold electrode can be modeled as series of dielectric slabs with RC meshes for the electrolyte buffer which possesses a resistive and low non-zero capacitance and the PEDOT:PSS which has a capacitive and measurable non-infinite impedance.[66] An approximation can be applied for the system for a PEDOT:PSS layer with pure capacitance and an electrolyte layer with pure resistance. The overall impedance in an electrical circuit is dominated by the circuit element with the greatest impedance in a series configuration and by the circuit element with the lowest impedance in parallel. As a result, a bare device composed of electrode coated with PEDOT:PSS and buffer exhibits a distinct profile due to the domination of the capacitive impedance at low frequencies and the resistive (electrolyte buffer and wires) impedance at high frequencies. This system can then be modeled as a capacitor in series with a resistor. The electrode surface can then be monitored as material is added or removed from the device as a change in the impedance profile and resulting component values in the equivalent electrical circuit (EEC) model.

When modeling a system as an equivalent electrical circuit the SLB can be described as a dielectric slab and the overall system is defined as a SLB RC mesh in series with the

aforementioned PEDOT:PSS capacitive component and electrolyte resistive component **[Fig 1.6a].**[65,67,68] Additional RC meshes can be added in series to account for the inclusion of other components to the bilayer and empirically fit to experimental data until an acceptable fitting error is obtained. For the application used in this work, the use of single SLB associated RC mesh is acceptable **[Fig 1.6c].** The capacitance of PEDOT:PSS scales volumetrically and its addition lowers the system impedance of the bare gold electrode[69] alone and allows for the resolution of the characteristic Bode 'chair' response upon the formation of an ideal SLB on the PEDOT:PSS surface. The Bode plot of the SLB device appears as the impedance profile of a bare device with the addition of a SLB dominated middle frequency range **[Fig 1.6b].** Upon addition of active substrates or molecules that modify the SLB permeability, changes to the derived membrane resistance (Rm) can be obtained. This has proven useful in the past at

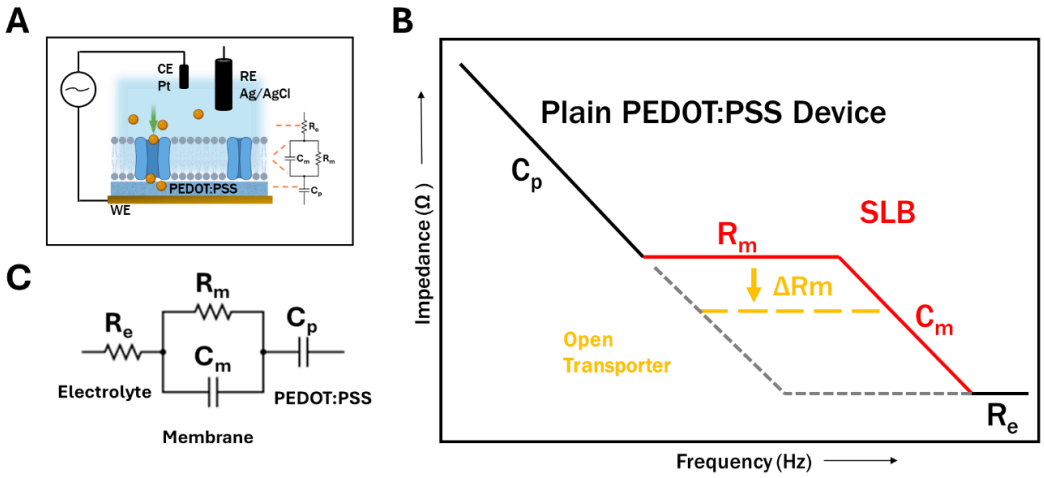

Figure 1.6: Electrochemical Impedance Spectroscopy
(A) *Depiction of SLB electrode device configured for Electrochemical Impedance Spectroscopy (EIS) measurements. RC-meshes are associated with system components (PEDOT:PSS, Electrolyte, SLB)* ***(B)*** *Representative Bode impedance profile of a device measured using EIS first with plain gold electrode (blue), a PEDOT:PSS coated gold electrode device (black/gray), addition of a SLB (red) to PEDOT:PSS device, activation of a transporter (yellow) in the SLB and resultant change in membrane resistance (ΔRm). Log of the real impedance is plotted vs the log of the frequency.* ***(C)*** *Simplified equivalent electrical circuit (EEC) model of SLB device used to fit impedance response and obtain a SLB associated resistance, Rm. EEC is derived from the series RC mesh model and confirmed empirically.*

Figure created with BioRender

measuring transport through membrane imbedded transmembrane proteins.[55,61] In chapter 2, I will further describe how I utilize these methodologies with a plant membrane derived SLB to explore the function of members of the AtCOPT family of Cu transporters.

CHAPTER 2: ELECTRICAL DETECTION OF HIGH-AFFINITY CU (I) TRANSPORTER FUNCTION IN A BIOMIMETIC PLANT MEMBRANE-ON-CHIP DEVICE

Barituziga Banuna[1], Miriam Huerta[1], Ju-Chen Chia[2], Zhongmou Chao[1], Juliana Carten[1], Olena Vatamaniuk[2,3], Susan Daniel[1]

[1] Robert Frederick Smith School of Chemical and Biomolecular Engineering, Cornell University, Ithaca, NY, USA

[2] Soil and Crop Sciences Section, School of Integrative Plant Science, Cornell University, Ithaca, NY 14853, USA

[3] Plant Biology Section, School of Integrative Plant Science, Cornell University, Ithaca, NY 14853, USA

Abstract

Transporter proteins with electrogenic and slow transport are fundamental to many biological processes in plants. However, due to their properties and membrane localization, they have posed a significant challenge to their direct characterization and our understanding. Provided the limitations of exogenous expression systems and the difficulties of *in planta* assays, it is crucial that we identify new platforms that can recapitulate the plant membrane environment|. Our biomembrane platform allows for the incorporation of electrical components and leverages the use of resistive analysis modalities to measure transport activity irrespective of a protein's electrical nature. We find that through the incorporation of native membrane components and transporter proteins onto a biocompatible substrate we can directly electrically detect the function of transporter widely believed to be electroneutral and undetectable by electrical means. We utilize COPT1 in *Arabidopsis thaliana* as a basis for our initial work, but we envision a future where this platform can be extended to study a wide range of transporters regardless of plant biological origin, cell type and localization.

2.1 Introduction

Membrane proteins play a critical role in the regulation of cellular homeostasis by mediating biological processes that include cellular transport, cell-to-cell communication, reactions, and signal transduction. Transport proteins in particular are of major interest due to their ability to uptake and redistribute important micronutrients in a wide range of organisms from mammals to plants and bacteria. In plants, the regulation of physiological concentrations of ions is critical for survival. There are eight micronutrients that are considered essential to higher plants: B, Cl, Cu, Fe, Mn, Mo, Ni, and Zn.[70] Deficiencies in these micronutrients result in major abnormalities in plants such as decreased growth and reduced fruit formation. When present in excess, these ions can induce toxicity in plants producing of reactive oxygen species (ROS), leaf malformation, reduced root length and death.[1,70] Transport proteins help maintain optimal concentrations of these micronutrients by intaking and distributing ions into plant tissues in times of scarcity and reducing intake through negative feedback loops when they are in abundance. Not surprisingly, the loss of these transporters disrupts this delicate balance, resulting in deleterious effects.

Copper ions play a major role as a cofactor in respiration, photosynthesis, and oxidative stress management. In plants, copper ions have been also tied to the processes of ethylene signaling,[71,72] senescence,[73] plant defense mechanisms,[74,75] and reproduction.[25,76] Copper deficiency greatly impacts fertility leading to decreases in grain yield, disturbed iron homeostasis and observable changes to reproductive structures such as pollen malformation.[3] AtCOPT1 is a member of a large family of high-affinity Cu(I) specific transporters known as COPT (COPper Transporters) present in *Arabidopsis thaliana* and other plant species. In *A. thaliana* six members of the COPT family have been identified. Denoted as AtCOPT1/2/3/4/5/6, all have been associated with Cu(I) transport except COPT4 whose function remains unknown.[1,4] Each AtCOPT occupies a functional niche in the plant;

AtCOPT1 and AtCOPT2 are highly expressed in the roots where they mediate Cu(I) uptake,[11] AtCOPT5 is found throughout the plant as is AtCOPT6[9] though its primary expression is in vascular tissues.[10] AtCOPT3/5 have been shown to be localized to the internal membrane compartments. AtCOPT5 is believed to facilitate Cu efflux from vacuole storage under copper deficiency[3,13] and AtCOPT3 is thought to be associated with membranes of the ER, but limited evidence of this is available[77]. COPT proteins are also suspected to serve an important role in plant reproduction; however much of our knowledge of their function and structure is derived from studies of the homologous CTR (Copper Transporter) family found in mammals and yeast.[8,9,11,31] Protein folding simulations and X-ray crystallography experiments carried out with human CTR1 (hCTR1) suggest that COPT proteins have three transmembrane domains and function as a trimeric complex. These transmembrane domains within a trimeric complex interact to form a pore and conserved internal methionine residues facilitate unidirectional Cu(I) shuttling.[78] N-terminal motifs in COPT1 are primarily responsible for the recruitment of Cu(I) from the microenvironment and COPT/CTR C-terminal motifs interact with cytosolic Cu chaperones.[8,14,20]

Studying these membrane transporters has proven to be a challenge arising, in part, from the presence of the protective plant cell wall and the limited availability of tools to directly study these membrane transporters' biophysiological behavior and mode of operation. Standard *in vivo* cell-based copper uptake and complementation assays completed using *S. Cerevisiae* Cu uptake deficient mutants *ctr1*Δ, *ctr2*Δ, and *ctr3*Δ have functionally identified the *A. thaliana* Cu transporters AtCOPT1, AtCOPT2, AtCOPT3, AtCOPT5, and AtCOPT6. Functional assays with heterologous expression of nonendogenous plant transporters in yeast, however, can carry inherent risks, namely the potential for non-native interactions.[4,9] Alterations to native protein behavior and potential toxicity limits the compatibility of some transporters such as AtCOPT4 with these methods.[8] Since yeast complementation assays do

not provide direct measurements of protein activity, it is becoming increasingly common to use electrophysiological techniques. One such method to directly measure transporter function is patch-clamp, which is commonly used to study ion channels in animals. Patch-clamp relies upon detecting changes in membrane polarization during activation of channel proteins. However, patch-clamp is difficult to master and many transport proteins including COPTs have been found to be incompatible with patch clamp due to either their non-electrogenic nature or slower transport kinetics.[17]

The ideal experimental system would allow direct measurement of copper transport activity whilst maintaining an environment like that of the native plant. *In vitro* assays and membrane mimics present alternative and complementary methods to study the direct function of transmembrane proteins, such as COPTs. In particular, the functional study of transmembrane proteins has benefitted from the use of supported lipid bilayers (SLBs) to house the proteins and couple with various sensing schemes. Membrane proteins require stabilization of their transmembrane domains via incorporation into membranes and SLBs can be customized with native membranes and specific lipid compositions.[44,45] Supported lipid bilayers have been used successfully to model biological membranes, and when formed from native membrane materials, can recapitulate many of the properties of native membrane systems, such as lipid fluidity and protein retention, activity, and orientation.[52] Prior work has shown that integration of SLBs with electrical and biologically compatible surfaces can enable protein function and surface interactions to be translated into electronic readouts.[54] Recently, we showed that SLBs can be formed from native protoplast membrane material while retaining properties of the native membrane and the expressed proteins of interest.[79] Herein we demonstrate an alternative tool for the study of transport proteins through the integration of a plant derived SLB with a biocompatible electronic chip. This approach enables sensory readout of transporter function that, to date, has not been possible in plant

systems **[Fig. 2.1].** We show that SLBs containing AtCOPT1 proteins can be successfully formed on electrically compatible surfaces. Importantly we demonstrate that transport of copper can be directly detected through resistance based electronic methodologies bypassing the challenge imposed by electroneutral proteins with traditional methodologies. Furthermore, we demonstrate how this tool can be used to investigate key protein properties such as ligand affinity. This work presents a new tool to understand the function of a wide range of membrane-associated processes including metal micronutrient transport in plants.

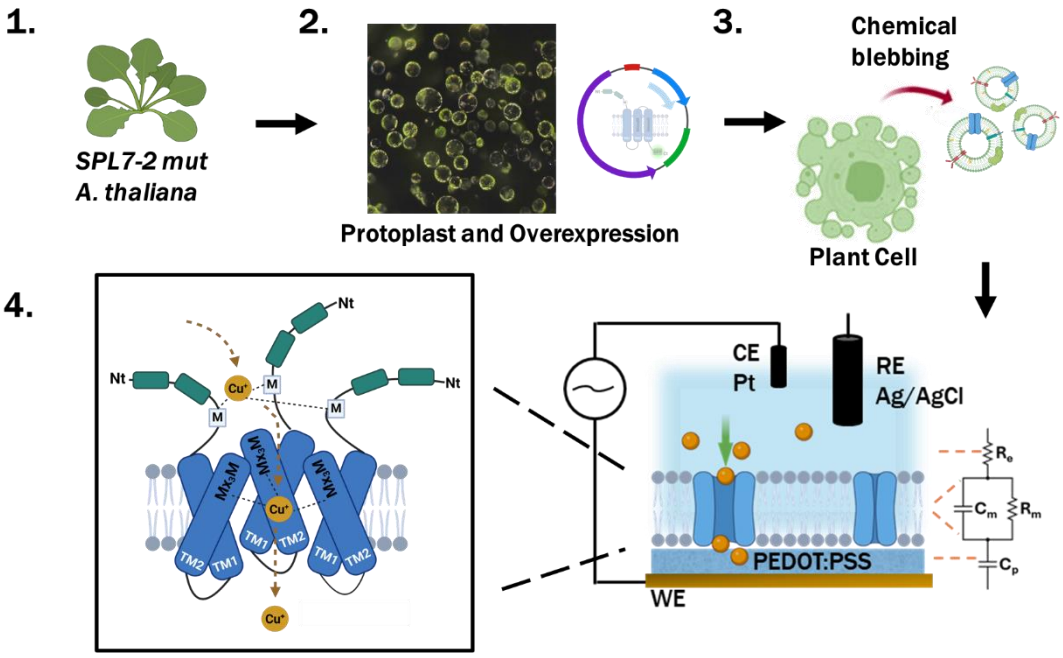

Figure 2.1: Overview of Plant Membrane-on-Chip experimental process
(1) *A. thaliana* SPL7-2 mutant *seedlings were grown for 14 days.* ***(2)*** *Seedlings were then harvested, and the cell walls were digested away to generate protoplasts, which were transfected with plasmids to overexpress the gene of choice.* ***(3)*** *After transfection, the protoplasts were chemically treated to induce the formation of small unilameller vesicles (termed 'blebs'). (4) These membrane blebs were used to form supported lipid bilayers (SLBs) on PEDOT:PSS electrode devices. The resulting Plant Membrane-on-Chip device contains the integrated transporter protein (TM3 & C-terminal not shown) and its response to stimuli can be measured electrically.*
Figure created with BioRender

2.2 Results and Discussion

2.2.1 Design Parameters for a Plant Membrane-on-Chip Device

To design a platform that would recapitulate the behavior and microenvironment of the native plant membrane and allow for the direct detection of the response of electroneutral proteins non-amenable to traditional electrical characterization techniques we set out to achieve three essential qualities in our Plant Membrane-on-chip: 1) the successful incorporation of COPT1 in its native orientation, 2) the confirmation of protein activity, and 3) direct and quantifiable readouts.

2.2.2 Chemically- Induced Vesiculation of Protoplast Results in Blebs That Retain AtCOPT1

We first selected AtCOPT1 as our target transport protein because it is one of the most characterized COPT proteins and also due to its natural plasma membrane localization. Additionally, prior attempts to directly measure AtCOPT1's activity with patch-clamp were unsuccessful, suggesting an electroneutral mechanism for transport.[17] As our platform does not require electrogenic processes for detection, AtCOPT1 should provide a good validation of the benefits to the Plant Membrane-on-Chip. To minimize the contribution of other copper transporters in our assay, experiments were conducted in an *A. thaliana spl7-2* (SQUAMOSA PROMOTER BINDING PROTEIN-LIKE7) mutant lacking the function of the *SPL7* transcription factor.[80] In *Arabidopsis,* SPL7 plays a major role in the upregulation of copper transporter and mobilization genes, including COPT1, under conditions of Cu-deficiency. The *spl7-2* mutant has minimal expression and activity of endogenous Cu transporters,[27] so we selected these plants as a clean "chassis" with which to derive our protoplast from with the goal to have COPT1 as the predominant copper transporter in the protoplast membrane after transfection of the protoplasts with appropriate genes.

Mesophyll protoplasts were harvested from 14-day old *spl7-2* mutant plants and then

transfected on the same day. Protoplast were transiently transfected with a C-terminal eGFP-tagged COPT1 construct (AtCOPT1:eGFP) under a CaMV 35S constitutive promoter to maximize the expression of COPT1 and monitor its synthesis and localization. Similarly, protoplasts were transfected with the empty vector eGFP construct or with water in a Mock transfection to serve as controls. Protoplasts overexpressing AtCOPT1:eGFP exhibited GFP fluorescence localized to the plasma membrane, in comparison to the eGFP empty vector control which was present primarily in the cytosol **[Fig. 2.2A].** Expression of full-length AtCOPT1:eGFP was confirmed by GFP immunoblotting of harvested protoplasts following transfection. Bands can be seen at the predicted molecular weight of AtCOPT1:eGFP (45 kDa) and eGFP alone (27 kDa) on the GFP immunoblot **[Fig. 2.2B].**

After confirming the synthesis and plasma membrane localization of the COPT1-eGFP construct, we then tested if the AtCOPT1:eGFP fusion construct was functional. This was confirmed by yeast complementation assay **[Fig. S2.1].**

Protoplasts were then chemically induced to form blebs which are small unilamellar vesicles (SUVs) that bud off from the plasma membrane. Bleb size distribution and concentration were measured by nanoparticle tracking analysis (NTA) **[Fig. S2.2].** Isolated blebs were found to be polydisperse in size with an average diameter of ~250-300 nm and were within the expected size range for native blebs previously reported.[79] NTA results indicated that particle counts were on the order of ~10^9 particle/ml and there was not a significant difference in particle number between blebs isolated from eGFP and COPT1:eGFP protoplasts. To determine if the COPT1:eGFP transporters were retained in the blebs, we first labeled the vesicle membranes with a membrane intercalating dye, octadecyl rhodamine B chloride (R18). We then adsorbed the labeled blebs onto glass slides and imaged them using confocal microscopy **[Fig. 2.2D].** Colocalized fluorescence of R18 and eGFP indicated that the COPT1:eGFP fusion constructs were still present in the vesicles. The presence of

fluorescence in control eGFP blebs suggest the to the possibility of cytosolic encapsulation during the budding process.

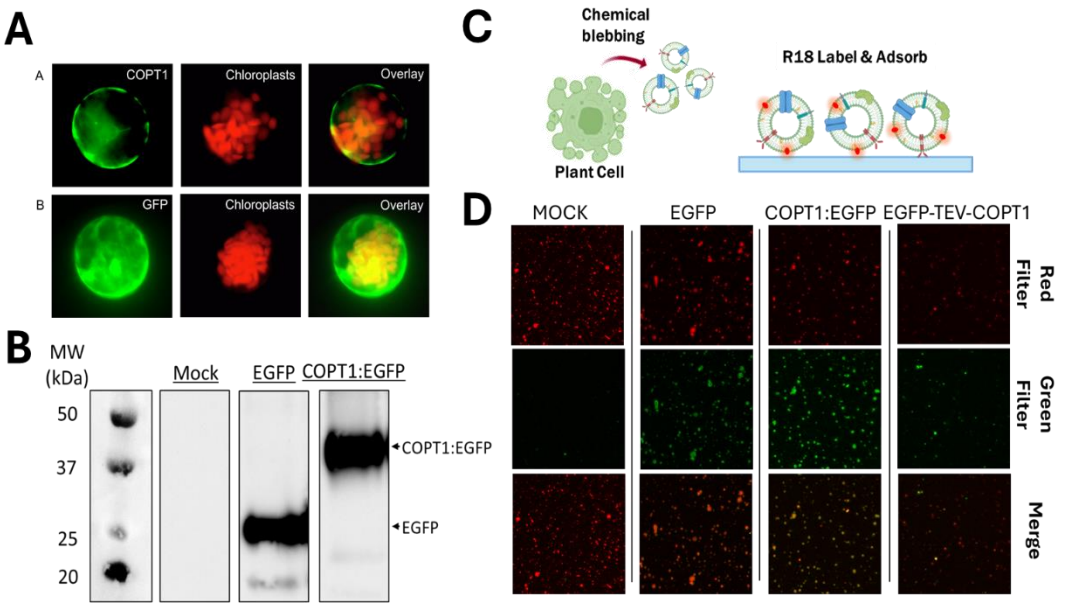

Figure 2.2: Confirmation of the synthesis and membrane localization of COPT1:eGFP in protoplasts and small unilamellar vesicles.
(A) *Fluorescence images of* spl7-2 mut *A. thaliana protoplast transfected with COPT1-eGFP (top) or GFP encoding (bottom) constructs. From left to right appear the GFP channel (FITC), chlorophyll auto-fluorescence (LPFITC) and image overlays. Note that the COPT1-GFP fluorescence is localized primarily to the plasma membrane in contrast to the protoplast transfected with the empty vector (eGFP), which displays more cytosolic fluorescence.* ***(B)*** *GFP immunoblots of protoplast samples following transfection. Lanes from left to right are: ladder, mock transfection, protoplasts transfected with p-SAT6 COPT1:eGFP (~45kDa), protoplasts transfected with empty vector pSAT6-eGFP (~27kDa).* ***(C)*** *Depiction of Protoplast Blebbing. Protoplast are exposed to a low concentrations of chemical agents dithiothreitol and formaldehyde to induce membrane vesiculation to form blebs that contain native membrane components* ***(D)*** *Confocal images of small unilamellar vesicles (SUVs) derived from transfected* spl7-2 *protoplasts labeled with the intercalating membrane dye, R18. Transfection conditions are indicated along the top and filters/channels along the right side. R18 labeled SUVs appear in red, eGFP presence is indicated by green fluorescence, and colocalization of R18 and eGFP as yellow.*
Figure created with BioRender

2.2.3 Supported Lipid Bilayers Containing COPT1 Transporter Can Be Made Using *A. thaliana* Derived Membrane Vesicles

To generate SLBs that can be used in electronic sensing, it is necessary to form them on biocompatible and conductive surfaces. PEDOT:PSS (poly(3,4-ethylenedioxythiophene)

polystyrene sulfonate) is a conductive biocompatible polymer that is transparent, making it amenable to a variety of optical and electrical characterization techniques. To more closely mimic the cell membrane, SLBs can be made from cell blebs derived from cell lines expressing the protein of interest in the plasma membrane. While there are many methods to form SLBs, we utilized a technique known as vesicle fusion where cell blebs are induced to rupture on a support using fusogenic liposomes that have a natural propensity to rupture and form planar bilayer sheets on surfaces. Briefly, the SLB formation process involves optimizing the surface properties of the surface and fusogenic liposomes to tailor them to the specific properties of the membrane blebs **[Fig. 2.3].** The charge and properties of the fusogenic liposomes can be modified by changing the lipid composition.[81] In this work, POPC (1-Palmitoyl-2-oleoyl-glycero-3-phosphocholine) liposomes were used because of their abundance in the native plant membrane and their compatibility with PEDOT:PSS.[82,83]

To visualize and confirm the formation of the SLBs with bleb material, we used fluorescence recovery after photobleaching (FRAP). Liposomes and blebs labeled with R18 were used as a starting material for SLB formation and the fluorescence intensity recovery of a laser-bleached spot was monitored over time. Images show the increase in bleach spot intensity over time as unbleached fluorophores diffuse into the bleach spot. This serves as evidence of the formation of a contiguous SLB, at least over the length scale of the bleach spot **[Fig. S2.3].** By fitting the intensity recovery to a 2D diffusion equation we obtained diffusion coefficients for R18 in AtCOPT1:eGFP, empty vector eGFP, and mock transfection SLBs in the range of ~0.4-0.6 $\mu m^2/s$ and comparable mobile fractions of ~100%. These characteristics are aligned with prior work and confirm bleb rupture and contiguous bilayer formation on the surface.

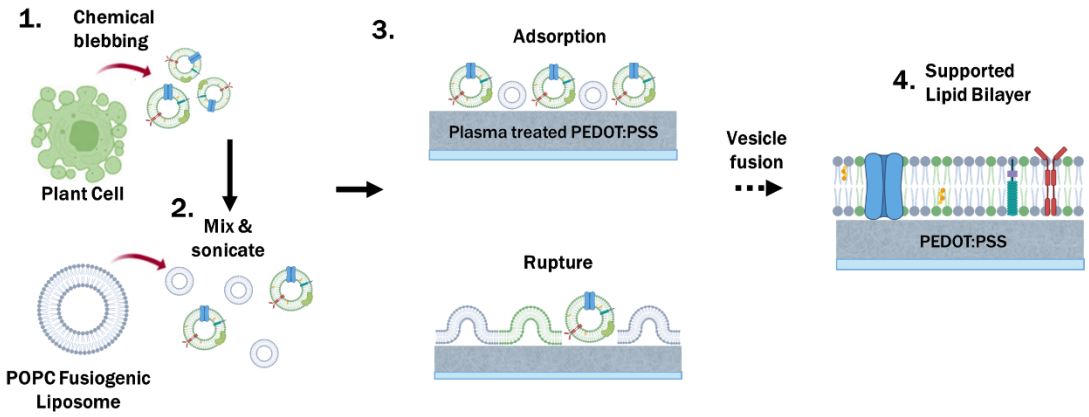

Figure 2.3: Cartoon representation of the vesicle fusion process and the formation of a protoplast-derived SLB
(1) Plasma membrane vesicles are isolated via chemical induction of protoplast blebbing (2) POPC fusiogenic vesicles are mixed with blebs and sonicated (3) bleb-liposome mixture applied to a plasma treated PEDOT:PSS surface adsorb and electrostatic and Van der Wals forces induce their rupture (4) Ruptured vesicles fuse and components redistribute to form a contiguous SLB.
Figure created with BioRender

2.2.4 AtCOPT1 transporters are incorporated into SLBs and retain their native membrane orientation

To confirm the incorporation of COPT1 in our SLBs we carried out additional characterization using total internal reflection fluorescence microscopy (TIRF). TIRF is an optical microscopy technique that is highly amenable to the study of interactions near SLB interfaces because an evanescent wave created between the glass and buffer interface penetrates only about 100 nm deep into the aqueous phase. Since the SLB is positioned near the interface, only fluorophores within this zone can be excited, eliminating interference from fluorescence in the bulk. Due to its proposed unidirectional transport of copper, it was important that the COPT1 be oriented correctly in the SLB for any functional characterization to be interpretable. In the native plant, AtCOPT1 is believed to be oriented such that the N-terminal is accessible to the extracellular space with a luminal C-terminal.

Prior work indicates that proteins in SLBs formed by vesicle fusion largely retain their native membrane orientation, with the extracellular portion facing up in the SLB.[46,52,79] To

investigate the orientation of AtCOPT1 in our SLB platform, an eGFP-TEV-AtCOPT1 construct was generated in the same vector with a N-terminus eGFP tag linked to COPT1 by and a TEV protease cleavable linker. Expression and the plasma membrane localization of the n-terminal construct was confirmed by protoplast fluorescence imaging **[Fig. S2.4A].** GFP immunoblotting was used to determine if the fusion protein was cleavable, by treating protoplasts expressing eGFP-TEV-AtCOPT1 with TEV protease. Results indicated that the cleavage site was accessible, and the construct and cleavage product were of the expected size **[Fig. S2.4B].** Transfected protoplasts were blebbed and the retention of the N-terminal construct was confirmed by imaging R18 labeled blebs for colocalization **[Fig. 2.2D].** We then formed SLBs from blebs containing eGFP-TEV-AtCOPT1 and imaged them before and after the addition of TEV protease using TIRF. Fluorescently tagged COPT proteins are visible in the SLBs as fluorescent puncta following a typical point spread function. Should the TEV cleavage site be accessible the eGFP will be cleaved from the fusion protein and enter the bulk where it will no longer be illuminated by the TIRF evanescent wave. Following TEV addition, the average number of fluorescent puncta decreased by 83% **[Fig. S2.5].** Loss of fluorescence after the addition of TEV protease indicates that the n-terminal cleavable linker was accessible and thus not under the SLB. This serves as evidence that COPT1 is primarily orientated in the same configuration as the native protein.

2.2.5 Direct Detection of AtCOPT1-Mediated Copper Transport Using Electrical Impedance Spectroscopy

With the confirmation of SLB formation and the retention of the transporter in the native orientation, protein function could be assessed. Electrochemical Impedance Spectroscopy (EIS) is a powerful tool to study SLBs owing to its non-destructive and sensitive properties. EIS utilizes a system of electrodes wherein a current is swept through a range of frequencies, and the corresponding impedance response is recorded **[Fig. 2.4A].** Impedance is the inverse

of the admittance in an alternating current and is a complex quantity composed of both real and imaginary components. For simplicity, here we will present it as the resistance to current flow in an alternating current. Changes to surface properties result in shifts in impedance at specific frequencies. For example, SLB formation on electrodes results in an attenuation of ion flux and subsequent increase in impedance. When a pore opens in an SLB such as when a transport protein is opened, there is a small decrease in SLB impedance as ions pass through. The volumetric capacitive properties of the PEDOT:PSS on the electrode make it ideal for EIS measurements as it significantly reduces the gold electrode's impedance. This lower impedance allows small changes in SLB properties to be observed which would otherwise be masked without the PEDOT:PSS present.

A plain device, consisting of a PEDOT:PSS coated gold electrode and electrolyte

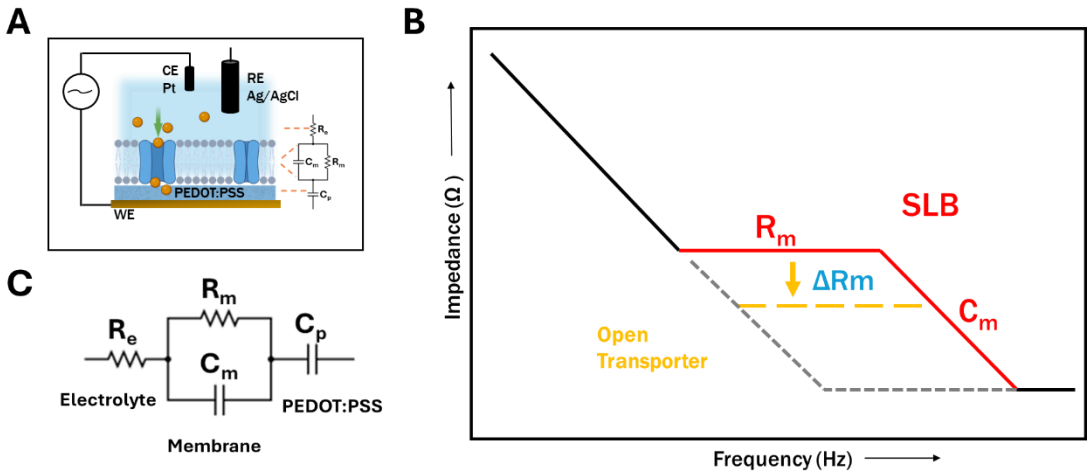

Figure 2.4: Electrochemical Impedance Spectroscopy
(A) *Schematic of Plant-on-chip device set-up for Electrochemical Impedance Spectroscopy (EIS) measurements. Platinum counter electrode (CE) and Ag/AgCl reference electrode (RE) are placed in the bulk electrolyte buffer. PEDOT:PSS coated gold electrode serve as the working electrode (WE)* ***(B)*** *Representative Bode impedance profile of a SLB device measured using EIS first with plain PEDOT device (black/gray), SLB (red), and activation of a transporter (yellow). Log of the real impedance is plotted vs the log of the frequency* ***(C)*** *Equivalent electrical circuit model of SLB device used to fit impedance response and obtain a SLB associated resistance, Rm.*
Figure created with BioRender

buffer, has an impedance response that is modeled as a resistor-capacitor in series, ReCp, where Re is the electrolyte associated resistance and Cp is the PEDOT:PSS associated capacitance. Upon formation of an SLB, the impedance profile of the device changes and can be represented as the addition of a resistor-capacitor in parallel to the plain device model **[Fig. 2.4B].** The derivation of the equivalent electrical circuit model is described more in the Methods. The final SLB impedance profile can be modeled as an ReCp(RmCm) where the membrane resistive (Rm) and capacitive (Cm) behavior associated with the SLB can be extracted from the fits to the data **[Fig. 2.4C].** This Rm provides a quantifiable and direct means of measuring the ion flux through the SLB that is associated with the activity of transporter protein. Cm provides us with a secondary check on SLB formation given that an approximately 4 nm thick lipid layer would have a theoretical capacitance on the order of 10^{-9} F, and we report here Cm in the range of 1-5 nF.

2.2.6 Detection of AtCOPT1 copper transport activity in a concentration dependent manner

To test the functionality of AtCOPT1:eGFP proteins in SLB devices, we used (EIS) to measure the quantifiable decrease in membrane impedance associated with transporter activity. We first formed SLBs on PEDOT:PSS devices using blebs with AtCOPT1:eGFP and with empty vector eGFP blebs as a control. As expected SLBs formed from using these blebs possessed a stepped impedance profile. To compare the response of SLBs with COPT1 to our control, the response of Plant Membrane-on-chip devices were recorded as they were exposed to a range of physiologically relevant Cu concentrations (0.1-40 µM Cu). Bio-available copper is most commonly found in the +2 oxidation state, but COPT1 is believed to be Cu(I) specific so a molar excess of Ascorbic Acid (100 µM) was added to the copper solutions to reduce Cu(II) to Cu(I) and maintain the +1 oxidation state.[14] If there was COPT1 activity, we expected a decrease in the initial Rm as the COPT1 transmembrane pore opens and allows ion

flux. We report this as the %Δ Rm given as:

$$\frac{R_m(initial) - R_m([ion])}{R_m(initial)} \; x\; 100 \qquad (3)$$

where Rm(initial) is the Rm of the SLB upon formation and Rm([ion]) is the Rm of the SLB at any concentration of metal ion. Upon addition of increasing concentrations of Cu to AtCOPT1:eGFP devices, we saw a concentration-dependent decrease in Rm seen as a downward shift in SLB associated impedance of a Bode plot **[Fig. 2.5A].** AtCOPT1:eGFP and eGFP Plant Membrane-on-chip devices displayed decreases in Rm (31.03±1.43% and 20.56±1.71% respectively at 40 µM) when exposed to Cu(I) that saturates at higher concentrations. However, SLBs containing AtCOPT1:eGFP displayed a significantly higher degree of response (up to ~12% higher in Δ Rm), indicative of transport presence in the membrane **[Fig 2.5B].** We hypothesize that the background response measured in eGFP devices could be attributed to a combination of two main factors: 1) presence of other

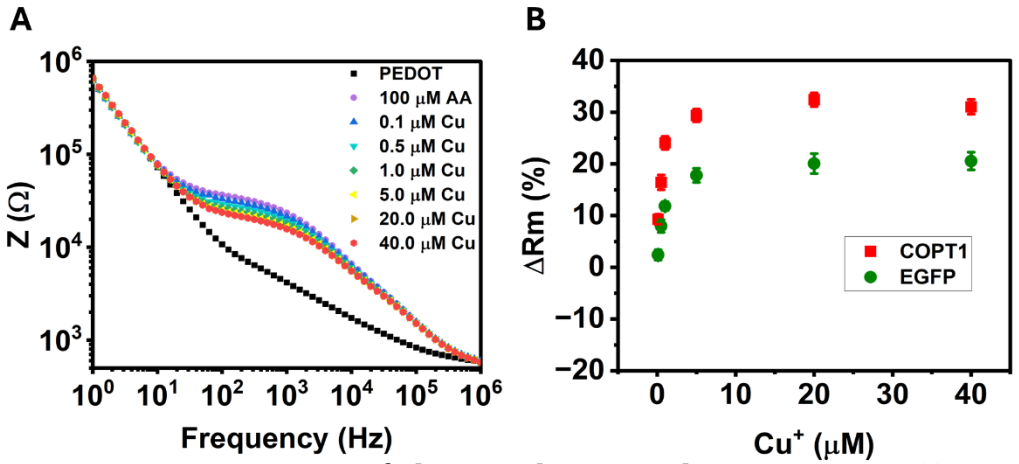

Figure 2.5: EIS measurement of Plant Membrane-on-Chip response to Cu(I)
(A) *Representative Bode impedance profile of a single experiment with a COPT1:eGFP SLB device measured using EIS first with plain PEDOT device (black), SLB with 100 µM Ascorbic Acid (AA) (purple), and Cu treatment from 0.1 µM (blue) to 40 µM (red). The drop in impedance is visible as the concentration of Cu increases corresponding to a shift in color from purple to red and indicating copper transport.* ***(B)*** *(A) Response SLB Rm of COPT1:eGFP and eGFP SLB devices with an increase in Cu concentration in the presence of Ascorbic Acid. A positive change in Rm indicates a drop in membrane resistance associated with ion transport for concentrations from 0.1 µM to 40 µM (Error Bars indicate standard errors of n=3 biological replicates.)*

membrane transporters still expressed despite the *spl7-2* mutant background, and 2) interactions of copper with biological membranes as copper is well established to interact with a number of phospholipids in membranes and has been shown to induce lipid-peroxidation leading to membrane damage.[84–86] However, these factors would be present in the control case as well, so any signal above the background can be attributed to the presence of the transporter.

While generally used to model enzyme kinetics, Michaelis-Menten can be used to model transport proteins provided that they display concentration dependent and saturable response with single-file transport.[56] To further characterize the Cu(I) response we modeled the percent change in Rm with a typical Michaelis-Menten fit to obtain an apparent affinity. This affinity is the combined contribution of the expressed AtCOPT1:eGFP protein, any additional transporters, as well as the effects of the Cu-membrane interactions. The resultant Cu affinity for AtCOPT1:eGFP SLBs (Km= 0.357 μM) was within the typical range of a high affinity transporter (Km < 5 μM) and more than double that of eGFP (Km=0.787 μM) **[Fig. S2.6I].** Reported values of Km for CTR and other copper transporters vary but generally range from 1-4 μM.[87] When compared to prior studies on ScCTR our calculated Km was lower but within an order of magnitude. This difference could be attributed to the direct nature of our assays compared to the indirect measure of Cu transport used *in vivo* uptake assays, but also the variations in Cu interacting n-terminal domains amongst the CTR/COPT family and levels of expression in distinct cell types.[14] Nonetheless, our results align well to these reported comparative cases and support that the activity we see is from the presence of these transporters.

After establishing a way of measuring COPT1-mediated copper transport activity, we tested COPT1's specificity by introducing other metal ions to our devices. To begin, we measured the response of AtCOPT1:eGFP Plant Membrane-on-chip devices to zinc, a divalent

cation reported to not be transported by CTR/COPT.[21] AtCOPT1:eGFP devices were exposed Zn concentrations (0.1-40 µM) while in the presence of excess Ascorbic Acid to maintain the same conditions as our Cu experiment. EIS results indicated that there was not a significant difference in response between devices containing AtCOPT1:eGFP and the eGFP control therefore any changes to Rm was unlikely to be associated with COPT1 transport on zinc. Interestingly, at low concentrations the addition of Zn caused a slight reduction in Rm by ~12% in plant derived SLBs **[Fig. 2.6A].** This decrease in Rm could be explained by the presence of Zn transporters present in both eGFP and AtCOPT1:eGFP.[50] Further additions of Zn resulted in an increase in Rm above that of the initial SLB by up to ~12% **[Fig. 2.6B].** The increase in resistance of an SLB is generally attributed to binding of additional material to the SLB surface or an increase in membrane order and packing leading to greater ohmic sealing. It has been proposed that Zn interacts with membranes by binding to neighboring phospholipids resulting in stabilization and further ordering of the lipid membrane.[88] Control experiments with pure POPC SLBs showed that the addition of Zn resulted in an increase in Rm by

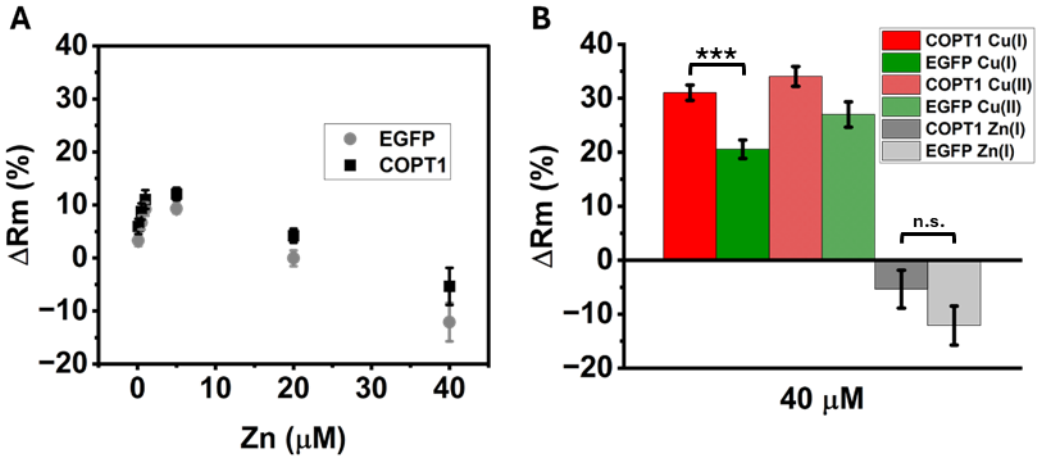

Figure 2.6: Changes in Membrane Resistance in Plant Membrane on Chip Devices with ion addition
(A) *Response of COPT1:eGFP and eGFP SLB devices with an increase in Zn concentration in the presence of Ascorbic Acid. A negative change in Rm indicates an increase in membrane resistance associated with ion interaction with membrane materials* ***(B)*** *Response of COPT1:eGFP and eGFP SLB devices at a concentration of 40 µM Cu or Zn. (Error Bars standard error of n=3 biological replicates. *** = P≤0.001)*

64±10% **[Fig. S2.8].** The observed response is therefore likely a combination of endogenous Zn transporters with the effect of Zn-lipid interactions at higher concentrations.

2.2.7 Plant Membrane-on-chip Devices Recapitulate Cu Transporter-Metalloreductase Interactions

As an additional test of specificity we wanted to see if AtCOPT1:eGFP devices could distinguish between the oxidation state of copper. Based on metal competition uptake assays performed in yeast, members of the CTR/COPT family are believed to be specific for Cu(I).[8,14] To test this, we once again formed SLBs using AtCOPT1:eGFP blebs and eGFP blebs and added copper however without the addition of Ascorbic Acid. Deprived of Ascorbic Acid to reduce Cu(II) to Cu(I), copper should primarily be in its +2 oxidation state. Since Cu(II) should not be transported we expected that AtCOPT1:eGFP and eGFP devices would display similar response, but we observed a higher response in AtCOPT1:eGFP devices compared to the eGFP control (~7% difference in ΔRm) though not very statistically significant. When treated with Cu (0.1-40 μM), AtCOPT1:eGFP and eGFP devices showed a similar decrease in Rm to devices tested with Ascorbic Acid (34.06±1.83% and 26.98±2.34% respectively at 40 μM) **[Fig. S2.7].** This suggests that COPT1 is active and some of the Cu present in the system might exist as Cu(I) rather than Cu(II).

A literature review reveals that present in the plasma membrane of protoplast are a family of iron reductases known as FRO (ferric reduction oxidase) that are also capable of reducing Cu(II) to Cu(I).[27] Therefore it is likely that our Plant Membrane-on-chip device is recapitulating the proposed two-step process of Cu uptake involving the reduction of Cu(II) to Cu(I) by membrane surface metaloreductases and subsequent CTR/COPT mediated transport. Indeed when we model the device response with Michaelis-Menten kinetics the Cu affinity of the AtCOPT1:eGFP (Km = 0.65 μM) device is nearly half that of the devices treated with

Ascorbic Acid and yet the ensemble Km of the eGFP device (Km = 0.805 µM) remained largely the same **[Fig S2.6II].**

2.4 Conclusion

The direct measurement of transporter proteins has largely remained a challenge in plants. Due to their membrane localization, transport proteins are difficult to access, and their slower rates of transport make them unamenable to patch clamp. *In vivo* metal uptake assays have proven to be a useful tool in the study of transport proteins, but they don't provide direct detection of transport activity and, due to ectopic expression, may not be compatible with all proteins. Here we demonstrate the use of a plant native membrane SLB integrated with an electrode to directly translate transporter activity to electrical readouts. Using a combination of conventional techniques, we have developed a biomimetic Plant Membrane-on-chip platform for functional detection of the *Arabidopsis thaliana* Cu(I) transport protein AtCOPT1.

We show that: 1) AtCOPT1:eGFP can be incorporated into a supported lipid bilayer by using vesicles harvested from transfected protoplast 2) These supported lipid bilayers formed via vesicle fusion can maintain the native membrane physical properties of fluidity and protein orientation 3) Electrical impedance measurements can directly capture AtCOPT1:eGFP activity through electronic sensing modalities 4) Electrical measurements of AtCOPT1:eGFP activity can be incorporated in enzyme models to derive transporter kinetic parameters 5) Our Plant Membrane-on-chip devices can recapitulate known Cu vs Zn selectivity properties of AtCOPT1. Additionally, based on evidence from our experiments, it may be possible that this platform could also be used to study Cu(I) transporter-metaloreductase interactions with appropriate cell line knock outs or inhibiting compounds. Our findings indicate that a Plant Membrane-on-chip device provides a powerful tool to directly investigate the function and properties of transporter proteins in a stable *in vitro* platform without the necessity of ectopic expression.

2.5 Materials and Methods

2.5.1 Materials

1-Palmitoyl-2-oleoyl-glycero-3-phosphocholine (16:0–18:1 PC, POPC) used for the preparation of fusogenic liposomes was obtained from Avanti Polar Lipids (700 Industrial Park Dr, Alabaster, AL 35007). Whatman Nucleopore polycarbonate filters (50 nm) (Cytiva-Marlborough, MA) were used for liposome extrusion. The octadecyl rhodamine B chloride (R18) used in optical experiments was obtained from Thermo Fisher Scientific (Waltham, MA). Microscope coverslips (VWR 25 mm × 25 mm glass) were prepared for use by Piranha wash using sulfuric acid (95- 98%, VWR) and hydrogen peroxide (50 wt.% solution, Krackler Scientific). 4-(2-Hydroxyethyl)piperazine-1-ethanesulfonic acid (HEPES), dithiothreitol (DTT), formaldehyde solution, and Calcium Chloride dihydrate were all purchased from Millipore Sigma. PEDOT:PSS (PH 1000) was purchased from Ossila (Sheffield, UK). (3-glycidyloxypropyl) trimethoxysilane (GOPS) Bathocuproinedisulfonic acid disodium salt hydrate (BCDS) and MES Sodium salt were purchased from Sigma-Aldrich (St. Louis, MO, USA). Tris hydrochloride (Tris-HCl) was purchased from Roche Diagnostics (Mannheim, Germany). Potassium Chloride (KCl) was purchased from MP Biomedicals (Solon, OH). MES was purchased from Calbiochem. L(+)-Ascorbic Acid (AA) and Zinc Sulfate heptahydrate was purchased from EMD Chemicals. Sodium Citrate dihydrate was purchased from Fisher Scientific. Tween-20 was purchased from Sigma. Sylgard 184 elastomer/crosslinker mixture was obtained from Robert McKeown company (Branchburg, NJ)

For Western Blots Monoclonal Mouse anti-GFP IgG2a JL-8 was obtained from Takara Bio and Goat anti-Mouse IgG H+L IgG was purchased from Abcam.

For plant culture, enzyme digestion and transfection Murashige and Skoog (MS) medium and Polyethylene Glycol 4000 (PEG-4000) was purchased from Sigma-Aldrich. D-Sorbitol, D-

Mannitol, Sucrose, Pure bright bleach, and Magnesium Chloride anhydrous were purchased from VWR. Cellulase Onozaka R-10 and Macerozyme R-10 were both purchased from Research Products International (RPI).

ImageJ 1.53 A and Fiji (NIH), AxioVision rel. 4.8, Zen 3.4 were used to acquire and analyze optical data. NOVA 2.1.7 was used to collect electrical data. Origin 2024 was used to plot data found in the main and supporting figures. All plasmid sequences were confirmed by full length Nanopore plasmid sequencing through Plasmidasaurus or Eurofin Genomics.

2.5.2 Buffers and other Solutions

GPMVM Buffer: (500 mM Mannitol, 150 mM NaCl, 2 mM $CaCl_2$, 10 mM HEPES pH 5.6)

Blebbing Buffer: (2 mM DTT (2 µL/mL), 25mM Formaldehyde (2.25 µL/mL) GPMVM pH5.6)

W5 medium: (0.1% glucose, 0.08% KCl, 0.9% NaCl, 1.84% $CaCl_2$ 2H2O, 2mM MES-KOH pH 5.7)

TVL: (0.3 M Sorbitol, 50 mM $CaCl_2$, sterilize with 0.45 µm filter)

Enzyme Solution: (0.5 M Sucrose, 20 mM $CaCl_2$, 40 mM KCl, 20 mM MES-KOH pH 5.7, 1w/v% Cellulase, 1w/v% Macerozyme sterilized with 0.45 µm filter)

Bleach Sterilization Solution: (30% bleach, 70% sterile Di H_2O and 0.1% Tween-20)

MMG: (0.4 M mannitol, 15 mM $MgCl_2$, 4 mM MES-KOH pH 5.7)

PEG-Calcium Transfection Solution: (40% PEG-4000, 0.2 M mannitol, 100 mM $CaCl_2$)

Tris-HCl KCl Buffer: (150 mM KCl, 10 mM Tris-HCl pH7.4)

2.5.3 Plasmid Generation

To amplify plasmids, transformed NEB 5-alpha cells (NEB) cells containing the desired plasmids were grown overnight in LB Media (25g/L LB Millipore Sigma) with 1mg/ml Ampicillin (Fisher BioReagents) as a selector and isolated using a ZymoPURE II Maxiprep

Plasmid prep kit (Zymo Research). For transit expression of COPT1 in the protoplasts, full-length COPT1 cDNA without stop codon was fused with the modified green fluorescent protein (EGFP) using the pSAT6-N1-EGFP-Gate vector.[9] The resulting pSAT6-COPT6-EGFP construct expresses COPT6:EGFP fusion protein under the control of the cauliflower mosaic virus 35S promoter. For yeast functional complementation, the COPT1 cDNA with stop codon was subcloned into the pYES3-Gate vector.[9,89] The primer sequences used for cloning are listed in Supplemental Table 1. The n-terminal GFP tagged orientation construct eGFP-TEV-GGSG-AtCOPT1 was generated by Gibson cloning into the pSAT6 vector. A short GGSG linker sequence was incorporated to improve the accessibility of TEV protease to the cleavage site.

2.5.4 Functional Complementation of the Saccharomyces cerevisiae

Budding yeast (*Saccharomyces cerevisiae*) wild-type strain SEY6210 (*MATa ura3-52 leu2-3, −112 his3Δ200 trp1Δ901 lys2-801 suc2Δ9*) and the copper uptake-deficient mutant strain *ctr1Δctr2Δctr3Δ* (*MATa ura3-52 his3Δ200 trp1-901 ctr1::ura3::Knr ctr2::HIS3 ctr3::TRP1*) were used for functional complementation assays. The YES3-Gate-COPT1 construct, YES3-Gate-COPT2[9] or YES3-Gate lacking the cDNA insert was transformed into the appropriate yeast strains and selected for uracil prototrophy on YNB–URA medium containing 6.7% (w/v) yeast nitrogen base without amino acids (Difco), 0.77% (w/v) CSM–URA (MP Biomedicals), 0.5% (w/v) NaCl, 2% glucose, 2% (w/v) agar and the respiration competence of different colonies was tested by their ability to grow on non-fermentable carbon sources.[9,90] Single colonies were grown in liquid YNB–URA to an OD600 nm = 1.0 before diluted 10-fold serially and spotted onto YNB–URA medium or YPEG medium containing 1% (w/v) yeast extract, 2% (w/v) bacto-peptone, 3% (v/v) glycerol, 2% (v/v) ethanol, and 2% (w/v) agar and the indicated concentrations of $CuSO_4$. Plates were incubated for 3 days at 30°C.

2.5.5 Isolation of Protoplast

Protoplast were isolated from 14-day old *A. Thaliana spl7-2* mutant (SQUAMOSA PROMOTER BINDING PROTEIN-LIKE7) seedlings grown on half-strength MS medium with 1% (w/v) sucrose and 0.7% (w/v) agar.[91] To sterilize, 100 mg of seeds were incubated in 1 mL of 70% Ethanol solution for 1 min in a laminar flow hood before spinning down and aspirating the supernatant. Seeds were immersed in 1 mL bleach sterilization solution under vortex for 10 minutes before being spun down and the bleach solution removed. To wash the seeds 1 mL of sterile Di H_2O was added to the seeds and well mixed. The seeds were then spun down and the water aspirated. This step was repeated 5 times before adding 1 mL of sterile water and incubating the seeds at 4 °C for two days in the dark before agar germination. To isolate protoplast ~5 grams of fresh shoots were collected, submerged in 15 mL TVL solution and chopped with a fine razor. To digest the cell wall, 20 mL of Enzyme solution was added and allowed to incubate in the dark for 15-16 hrs at room temperature under light shaking. Free protoplasts were sieved through 2 layers of Miracloth and collected. 10 mL of W5 medium was slowly added to the top of the protoplast solution to create an interface and then centrifuged in a swing bucket rotor for 7 minutes at 100 RCF with slow acceleration/deceleration. Protoplasts were collected from the interface of the enzyme solution-W5 medium and 15 mL of W5 was used to wash the protoplast. Rinsed protoplasts were then centrifuged for 5 minutes at 60 RCF, the supernatant removed, and the protoplast resuspended with 15 mL W5 medium. Protoplast were once again centrifuged, and the supernatant removed before finally gently resuspending with 1 mL W5 medium and counted under a microscope to determine the yield.

2.5.6 Protoplast Transient Transfection

Arabidopsis thaliana protoplasts isolated from leaf mesophyll tissue were transfected using previously established procedures.[91–93] Protoplasts were prepared to a concentration of 10^6

cells/mL in W5 medium and allowed to rest on ice for 30 minutes to an hour before removing as much W5 medium as possible without disturbing the protoplast pellet. At room temperature the protoplasts were then resuspended with MMG solution to a concentration of 10^6 cells/mL. pSAT6-N1-EGFP-Gate construct[9] plasmid DNA (100 µL of 1 µg/µL) were added to the protoplast and gently mixed. To the protoplast solution 1.1 mL of PEG-Calcium transfection solution and mixed completely by gentle agitation for 1 minute. Following the mixing, the mixture was allowed to incubate at room temperature for 6-7 mins before diluting with 10 mL W5 medium and mixing well by inverting the tube gently twice. The transfection mixture was then centrifuged at 100 RCF for 2 minutes at room temperature to collect the protoplast and the supernatant discarded. The protoplast pellet was then gently resuspended with 10 mL of W5 medium and cultured at room temperature overnight in the dark. After the overnight incubation the transfected protoplasts were collected by centrifuging at 100 RCF for 2 minutes, resuspended in 1 mL of W5 medium. For experiments, the transfection was scaled up or down as needed. EGFP-mediated fluorescence and chlorophyll autofluorescence were visualized using FITC (for EGFP) or rhodamine (chlorophyll) filter sets of the Axio Imager M2 microscope equipped with the motorized Z-drive (Zeiss) to assess transfection efficiency and localization. Images were processed using Image J. Small scale ($< 2.5x10^5$ cells) yielded higher transfection rates. For all electrical experiments batches with a minimum transfection efficiency of 70% were used **[Table S2.2].**

2.5.7 Bleb Isolation

To isolate membrane blebs, protoplasts were centrifuged at 100 RCF for 5 minutes to obtain a pellet without rupturing cells. The W5 buffer was then removed and replaced with blebbing buffer at a ratio of 4 mL per 10^6 cells and allowed to incubate for 2 hours at room temperature to induce the production of membrane blebs. Following incubation, protoplasts in the blebbing buffer were centrifuged at 200 RCF for 5 minutes to collect the protoplast without rupturing

them. The supernatant was centrifuged at 2000 RCF for 5 minutes to clear the supernatant of remaining debris and the remaining suspended blebs collected.

2.5.8 Protoplast Western Blot

The expression in protoplast was assessed via immunoblotting. Protoplast were pelleted and lysed by physical agitation before addition of a western blot mix (Bolt Blue LDS and Bolt Reducing Agent Buffer at final concentration 1x and 5%w/v SDS). To confirm the cleavage of eGFP:TEV:COPT1, protoplast were treated with TEV protease (New England Biolabs) at 30 °C for 2 h followed by an overnight incubation with additional TEV protease. TEV treated and protoplast samples were then added to the western blot mix and heated at 90 °C for 10 mins before running in Bis-Tris gel (NuPage) with a Precision Plus Protein ladder (Bio-Rad) followed by a transfer to a PVDF membrane (Immobilon-P, Millipore). Blots were then stained with Ponceau S and imaged Chemidoc (Bio-Rad) to assess transfer and serve as a loading control. The blot was then blocked with milk (5% milk powder in TBST buffer) before immunoblotting with 1:4000 Mouse anti-GFP JL-8 (Takara) overnight at 4 °C and 1:4000 Goat anti-mouse (Abcam) for 1 hr at room temperature. Blots were imaged for GFP with a Chemidoc (Bio-Rad) after staining with an ECL kit (Clarity) and analyzed using Image Lab software (Bio-Rad).

2.5.9 Glass Slide Preparation

To clean, microscope coverslip slides were immersed in a Piranha solution for 15 minutes and then washed with deionized water for 30 mins. Cleaned slides were then stored for later use under deionized water (18.2 MΩ cm), rinsed with deionized water and dried with nitrogen gas before use.

2.5.10 PEDOT:PSS Slide Preparation

To make the PEDOT:PSS solution PEDOT:PSS was filtered through a 0.45 µm syringe filter and then combined with, 1% (3-glycidyloxypropyl) trimethyoxysilane in a scintillation vial.

The solution was then sonicated for 30 mins in a chilled bath sonicator (ultrasonic cleaner, VWR) and passed once through a 0.45 µm syringe filter. Clean glass slides were prepared for spin coating via oxygen plasma cleaning at 7.2 W and 105 Micron for 30 s (Harrick Plasma, Ithaca, NY). Three drops of PEDOT:PSS solution were then applied to each slide and spin coated (Apogee Spin coater, Cost Effective Equipment) at 4000 rpm for 30 s. The coated slides were then baked at 140 °C for 1 hr and immersed in deionized water overnight. Before use slides were rinsed with deionized water and dried with nitrogen gas.

2.5.11 Fusogenic Liposome Preparation

Fusogenic liposomes were formed using thin-film hydration and extrusion from a suspension of POPC lipids in chloroform. The chloroform was evaporated using nitrogen gas to form a lipid thin film and were placed under vacuum for a minimum of 4 hr to remove trace solvent. The lipids were then rehydrated with Tris-HCl KCl buffer to a concentration of 2 mg/mL. The rehydrated suspension was then vortex and water bath sonicated for 15 mins before extruding at least 10 times through a 50 nm Nucleopore polycarbonate filters using an Avanti Extruder (Avanti Polar Lipids, Birmingham, AL).

2.5.12 Liposome and Bleb characterization

The average hydrodynamic size of liposomes and protoplast blebs in GPMVM buffer were measured on a Zetasizer Nano-ZS instrument (Malvern Instruments) using a 4 mW He-Ne laser (λ = 632 nm) and a backscattered detector angle of 173°. The size of the liposomes were monodisperse with an approximate diameter of 100 nm. The size and concentration of protoplast blebs diluted 0.1x in GPMVM buffer were measured using nanoparticle tracking analysis (NTA) on a Malvern NS300 Nanosight (Malvern Instruments) with a 532 nm laser. Each sample was measured 5 times at room temperature.

2.5.13 Plant Bleb Confocal Microscopy

To visualize the retention of overexpressed proteins following blebbing, blebs were labeled

with 1 µL of R18 (0.36 mM) per 50 µL of protoplast blebs and absorbed onto a clean glass slide. Following a 1 h incubation, excess material was then rinsed off with Tris-HCl KCl buffer before subsequent characterization. Adsorbed blebs were then imaged with a 488 nm and 561 nm laser using a Zeiss Elyra Super Res and Zeiss LSM 710 AxioObserver.

2.5.14 Supported Lipid Bilayer Formation

To form Supported lipid bilayers, sample wells were affixed to PEDOT:PSS coverslips/electrode devices in the form of polydimethylsiloxane (PDMS) punched with a well area of ~1 cm^2. PDMS was prepared in a petri-dish using a 10:1 Sylgard 184 elastomer/crosslinker mixture cured overnight at 70°C. PEDOT:PSS coated surfaces were soaked in Tris-HCl KCl buffer for at least 2 hrs prior to use. To prepare for SLB formation, PEDOT:PSS coated coverslips/electrodes surfaces were oxygen plasma treated at 7.2 W and 105 Micron for 30 s. These plasma conditions must be tuned for each plasma cleaner and surface to obtain the proper surface conditions for SLB self-assembly. Protoplast blebs and POPC liposomes were mixed and sonicated for 20 mins before adding to the well. Contents in the well were allowed to incubate at least 1 h before rinsing well with Tris HCl KCl buffer to remove excess material before further characterization.

2.5.15 Fluorescence Recovery After Photobleaching (FRAP)

A 85:15 by volume mixture of sonicated POPC:Bleb was labeled with 3 µL of R18 (0.36 mM) lipophilic dye per 100 µL of vesicle/liposome solution and sonicated for 10 m (kept under 25 °C with ice pad). The formation process of the SLB was then followed as previously described on a PEDOT:PSS coated glass slide. An inverted Zeiss Axio Observer Z1 microscope with an α Plan-Apochromat 20× objective and a 150 mW 561 nm optically pumped semiconductor laser (Coherent, Inc) was used in the FRAP setup. The 561nm laser was used to bleach an approximately 20 µm diameter spot in the labeled supported bilayer and the recovery of the bleached spot's intensity was measured over time. The fluorescence

intensity recovery data was then fit to the 2D diffusion equation as described in Soumpasis et al.[94] following corrections for background and photobleaching effects. The diffusion coefficient (D) was calculated using the equation:

$$\boldsymbol{D = \frac{w^2}{4t_{1/2}}} \qquad \textbf{(4)}$$

where w is the radius of the bleach spot and $t_{1/2}$ is the time required to reach half the maximum recovery intensity.

2.5.16 Protease Cleavage Orientation Assay

To determine the orientation of COPT1 in bilayers formed via vesicle fusion, SLBs were formed using blebs derived from protoplast expressing n-terminal tagged eGFP construct eGFP:TEV:COPT1 on plasma treated glass slides. Plain glass slides were used for TIRF microscopy as opposed to PEDOT:PSS slides due to the thickness of the PEDOT:PSS layer and to minimize PEDOT:PSS associated background. To maximize the amount of fusion protein in the final SLB, protoplast blebs were allowed to incubate for 10 mins before the addition of an equal-volume of POPC and then subsequently well rinsed after 1 h with Tris-HCl KCl buffer. SLBs were treated with TEV protease (5 µL for 2 hrs at 30 C, overnight at 4 °C, in dark to prevent photobleaching) to cleave off eGFP from the fusion protein, followed by a final TEV protease treatment (5 µL for 1 h at 30 °C) and rinsed with Tris-HCl KCl buffer before subsequent imaging. Total internal reflection fluorescence (TIRF) microscopy on a Zeiss Axio Observer Z1 microscope with an α Plan-Apochromat numerical aperture (NA) 1.46 100× objective, Semrock LF488-B-ZHE filter cube, Laser TIRF 3 slider (Carl Zeiss, Inc) and 488 nm sold-state laser angle of incidence adjusted to ~68° to insure an evanescent wave of 100 nm with total internal reflection was used to view eGFP particles before and after TEV protease addition. Fluorescent puncta images were taken using an electron-multiplying CCD camera (ImageEM C9100-13, Hamamatsu) and ImageJ software was used to count the puncta.

2.5.17 Electrochemical Impedance Spectroscopy

For electrical impedance spectroscopy measurements supported lipid bilayers were formed inside PDMS wells on top of PEDOT:PSS electrode devices as previously described. PEDOT:PSS electrode devices were fabricated as previously reported.[54] Devices were then connected to a Potentiostat (Autolab PGSTAT128N) with a working electrode and a Pt mesh as the counter and reference electrode in the buffer above the SLB. The impedance response was recorded to an A.C. current from 1 to 10^6 Hz with applied A.C. voltage of 0.01 V and a DC voltage of 0 mV versus OCP (open circuit potential). A 85:15 POPC:bleb mixture by volume was used to form SLBs on the PEDOT:PSS device. This bleb to liposome composition was chosen to maximize the amount of native membrane components in the resultant SLB while maintaining a sufficiently resistive bilayer. For experiments with Ascorbic Acid the SLB was allowed to incubate for 5 mins in a Tris HCl KCl Ascorbic Acid (100 μM) solution prior to measurements. Copper and zinc were then added by rinsing with $CuSO_4$ or $ZnSO_4$ solutions. To control the oxidation state solutions were either prepared with or without excess Ascorbic Acid (100 μM) as a reducing agent to maintain the +1-oxidation state. After each addition the system was allowed to equilibrate for 11 min before the subsequent measurement. The impedance profile was then fit to a RC(RC) equivalent electrical circuit model using NOVA software.[65,67,95] The derivation of the electrical model is formulated from the assumption of dielectric 'slab' with an ionic current arising from ion flux and a capacitive current due to the variation over time of ions buildup at the slab boundary.[65] The total resultant current is the sum of these two values and is thus simulated by a resistor (for ionic current) and a capacitor (for capacitive current). This behavior is observed on a Bode plot as resistive and capacitive components respond differently to alternating current – the impedance of a resistive element is constant, and the impedance of a capacitive component is $1/iwC$ where, w is the angular frequency and, °C the capacitance. In this model the series

resistance is representative of the resistance of the buffer wires and other electrical elements. The series capacitor arises from the volumetric capacitor properties of PEDOT:PSS. The in parallel resistor and capacitor is representative of the bilayer that displays both capacitive and resistive properties **[Fig. 2.4].** This model was then used to extract the resistance of the bilayer and normalized against electrode area. Following measurements 70% ethanol was used to remove the bilayer and the baseline of the PEDOT:PSS electrode was measured and fit to a RC circuit.

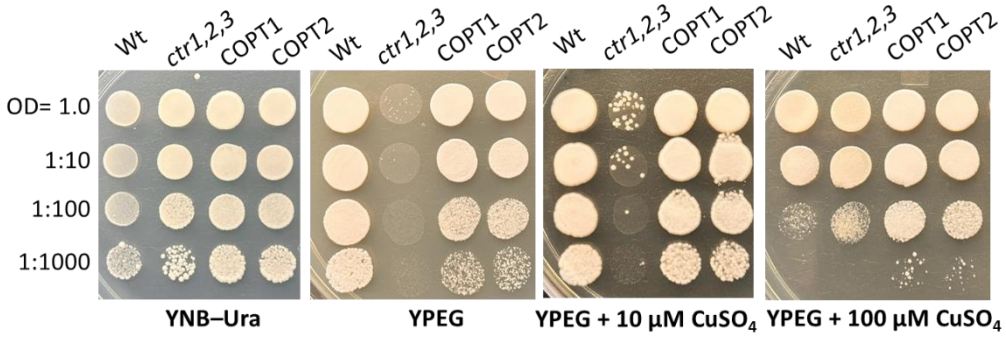

SI Figure S2.1: COPT1 rescues growth defect of the *ctr1Δctr2Δctr3Δ S. cerevisiae* triple mutant on ethanol/glycerol medium (YPEG). *The wild-type SEY6210 strain transformed with the empty vector (Wt), and the ctr1Δctr2Δctr3Δ mutant transformed with the empty vector (ctr1,2,3) or the vector containing COPT1 (COPT1) or COPT2 (COPT2) cDNA inserts were grown overnight in liquid YNB-URA medium to an A600 nm 1.1. Cells were then serially diluted at 10-fold (indicated on the left) and spotted either onto solid YNB-URA medium (YNB-URA) or YPEG (YPEG) with the indicated concentrations of $CuSO_4$.*

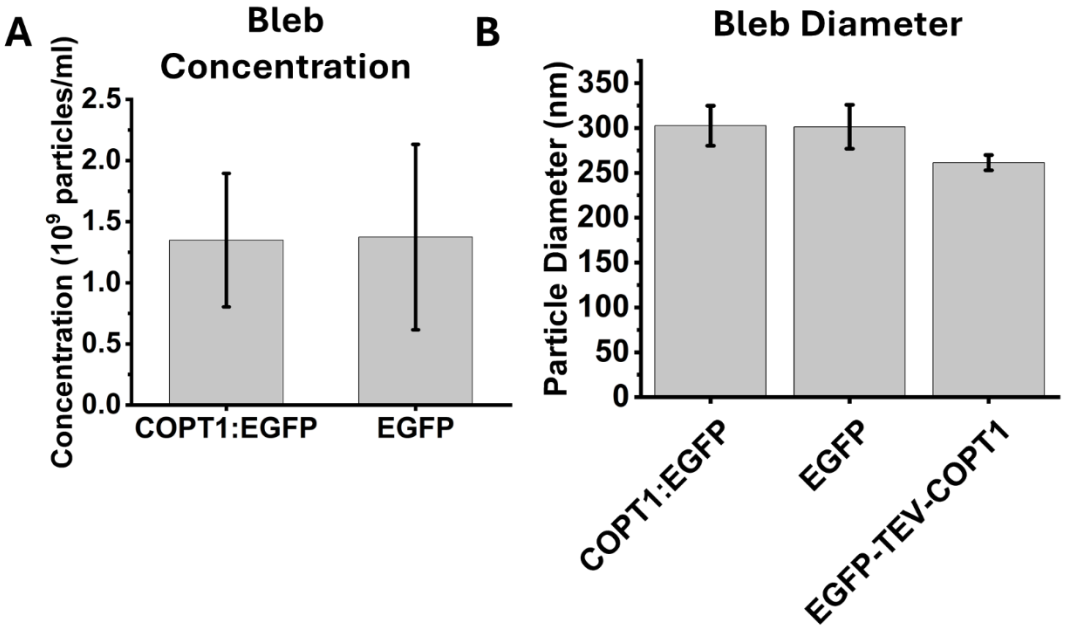

SI Figure S2.2: *SPL7-2 mut* Bleb Particle Characterization by Nanoparticle Tracking Analysis

(A) *Bleb Mean particle concentration as measured by Nanoparticle tracking analysis (NTA) of blebs derived from COPT1:eGFP & eGFP transfected protoplast. (n=3 biological replicates)* ***(B)*** *Bleb Mean particle diameter as measured NTA for COPT1:eGFP (n=3), eGFP (n=3), and eGFP-TEV-COPT1 blebs (n=1). All measurements were conducted in GPMVM pH5.6 buffer and with 5 technical replicates. Error bars indicate Standard Deviation*

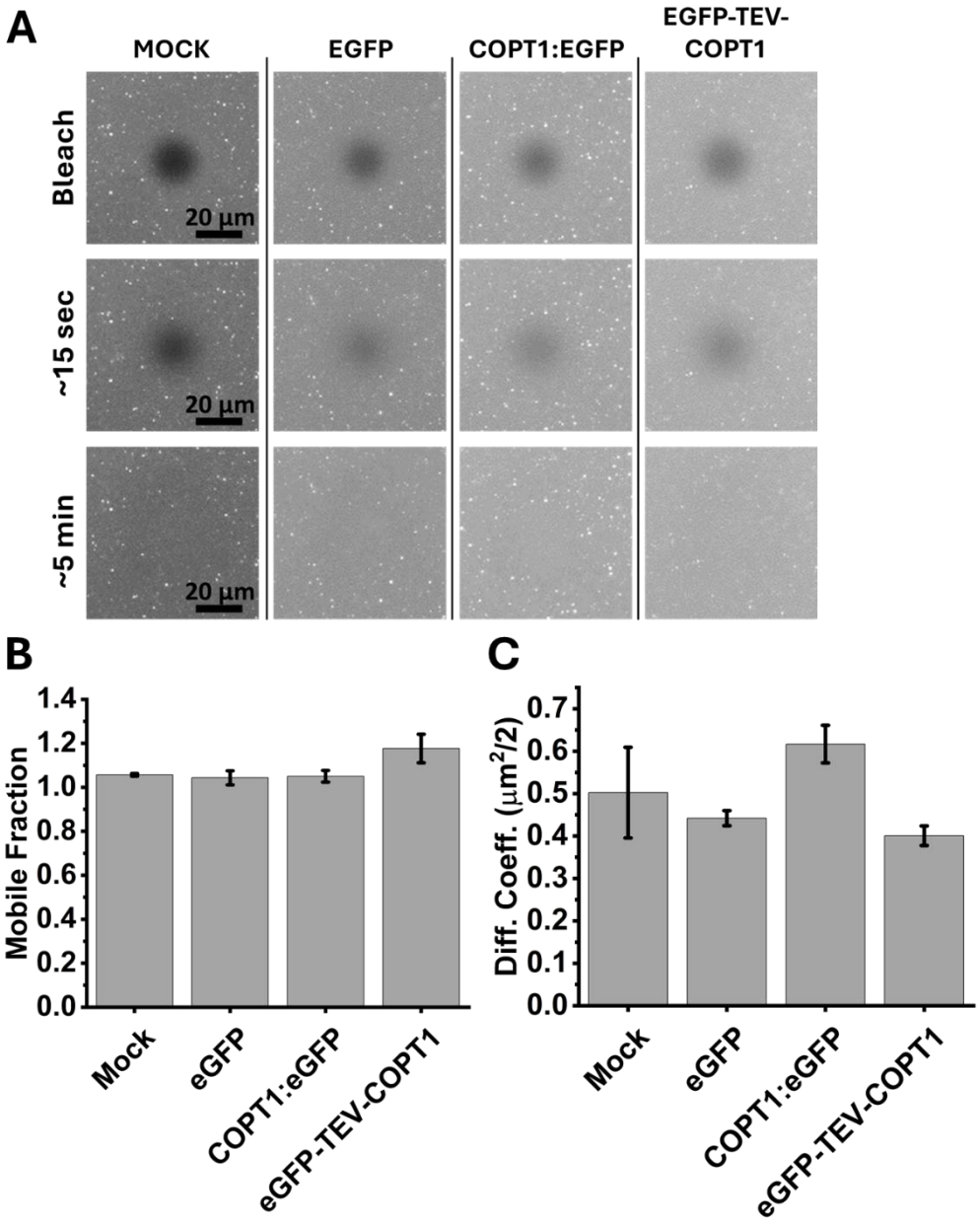

SI Figure S2.3: *SPL7-2 mut* SLB Fluorescence Recovery After Photobleach
(A) *Fluorescence Recovery after Photobleach representative images of R18 labeled 85:15 POPC:Bleb SLBs at approximately 15 seconds and 5 minutes after photobleaching with a 561nm laser. From left to right: SLBs formed using Mock, eGFP, COPT1:eGFP and eGFP-tev-COPT1 blebs. SLB formation is indicated by the full recovery of bleach spot fluorescence* ***(B)*** *Mobile Fraction (MF) of R18 in Mock, eGFP, COPT1:eGFP, eGFP-tev-COPT1 SLBs* ***(C)*** *R18 diffusivities of 85:15 POPC:Bleb Mock, eGFP, COPT1:eGFP, and eGFP-tev-COPT1 SLBs. n=1 with 3 technical replicates*

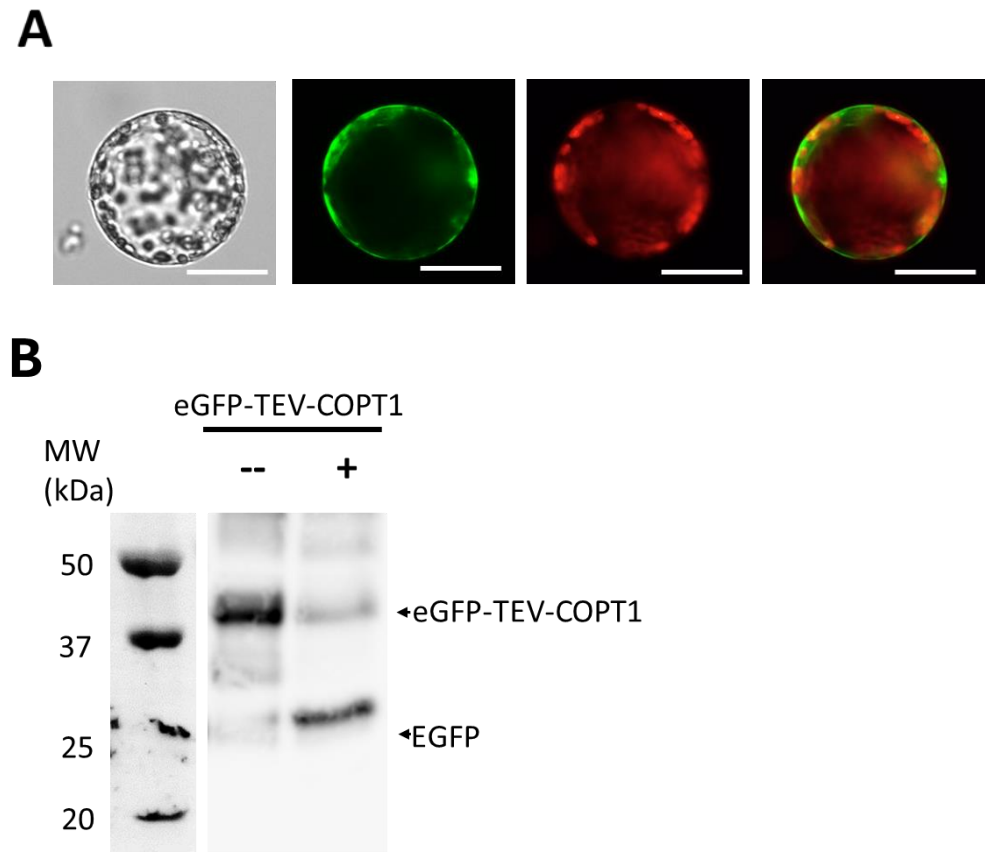

SI Figure S2.4: eGFP-TEV-COPT1 Protein Expression *in spl7-2 mut* Protoplast
(A) *Subcellular localization of COPT1 in Arabidopsis thaliana protoplasts. A. thaliana leaf protoplasts were transfected with water, the vector expressing COPT1 fused with EGFP at N terminus (eGFP-TEV-COPT1). GFP-mediated fluorescence and chlorophyll autofluorescence were visualized using FITC or rhodamine filter sets. Superimposed images of chlorophyll autofluorescence and GFP-mediated fluorescence (Overlay) were created to demonstrate that green fluorescence was derived from GFP. Bar = 20 µm.****(B)*** *Western Blot of Protoplast material treated with TEV protease. From left to right: Protein Ladder, untreated protoplast expressing N-terminal tagged construct eGFP-TEV-COPT1 (~45kDa), eGFP-TEV-COPT1 protoplast treated with TEV protease with cleavage products (~27kDa) and uncleaved protein (~45kDa).*

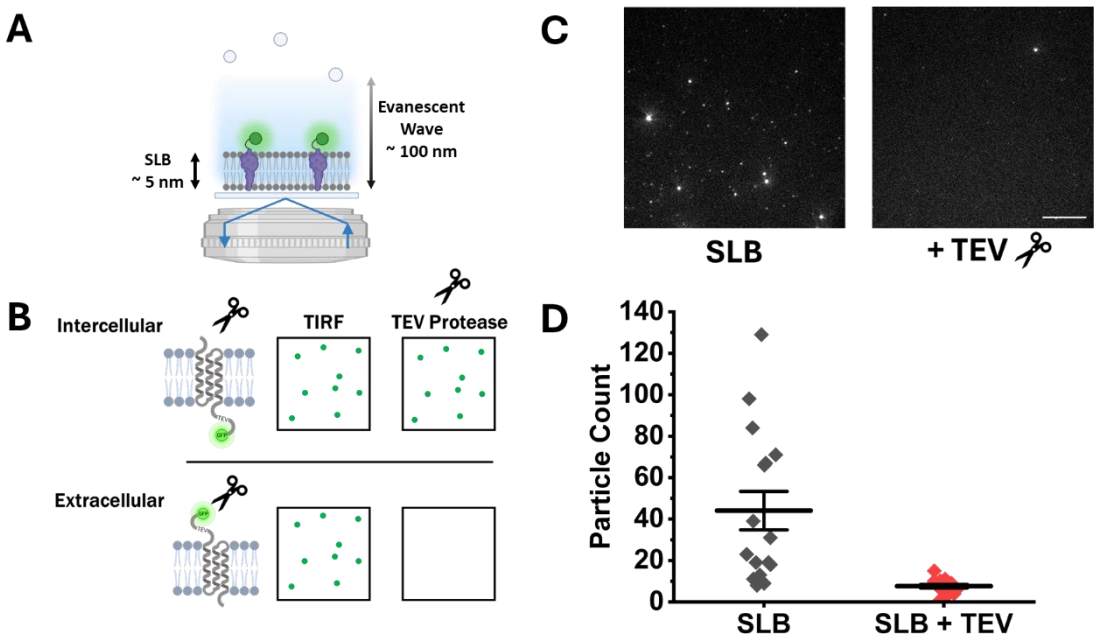

SI Figure S2.5: *SPL7-2 mut* Total Internal Reflection Fluorescence TEV Protease Orientation Assay

(A) *Depiction of Total Internal Reflection Fluorescence (TIRF) phenomenon allowing excitation of only particles close to the SLB and out of the bulk solution.* ***(B)*** *TEV Protease Assay allows for determination of protein orientation on TIRF based upon the accessibility of a cleavage marker. Intercellularly oriented markers are inaccessible while extracellular markers are cleaved and enter the bulk solution resulting in fluorescence loss.* ***(C)*** *Representative TIRF microscopy images of SLBs on glass treated and untreated with TEV protease N-terminal tagged eGFP-TEV-COPT1 proteins are visible are puncta and following TEV there is a loss in total fluorescence (scale bar 10 µm)* ***(D)*** *Quantification of fluorescence puncta in N-terminal tagged eGFP-TEV-COPT1 SLBs following cleavage with TEV protease vs untreated indicates that the N-terminal cleavage site is largely accessible. Figure created with BioRender*

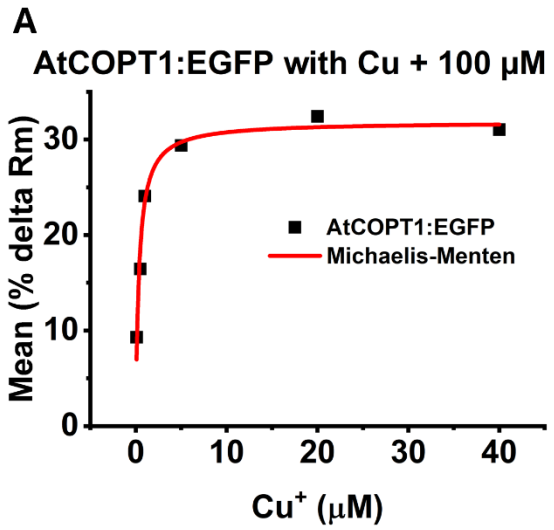

Model	MichaelisMenten
Equation	y = Vmax * x / (Km + x)
Plot	Mean
Vmax	31.84884 ± 1.10037
Km	0.35794 ± 0.06635
Reduced Chi-Sqr	3.00674
R-Square (COD)	0.97152
Adj. R-Square	0.9644

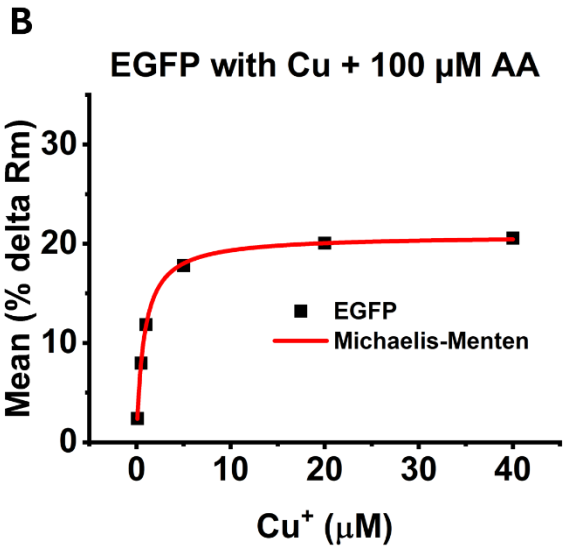

Model	MichaelisMenten
Equation	y = Vmax * x / (Km + x)
Plot	Mean
Vmax	20.84774 ± 0.11782
Km	0.78722 ± 0.02077
Reduced Chi-Sqr	0.02788
R-Square (COD)	0.99958
Adj. R-Square	0.99948

SI Figure S2.6I: Fittings of EIS Cu response data to Michaelis-Menten kinetics
EIS Cu response in presence of 100 µM of Ascorbic Acid ***(A)*** *AtCOPT1:eGFP device* ***(B)*** *eGFP device*

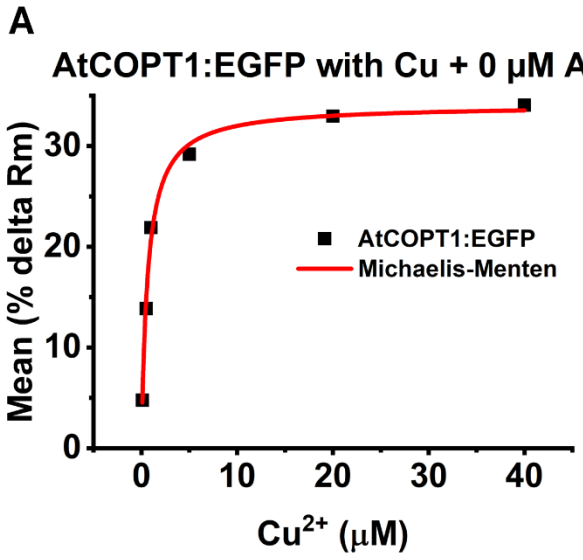

Model	MichaelisMenten
Equation	y = Vmax * x / (Km + x)
Plot	Mean
Vmax	34.07521 ± 0.66263
Km	0.65027 ± 0.06056
Reduced Chi-Sqr	0.93404
R-Square (COD)	0.99448
Adj. R-Square	0.99309

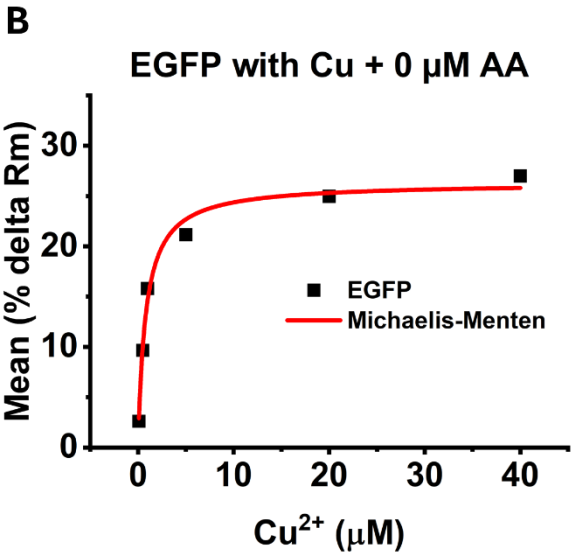

Model	MichaelisMenten
Equation	y = Vmax * x / (Km + x)
Plot	Mean
Vmax	26.32541 ± 0.83548
Km	0.80529 ± 0.11902
Reduced Chi-Sqr	1.3915
R-Square (COD)	0.98743
Adj. R-Square	0.98429

SI Figure S2.6II: Fittings of EIS Cu response data to Michaelis-Menten kinetics
EIS Cu response without Ascorbic Acid ***(A)*** *AtCOPT1:eGFP device* ***(B)*** *eGFP device*

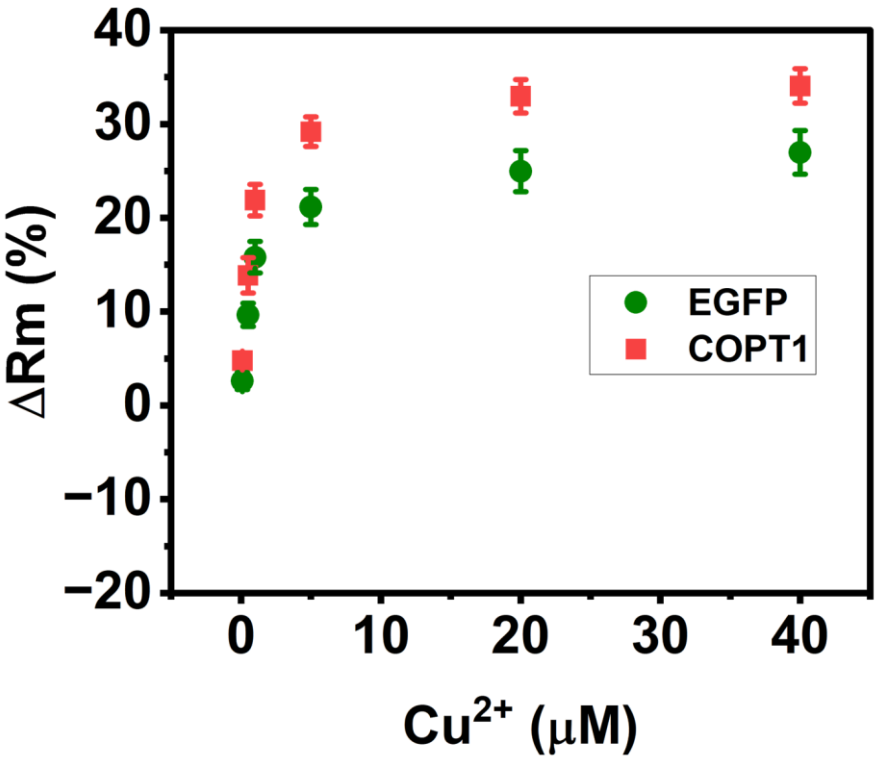

SI Figure S2.7: *SPL7-2 mut* EIS Plant Membrane-on-Chip response to Cu without Ascorbic Acid

Change in SLB Rm of COPT1:eGFP and eGFP SLB devices with an increase in Cu concentration without Ascorbic Acid. A positive change in Rm indicates a drop in membrane resistance associated with transport for concentrations from 0.1 μM to 40 μM) Error bars indicate standard error of (n=3) biological replicates

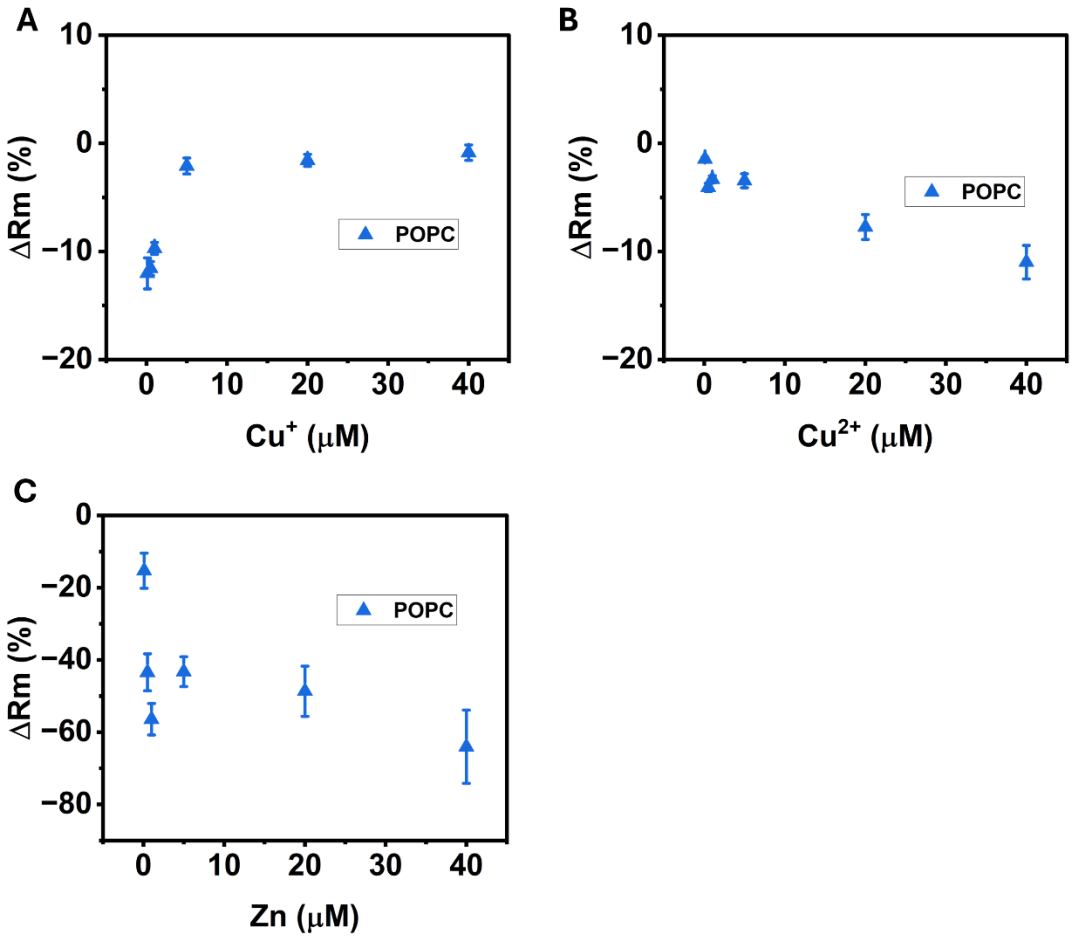

SI Figure S2.8: EIS POPC SLB Response to Ion Addition
(A) *Response SLB Rm of POPC SLB devices with an increase in Cu concentration (0.1-40 μM) in the presence of Ascorbic Acid (100 μM)* ***(B)*** *Change in SLB Rm of POPC SLB devices with an increase in Cu concentration (0.1-40 μM) without Ascorbic Acid. (inset first 5 data points)* ***(C)*** *Response of POPC SLB devices with an increase in Zn concentration (0.1-40 μM) in the presence of Ascorbic Acid. (n=+3 technical replicates)*

SUPPLEMENTAL TABLES

Oligo name	**Primer sequence (5' to 3')**
AtCOPT1_attB_F	GGGGACAAGTTTGTACAAAAAAGCAGGCTTCA CCGCCAAGAACAAAGAAACCATGGATCA
AtCOPT1_attB_R	GGGGACCACTTTGTACAAGAAAGCTGGGTCTC ATCAACAAGCACAACCTGAGGG
AtCOPT1_attB_nS_R	GGGGACCACTTTGTACAAGAAAGCTGGGTCAC AAGCACAACCTGAGGGA

Table S2.1: A list of used oligos in this study

***SPL7-2* Protoplast**	**eGFP Expression (#)**	**Total Live Cells (#)**	**Efficiency (%)**
B1 – AtCOPT1:eGFP	100	129	78
B1 – eGFP	70	93	75
B2 – AtCOPT1:eGFP	85	115	74
B2 – eGFP	61	84	73
BS1 – AtCOPT1:eGFP	82	112	73
BS1 – eGFP	83	91	91
S3 – eGFP-TEV-COPT1	79	90	88

Table S2.2: Tabulated Counts of *SPL7-2* mutant Protoplast Transfection Efficiency
From Left to Right: Transfection batch with indicated plasmid construct; cell counts of live protoplasts with eGFP fluorescence; cell counts of live protoplasts; batch transfection efficiency as determined by the percent of live cells with eGFP fluorescence

CHAPTER 3: AN ALTERNATIVE TOOL FOR ELECTROCEMICAL STUDIES - ORGANIC ELECTROCHEMICAL TRANSISTORS

3.1 Introduction

Chapter 2 discussed the use of a PEDOT:PSS coated electrode with a supported lipid bilayer (SLB) as a device for measuring protein transport. This chapter serves as an addendum and introduces the use of an organic electrochemical transistor (OECT) in place of an electrode to enable the use of double potential step chronoamperometry as an additional method of electrochemical analysis. The following sections will elaborate on how an OECT SLB device can be used to detect transport through the *Arabidopsis thaliana* (*A. thaliana*) COPT1 copper transporter protein.

3.2 Results and Discussion

3.2.1 Chemical Induced Vesiculation of Protoplast Results in Blebs That Retain AtCOPT1 and AtCOPT2

COPT1 and COPT2 were chosen as our target transport proteins due to their plasma membrane localization and suspected non-electrogenic nature. To minimize the contribution of other copper transporters in our assay, experiments were conducted in an *A. thaliana* COPT1/2/6 knockout (KO). *A. thaliana COPT1/2/6 KO* plants do not functionally express the known high-affinity copper transporters AtCOPT1, AtCOPT2 and AtCOPT6. We selected these plants as the starting material to for our assays with the goal to have our introduced COPT protein as the predominant copper transporter in the protoplast membrane after transfection.[80] Mesophyll protoplasts were harvested from 14-day old plants and then transfected the same day. Protoplast were transiently transfected with a c-terminal eGFP-tagged COPT constructs (AtCOPT1:eGFP) or (AtCOPT2:eGFP) under a CaMV 35S constitutive promoter to maximize the expression of COPTs and monitor its synthesis and

localization. Protoplasts transfected with the empty vector eGFP construct or with water in a Mock transfection served as the controls. Protoplasts overexpressing AtCOPT1:eGFP or AtCOPT2:eGFP exhibited GFP fluorescence localized to the plasma membrane, in comparison to the eGFP control which localized primarily to the cytosol **[Fig. 3.1A].** The expression of full-length constructs was confirmed by GFP immunoblotting of harvested protoplasts following transfection. Bands can be seen at the predicted molecular weight of AtCOPT1:eGFP (~45 kDa), AtCOPT2:eGFP (~45 kDa), and eGFP alone (~27 kDa) on the GFP immunoblot **[Fig. 3.1B].** Interestingly, additional higher bands were present in AtCOPT1:eGFP and AtCOPT2:eGFP blots that seem to correspond to the molecular weights of the COPT multimer forms (~90 kDa and ~135 kDa). Protoplasts were then chemically

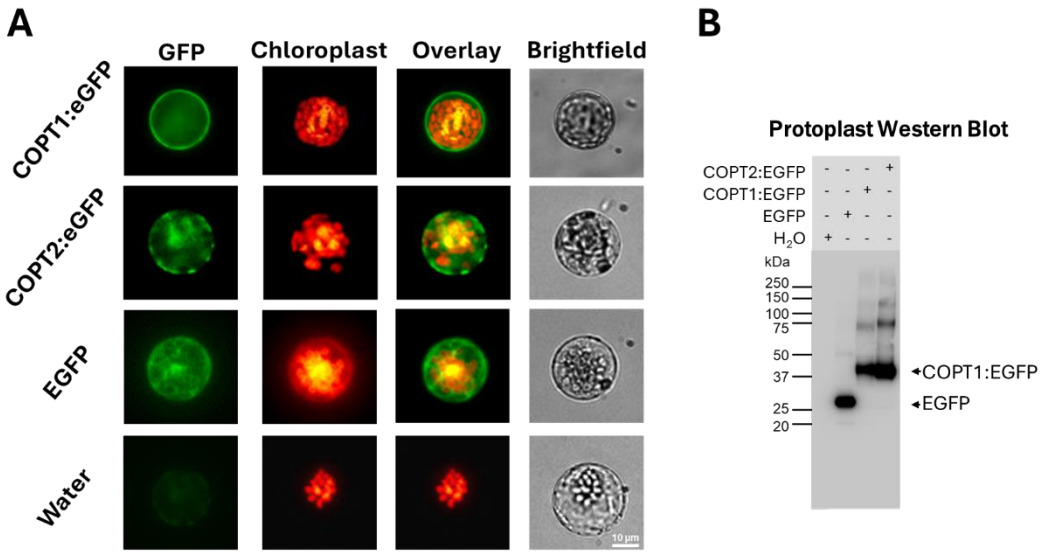

Figure 3.1: Confirmation of the synthesis and membrane localization of COPT1:eGFP & COPT2:eGFP in *COPT1/2/6 KO* protoplasts
(A) *Fluorescence images of* COPT1/2/6 KO A. thaliana *protoplast transfected with COPT1:eGFP (top), COPT2:eGFP (2nd), GFP encoding constructs (3rd) or Mock (bottom). From left to right appear the GFP channel (FITC), chlorophyll auto-fluorescence (LPFITC), merge image overlays and brightfield. Note that the COPT1:GFP fluorescence is localized primarily to the plasma membrane in contrast to the protoplast transfected with the empty vector (eGFP), which displays more cytosolic fluorescence.* ***(B)*** *Monoclonal Mouse anti-GFP IgG (Roche) immunoblots of protoplast samples following transfection. Lanes from left to right are: water Mock transfection, protoplasts transfected p-SAT6 empty vector EGFP (~27 kDa), p-SAT6 COPT1:eGFP (~45kDa), p-SAT6 COPT2:eGFP (~45kDa). Additional higher bands appear ~90kDa and ~135kDa that might indicate the presence of COPT1:eGFP & COPT2:eGFP dimer or trimer.*

induced to form blebs from the plasma membrane. Nanoparticle tracking analysis (NTA), and dynamic light scattering were used to characterize the bleb size distribution. Blebs isolated from COPT1/2/6 KO plants had an NTA measured diameter between ~100-200 nm and were within the expected size range for native blebs previously reported **[Fig. S3.1A].**[79] The Z-average size of COPT1/2/6 KO blebs measured by DLS ranged ~400-600nm and samples were highly polydisperse which may have influenced the accuracy of the reported Z-average diameter **[Fig. S3.1B].** The zetapotential of COPT1/2/6 KO blebs were negative and ranged between 10-20 mV **[Fig. S3.1C].** To determine if the COPT1:eGFP and COPT2:eGFP transporters were retained in the blebs, we first labeled the vesicle membranes with a membrane intercalating dye, octadecyl rhodamine B chloride (R18). The blebs were then adsorbed onto glass slides and imaged using confocal microscopy **[Fig. 3.2A].** Colocalized

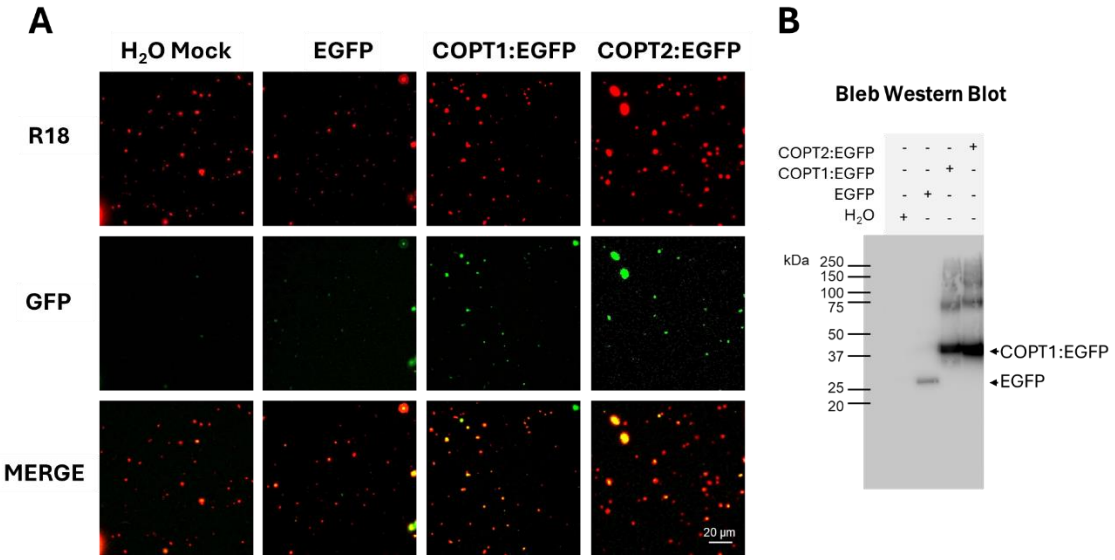

Figure 3.2: Confirmation of COPT1:eGFP & COPT2:eGFP retention in *COPT1/2/6 KO* blebs

(A) *Confocal images of blebs derived from transfected* COPT1/2/6 KO *protoplasts labeled with the intercalating membrane dye, R18. Transfection conditions are indicated along the top and filters/channels along the right side. R18 labeled SUVs appear in red, eGFP presence is indicated by green fluorescence, and colocalization of R18 and eGFP as yellow.* ***(B)*** *Monoclonal Mouse anti-GFP IgG (Roche) immunoblots of concentrated bleb samples. Lanes from left to right are: ladder, H_2O mock transfection, protoplasts transfected with p-SAT6 COPT1:eGFP (~45kDa), protoplasts transfected with empty vector p-SAT6 COPT2:eGFP (~45kDa) Additional higher bands appear ~90kDa and ~135kDa that might indicate the presence of COPT1:eGFP & COPT2:eGFP dimer or trimer.*

fluorescence of R18 and eGFP indicated that the COPT fusion constructs were still present in the vesicles. As an additional confirmation, isolated blebs were concentrated by ultra-centrifugation and immunoblotted for GFP. Bands found indicated that AtCOPT1:eGFP (~45 kDa) and AtCOPT2:eGFP (~45 kDa) were still present in the blebs **[Fig. 3.2B].**

3.2.2 Supported Lipid Bilayers Containing COPT Transporters Can Be Made Using *A. thaliana* Derived Membrane Vesicles

While there are many methods to form SLBs, for OECT devices we utilized a multi-step vesicle fusion method where cell blebs are induced to rupture on a support with fusiogenic liposomes **[Fig. 3.3].** The multi-step vesicle fusion method like the method described in Chapter 2 involves optimizing the surface properties of the substrate and fusiogenic liposomes, however additional steps and additives are added to account for the properties of the OECT **[Fig. S3.2].** To do this the charge and properties of the fusogenic liposome can be modified by changing the composite lipid composition[81] and treating the OECT surface with a polyelectrolyte. Fusogenic liposomes with a 1:1 molar ratio POPC:POPG (1-palmitoyl-2-

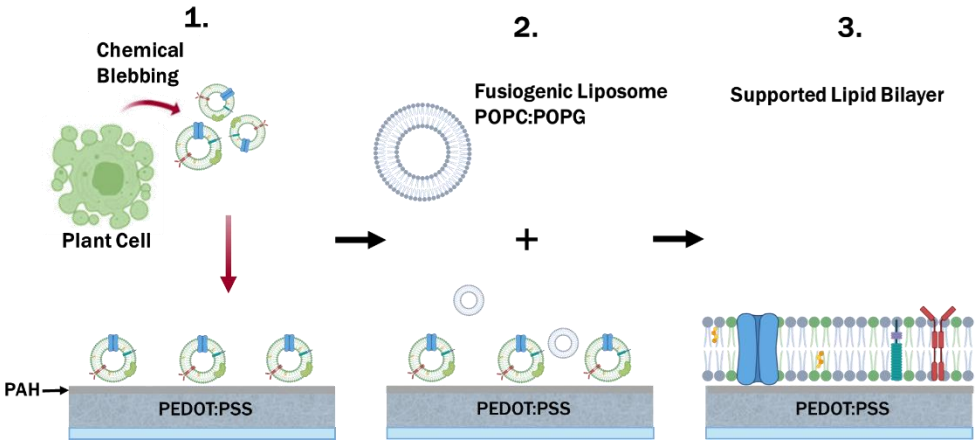

Figure 3.3: Cartoon representation of the multistep vesicle fusion process and the formation of a protoplast-derived SLB
(1) *PEDOT:PSS is plasma treated and coated with PAH before the addition of vesicles isolated via chemical induction of protoplast blebbing* ***(2)*** *1:1 molar POPC:POPG fusiogenic liposomes are added to adsorbed blebs on the support* ***(3)*** *Electrostatic and Van der Wals forces induce their rupture into a contiguous SLB.*
Figure created with BioRender

oleoyl-sn-glycero-3-phospho-(1′-rac-glycerol)) was used both due to their abundance in the native plant membrane and their compatibility with the OECT device.[82,83] To visualize and confirm the formation of the SLBs with our blebs we used fluorescence recovery after photobleaching (FRAP). By fitting the intensity recovery to a 2D diffusion equation we obtained diffusion coefficients for R18 in SLBs in the range from ~0.275-0.175 $\mu m^2/s$ and mobile fractions between ~90-100% **[Fig S3.3].**

3.2.3 AtCOPT1 activity measured with an OECT

To determine if proteins in SLB devices were functional we used double potential step chronoamperometry (voltage step analysis). As a starting point we focused on AtCOPT1 as it has been relatively more characterized than AtCOPT2. To accomplish this, PEDOT:PSS organic electrochemical transistors (OECT) devices were obtained from collaborators in Sweden. Briefly, voltage step analysis involves applying a constant current at the OECT source and measuring the drain current upon application of a voltage pulse **[Fig 3.4A].** For a more detailed explanation refer to section 2.4.17 in Materials and Methods. All OECT electrical experiments were conducted using blebs from COPT1/2/6 KO plants to minimize possible effects from endogenously expressed high affinity copper transporters.

Devices before SLB formation displayed a step like change in drain current with application of a voltage pulse **[Fig 3.4B].** The addition of the polyelectrolyte polyallylamine hydrochloride (PAH), resulted in minimal change in the response. SLBs formed from *COPT1/2/6 KO* background AtCOPT1:eGFP, eGFP, and Mock transfection blebs were formed on OECT devices and the response delay was tested. The formation of a SLB was appreciated as a delay in the drain current response that appears as a curve rather than a step. The degree of the time delay was used to assess SLB quality. Only the transistor on the device with the highest delay was selected for subsequent measurements. Bio-available copper is

most commonly found in the +2 oxidation state, but COPT1 is believed to be Cu(I) specific so a molar excess of Ascorbic Acid (100 µM) was added to the copper solutions to reduce Cu(II) to Cu(I) and maintain the +1 oxidation state.[14] Devices were then tested at a range of physiologically relevant Cu(I) concentration (0.01-50.0 µM) through subsequent additions of a concentrated copper sulfate solution. With the addition of Cu(I) there was a concentration dependent upward shift in the drain current response curve indicating a faster response and an increase in membrane permeability.

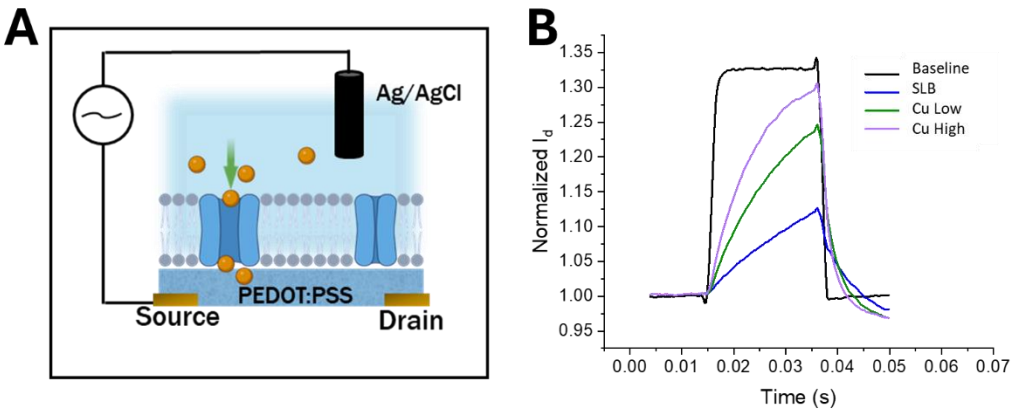

Figure 3.4: Voltage step measurements with OECT devices
(A) *Schematic of Plant-on-chip device set-up for Potential Step Chronoamperometry (voltage step) measurements. Ag/AgCl electrode is placed in the bulk electrolyte buffer. Source, drain and Ag/AgCl electrode are connected to the SMU (Keithley) device. PEDOT:PSS coated gold electrode serve as the working electrode (WE)* ***(B)*** *Representative drain current response of a single experiment with a COPT1:eGFP SLB device measured using Voltage Step analysis. Plain PEDOT device (black), SLB (blue), and Cu treatment at a low (green) and higher concentration (purple). The upward shift in the curve is indicative of a decrease in time delay as the transporter activates allowing ion flux. The length of the voltage pulse can be extended to capture the full length of the current delay*

Figure created with BioRender

In comparison to eGFP and Mock controls SLBs containing AtCOPT1:eGFP displayed faster response times which can be attributed to the activity of COPT1 **[Fig. 3.5].** There was not a significant difference in response between eGFP and Mock control devices, however while the average response of AtCOPT1:eGFP devices were higher than the controls it was also highly variable making it difficult to draw conclusions. As another test to confirm AtCOPT1 activity, an OECT device with an AtCOPT1 SLB was configured for Electrical

Impedance Spectroscopy measurements and used to test the response to increasing Cu(I) concentrations (0.01-50.0 µM). Results visibly indicated that the SLB associated resistance (Rm) decreased with increasing copper concentration as expected **[Fig S3.4].** Though generally used to model enzyme kinetics, Michaelis-Menten can be used to model transport proteins provided that they display concentration dependent and saturable response with single-file transport.[56] To characterize the Cu(I) response we modeled the inverse normalized response time with a typical Michaelis-Menten to obtain an apparent affinity. This affinity is the combined contribution of the expressed AtCOPT1:eGFP protein, any additional transporters as well as the effects of the Cu-membrane interactions. To see if it was still possible to extract kinetic information, we used Michaelis-Menten to model the response of

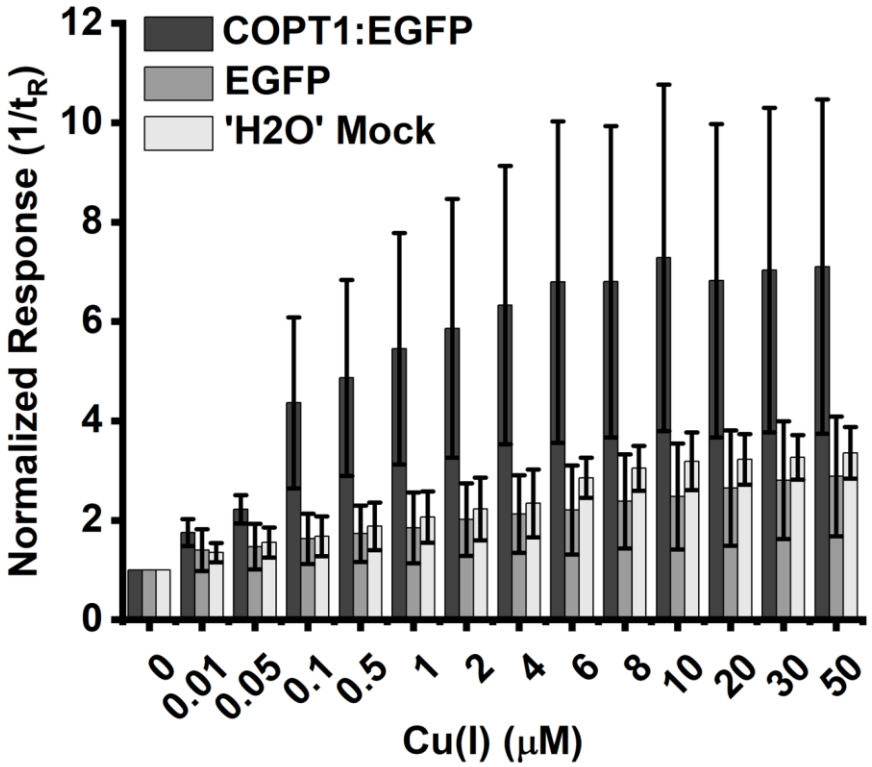

Figure 3.5: OECT Electrical measurements of *COPT1/2/6 KO* Supported lipid bilayers ***(A)*** *Normalized inverse responses from voltage step analysis measurements of COPT1:eGFP, Mock transfection, and empty vector eGFP SLBs at Cu concentrations from 0.01 to 50.0 µM in presence of 100 µM of Ascorbic Acid. The error bars represent the standard error of (Mock, eGFP; n = 3, COPT1:eGFP; n = 7) technical replicates*

the experimental run with the highest response. Calculated kinetic values for the AtCOPT1:eGFP OECT were Km = 0.182 ± 0.053 μM and Vmax = 16.41 ±0.61 with a coefficient of determination of R-square = 0.925 **[Fig. S3.5].** Attempts to fit the mean response of AtCOPT1:eGFP OECT devices resulted in a poor quality fit. The affinity determined with the electrode and EIS in Chapter 2 for an AtCOPT1:eGFP bilayer was Km= 0.357 μM which is within the same order of magnitude as the Km measured by this method. The difference in values could be attributed to inherent variations measurement modalities, sensitivity and statistical power.

The limitations of these experiments could be attributed to a variety of factors namely 1) variability in AtCOPT1:eGFP content between experiments 2) background signal from other transporters present 3) variability in initial SLB quality. To address the challenge of transporter content in experiments one approach used in Chapter 2 was the shift in protoplast transfection size from 10^6 cells to smaller batches ~2-2.5 x 10^5 cells which provided consistently higher transfection efficiencies. Another optimization of the experiment was the shift in plant lines from the *COPT1/2/6 KO* to a *spl7-2 mutant* which lacks the functional SPL7 copper deficiency response transcription factor. The absence of SPL7 should reduce the expression of a wider range of copper transporting proteins rather than just the COPT1/2/6 in the knockout. The switch to EIS for electrical measurements provided a faster and simpler method for determining SLB quality by simply measuring the SLB associated resistance in program and setting an optimal resistance range. This is opposed to voltage step analysis which would require a more in-depth fitting of the drain current response curve by exporting into a separate program or by first determining the SLB quality using EIS before proceeding to voltage step experiments.[53]

3.3 MATERIALS AND METHODS

3.3.1 Materials

1-Palmitoyl-2-oleoyl-glycero-3-phosphocholine (16:0–18:1 PC, POPC), 1-palmitoyl-2-oleoyl-sn-glycero-3-phospho-(1′-rac-glycerol) (sodium salt) (POPG) used for the preparation of fusiogenic liposomes was obtained from Avanti Polar Lipids (700 Industrial Park Dr, Alabaster, AL 35007). Whatman Nucleopore polycarbonate filters (100 nm) (Cytiva-Marlborough, MA) were used for liposome extrusion. The octadecyl rhodamine B chloride (R18) used in optical experiments was obtained from Thermo Fisher Scientific (Waltham, MA). Microscope coverslips (VWR 25 mm × 25 mm glass) were prepared for use by Piranha wash using sulfuric acid (95- 98%, VWR) and hydrogen peroxide (50 wt.% solution, Krackler Scientific). 4-(2-Hydroxyethyl)piperazine-1-ethanesulfonic acid (HEPES), dithiothreitol (DTT), formaldehyde solution, and Calcium Chloride dihydrate were all purchased from Millipore Sigma. PEDOT:PSS (PH 1000) was purchased from Heraeus Clevios GmbH depending on availability. 4-Dodecylbenzenesulfonic acid (DBSA), (3-glycidyloxypropyl) trimethoxysilane (GOPS), ethylene glycol (EG), polyallylamine hydrochloride (PAH), Polyetheylene Glycol 8k and MES Sodium salt were purchased from Sigma-Aldrich (St. Louis, MO, USA). Potassium Chloride (KCl) was purchased from MP Biomedicals (Solon, OH). MES was purchased from Calbiochem. L(+)-Ascorbic Acid (AA) was purchased from EMD Chemicals. Sodium Citrate dihydrate was purchased from Fisher Scientific. Tween-20 was purchased from Sigma. PDMS was prepared from a 10:1

For western blots Monoclonal Mouse anti-GFP IgG from Roche and Goat anti-Mouse IgG H+L IgG HRP was purchased from Abcam.

For plant culture, enzyme digestion and transfection Murashige and Skoog (MS) medium and Polyethylene Glycol 4000 (PEG-4000) was purchased from Sigma-Aldrich (M5519). D-

Sorbitol, D-Mannitol, Sucrose, Pure bright bleach, and Magnesium Chloride anhydrous were purchased from VWR. Cellulase Onozaka R-10 and Macerozyme R-10 were both purchased from Research Products International (RPI).

ImageJ 1.53 A and Fiji (NIH), AxioVision rel. 4.8, Zen 3.4 were used to acquire and analyze optical data. Origin 2024 was used to plot data found in the main and supporting figures. All plasmid sequences were confirmed by full length Nanopore plasmid sequencing through Plasmidasaurus or Eurofin Genomics.

Buffers and other solutions:

GPMVM Buffer: (500 mM Mannitol, 150 mM NaCl, 2 mM $CaCl_2$, 10 mM HEPES pH 5.6)

Blebbing Buffer: (2 mM DTT (2 uL/mL), 25 mM Formaldehyde (2.25 uL/mL) GPMVM pH5.6)

W5 medium: (0.1% glucose, 0.08% KCl, 0.9% NaCl, 1.84% $CaCl_2$ $2H_2O$, 2 mM MES-KOH pH 5.7)

TVL: (0.3 M Sorbitol, 50 mM $CaCl_2$, sterilize with 0.45-µm filter)

Enzyme Solution: (0.5 M Sucrose, 20 mM $CaCl_2$, 40 mM KCl, 20 mM MES-KOH pH 5.7, 1w/v% Cellulase, 1w/v% Macerozyme sterilized with 0.45-µm filter)

Bleach Sterilization Solution: (30% bleach, 70% sterile Di H_2O and 0.1% Tween-20)

MMG: (0.4 M mannitol, 15 mM $MgCl_2$, 4 mM MES-KOH pH 5.7)

PEG-Calcium Transfection Solution: (40% PEG-4000, 0.2 M mannitol, 100 mM $CaCl_2$)

D3 buffer (NaCl 0.09 g, MgCl 0.102 g, $CaCl_2$ 0.02 g, MES 1.09 g, H_2O 100mL pH6.0)

3.3.2 Plasmid Generation

Plasmids were amplified as described in **Chapter 2 Section 2.5.3**

3.3.3 Isolation of Protoplast, Transfection and Blebbing

Protoplast were isolated from 14-day old *A. Thaliana COPT1/2/6 KO* seedlings and ~10^6 cells

were transfected with either a Mock water transfection, AtCOPT1:eGFP, AtCOPT2:eGFP or empty vector eGFP pSAT6 plasmids under a CaMV 35S promoter as described in the Methods section of **Chapter 2 Sections 2.5.4 and 2.5.5**. Similarly, blebs were also produced as described in **Section 2.5.6**

3.3.4 Protoplast and Bleb Western Blot

Protoplast were pelleted and lysed by physical agitation before addition of a western blot mix (Bolt Blue LDS and Bolt Reducing Agent Buffer at final concentration 1x and 5%w/v SDS). Blots were then stained with Ponceau S and imaged Chemidoc (Bio-Rad) to assess transfer and serve as a loading control. The blot was then blocked with milk (5% milk powder in TBST buffer) before immunoblotting with 1:4000 Mouse anti-GFP (Roche) overnight at 4 °C and 1:4000 Goat anti-mouse (Abcam) for 1 hr at room temperature. Blots for blebs were similarly prepared but blebs were first concentrated by ultracentrifugation at 28,000 rpm for at least 4 hrs. Blots were imaged for GFP with a Chemidoc (Bio-Rad) after staining with an ECL kit (Clarity) and analyzed using Image Lab software (Bio-Rad).

3.3.5 Glass and PEDOT slide Preparation

Clean glass slides were prepared by Piranha wash as described in **Chapter 2 Section 2.5.8**. To make the PEDOT:PSS solution PEDOT:PSS (Clevios PH 1000) was filtered through a 0.45 µm syringe filter and then combined with ~1% (3-glycidyloxypropyl) trimethyoxysilane, 5% Ethylene Glycol, and ~0.33% Dodecylbenzenesulphonic acid in a scintillation vial. The solution was then sonicated for 30 mins in a chilled bath sonicator (ultrasonic cleaner, VWR) and passed once through a 0.45 µm syringe filter. Clean glass slides were prepared for spin coating via oxygen plasma cleaning at 29.6 W and 700 mm pressure for 2 mins (Harrick Plasma, Ithaca, NY). Three drops of PEDOT:PSS solution were then applied to each slide and spin coated (Apogee Spin coater, Cost Effective Equipment) at 2800 rpm for 30 s. The coated slides were then baked at 140 °C for 1 hr and immersed in deionized water overnight. Before

use slides were rinsed with deionized water and dried with nitrogen gas.

3.3.6 Fusiogenic Liposome Preparation

Fusiogenic liposomes were formed using thin-film hydration and extrusion with a suspension of phospholipids in chloroform. Chloroform solutions were prepared with the desired molar ratio of POPC and POPG. The chloroform was evaporated using nitrogen gas to form a lipid thin film and was placed under vacuum for a minimum of 4 hr to remove trace solvent. The lipids were then rehydrated with Tris-HCl KCl or GPMVM pH 5.6 buffer to a concentration of 2 mg/mL. The rehydrated suspension was then vortexed, and water bath sonicated for 15 mins before extruding at least 10 times through a 100 nm Nucleopore polycarbonate filters using an Avanti Extruder (Avanti Polar Lipids, Birmingham, AL).

3.3.7 Liposome and Bleb Characterization

The size distribution of liposomes and blebs were measured with nanoparticle tracking analysis (NTA) on a Malvern NS300 Nanosight (Malvern Instruments) and dynamic light scattering Zetasizer Nano-ZS instrument (Malvern Instruments) as described in **Chapter 2 Section 2.5.11**. Zetapotential of blebs diluted in GPMVM buffer were determined using the Zetapotential function of a Zetasizer Nano-ZS in a DTS1070 Folded Capillary Zeta Cell (Malvern Panalytical).

3.3.8 Plant Bleb Confocal Microscopy

Isolated blebs were optically confirmed to retain transfected constructs using confocal microscopy as described in **Chapter 2 Section 2.3.12**.

3.3.9 Multi-step Supported Lipid Bilayer Formation

The multi-step vesicle fusion method is optimized for the surface properties of the Swiss OECT devices. Each device contains six PEDOT:PSS transistors with areas of 10 or 100 μm^2. In the multistep process, PEDOT:PSS slides and OECT devices are first oxygen plasma treated at 29.6 W and 700 mm pressure for 2 mins. This plasma treatment step provides the

needed electrostatic properties to the substrate that allow for vesicle fusion. The plasma conditions must be tuned for each plasma cleaner and surface to obtain the proper electrostatic conditions for SLB self-assembly. Following plasma treatment, the well surface is coated with a layer of positively charged polyelectrolyte by 10 min incubation with 100 µL of poly(allylamine hydrochloride) (PAH) solution (~2.3 mg/mL in 0.5M NaCl) before rinsing with D3 buffer. This positive polyelectrolyte layer helps to minimize the negative charge of PEDOT:PSS and interacts electrostatically with the negatively charged native membrane blebs to improve rupture. For plant membrane blebs PAH performs the best but other vesicles have been ruptured using poly-L-lysine (PLL). Bleb can then be spun down at 2000 RCF and 50-100ul is added to the well and allowed to incubate for 10 mins before rinsing off any un-adsorbed blebs with D3 Buffer. To induce the rupture of the blebs 75-100 uLs of POPC:POPG (1:1 molar) fusiogenic liposomes were added and incubated in the well for at least 1 hr before rinsing with D3 buffer. PEG 8k (1 w/v %) was added for electrode and transistor devices to improve the rupture of blebs through induced osmotic shock. After 10 mins the device well was washed with D3 buffer and ready for use.

3.3.10 Fluorescence Recovery after Photobleach (FRAP)

To obtain fluorescently labeled supported lipid bilayers for FRAP, blebs were labeled with with 3 µL of R18 (0.36 mM) lipophilic dye per 100 µL of bleb solution and sonicated for 10 mins (kept under 25 °C with ice pad). SLBs were then formed with POPC:POPG liposomes using the labeled blebs on PEDOT:PSS coated slides as earlier described. The procedure for FRAP was then continued as described in **Chapter 2 Section 2.5.14**.

3.3.11 Organic Electrochemical Transistor Voltage Pulse

All measurements of OECT voltage step were conducted in 0.1x D3 buffer with a set up composed of a Source Measurement Unit (Keithley 2612B SourceMeter) connected to the

device source and drain electrode with an Ag/AgCl gate electrode. Supported Lipid bilayers were formed on OECTs with the multistep method and double potential step chronoamperometry was used to detect the activity of AtCOPT1:eGFP by applying a step voltage to OECT devices. The length of the voltage pulse was selected such as to allow for the extension of the drain current response. A baseline current was maintained at the source electrode and the current recorded at the drain as a +0.2 V pulse was applied at the gate electrode. The drain current response changes as the degree of doping of PEDOT:PSS transistor changes. On a bare device drain current response closely follows the applied voltage and appears stepped. Upon formation of a SLB the flux of ions to the PEDOT:PSS transistor is attenuated resulting in a delay in the current response **[Fig. S2.11C].** The current response can be fit using an exponential model of the form:

$$\boldsymbol{y = y_0 + A \cdot \exp(R_0 x)} \qquad \textbf{(4)}$$

where y is the current, x is the pulse time, R_0 is the OECT time constant τ and the response time, t, is given by -1/τ.[63] When a pore is formed in an SLB such as during the activation of a transporter protein there is a small increase in ion flux that causes a change in the doping state of the PEDOT:PSS. This change results in an increase in the drain current response time as compared to the of the SLB in the initial inactive transporter state. SLBs formed from COPT1:eGFP, eGFP, and H_2O mock blebs were exposed to increasing concentrations of Cu(I) as described, and measurements were taken after each addition following a 6 min equilibration. To compare devices, the response times following Cu(I) treatment were normalized to the SLB initial response times. Km and Vmax OECT values were obtained by modeling the inverse normalized device response time with a Michaelis-Menten model in Origin Lab.[56]

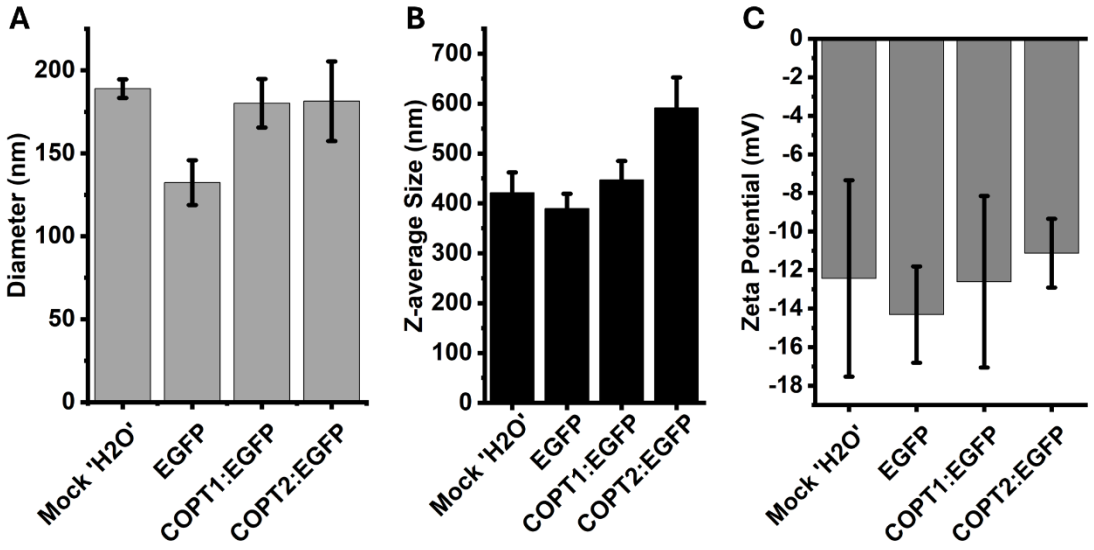

Figure S3.1: NTA and DLS Size and Zetapotential Measurements of *COPT1/2/6 KO* Blebs

(A) *Mean particle diameter as measured by Nanoparticle tracking analysis (NTA) of blebs derived from Mock transfection, empty vector eGFP, COPT1:eGFP COPT2:eGFP transfected protoplast. (n=5 measurements)* ***(B)*** *Bleb Z-average particle size as measured by dynamic light scattering (DLS) for Mock transfection, empty vector eGFP, COPT1:eGFP COPT2:eGFP blebs. (n=15 technical replicates)* ***(C)*** *Zetapotential measurements of isolated blebs. (n=3 technical replicates). All measurements were conducted in GPMVM pH5.6 buffer. Error bars represent the standard error of technical replicates*

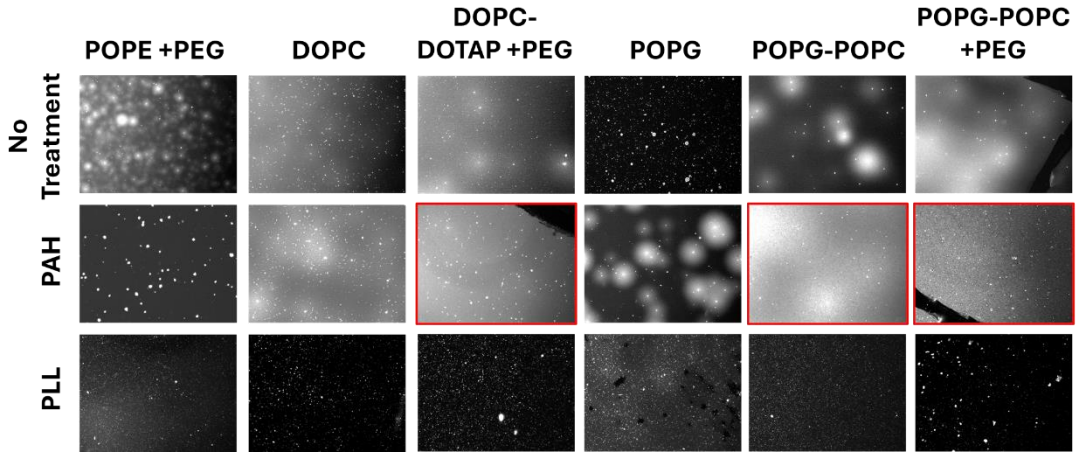

Figure S3.2: Optimization of Vesicle Fusion on PEDOT:PSS
Fluorescence images of R18 labeled wild-type A. thaliana *blebs ruptured on PEDOT;PSS coated glass slides with the multistep approach. Left indicates pretreatments applied to the PEDOT:PSS substrate (no treatment, PAH, PLL). Top indicates fusiogenic liposome compositions. (95:5 POPE:DSPE PEG5k, DOPC, 47.5:47.5:5 DOPC:DOPTAP: DSPE PEG5k, POPG, 1:1 POPG:POPC, 47.5:47.5:5 POPG:POPC: DSPE PEG5k) Promising combinations are highlighted in red.*

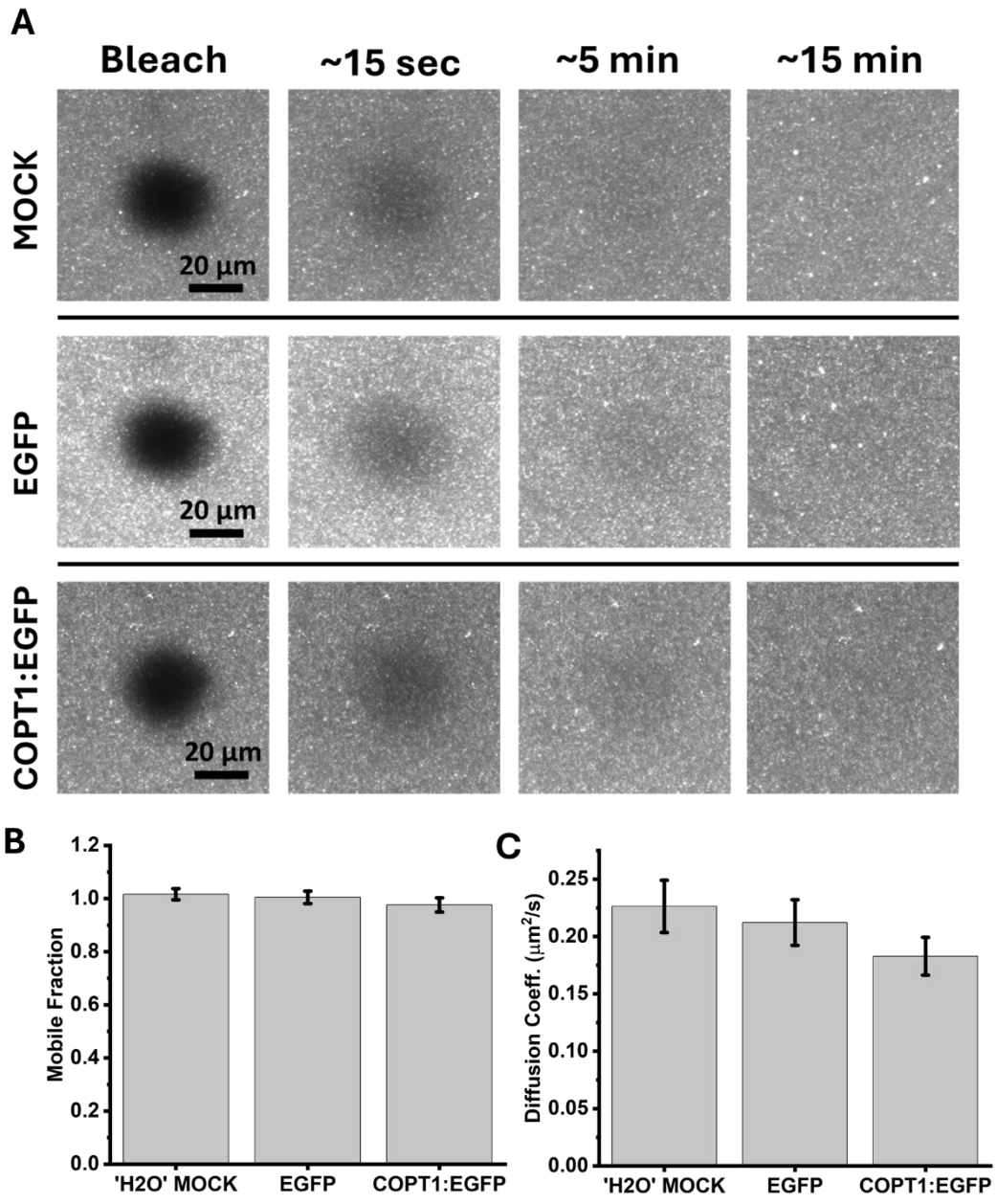

Figure S3.3: SLB formation and Fluorescence Recovery after Photobleach with *COPT1/2/6 KO* blebs

(A) *Fluorescence Recovery after Photobleach representative images of R18 labeled* COPT1/2/6 KO *bleb SLBs at approximately 15 seconds, 5 minutes and 15 minutes after photobleaching with a 561nm laser. From top to bottom: SLBs formed using H_2O Mock, empty vector eGFP, and COPT1:eGFP. SLB formation is indicated by the full recovery of bleach spot fluorescence* ***(B)*** *Mobile Fraction (MF) of R18 in H_2O Mock, empty vector eGFP, and COPT1:eGFP SLBs* ***(C)*** *R18 diffusivities of H_2O Mock, eGFP, and COPT1:eGFP SLBs.The error bars represent the standard error measurements of three technical replicates (n = 3)*

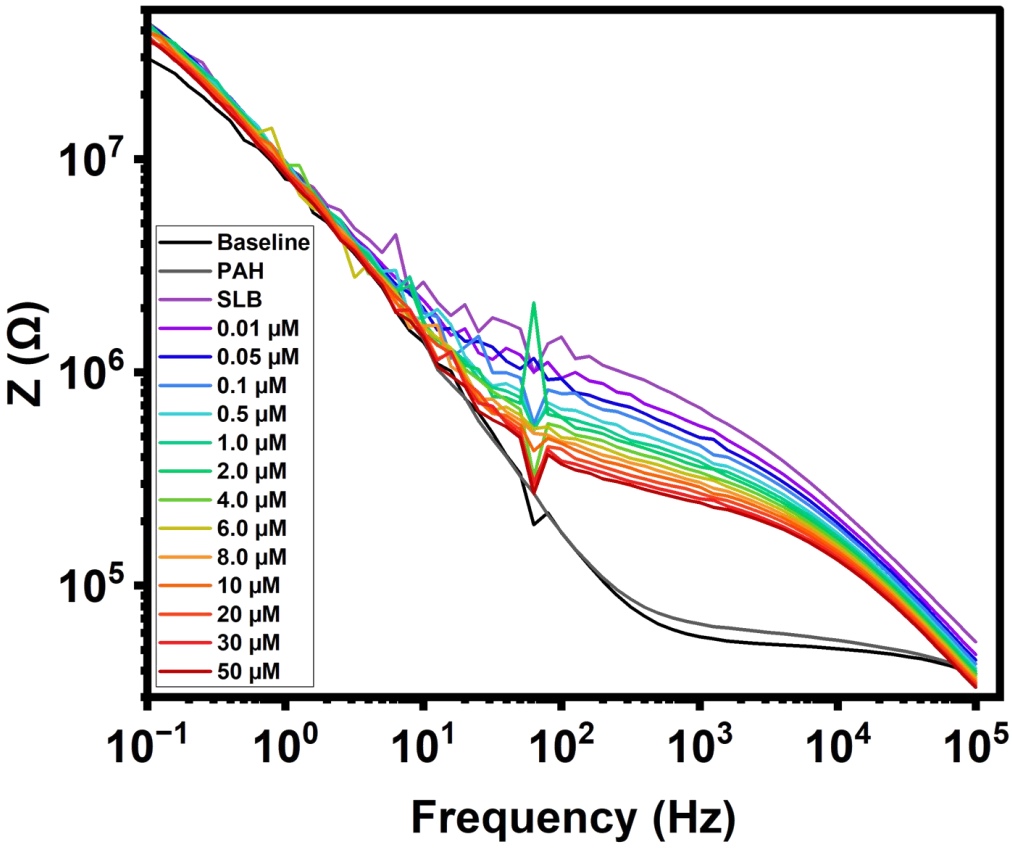

Figure S3.4: OECT EIS Measurement of *COPT1/2/6 KO* AtCOPT1:eGFP SLB
(A) *Representative Bode impedance profile of a single experiment with a AtCOPT1:eGFP SLB device measured using EIS first with plain OECT device (black), OECT treated with PAH (grey), AtCOPT1 SLB (violet), and Cu treatment from 0.01 µM (purple) to 50 µM (red). The drop in impedance is visible as the concentration of Cu increases corresponding to a shift in color from purple to red and indicating copper transport.*

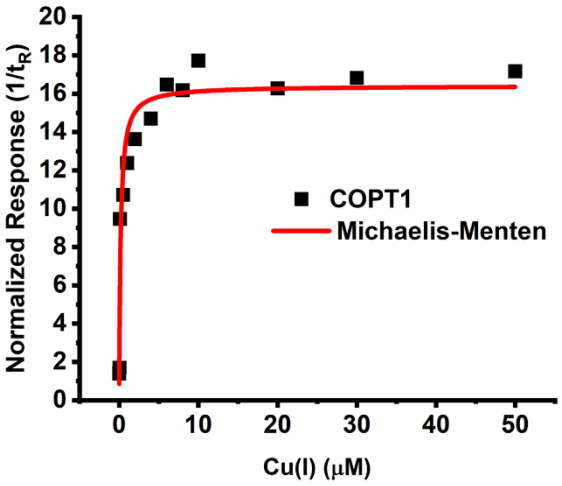

Model	MichaelisMenten
Equation	y = Vmax * x / (Km + x)
Plot	COPT1
Vmax	16.4121 ± 0.60798
Km	0.18192 ± 0.05259
Reduced Chi-Sqr	2.52319
R-Square (COD)	0.92486
Adj. R-Square	0.91803

Figure S3.5: Michaelis-Menten Fit for OECT Device Voltage Step
Michaelis-Menten fitting of the normalized inverse response of the COPT1/2/6 KO *AtCOPT1:eGFP OECT device with the highest response.*

CHAPTER 4: CONCLUSION AND FUTURE OUTLOOK

4.1 Conclusion

Transport proteins are key structures that play crucial roles in the biological compartments that allow for life. Their presence not only allows for the maintenance of the delicate balance of ions required in organisms, but also the support the critical role biological membranes play in providing unique chemical environments for biological reactions and signal transduction. Indeed, transporters have evolved to become efficient conveyors of ions and molecules. The chemical variations of pore structures, as well as selective moieties lining the pore, make it possible for transporters to discriminate between the vast number of possible ions and molecules present in biological systems. The highly tuned selectivity of transporters, however, also makes them vulnerable to mutations, which can limit function and result in disease and dysfunction on the organism level. This makes transporters a critical target for scientific inquiry; however, efforts to elucidate their molecule targets, specificity, and overall activity have been stifled particularly in plants by limited accessibility, imperfect exogenic models, and a lack of direct tools for measuring function.

The challenge of accessibility to plasma membrane transport proteins, in plants, has been largely addressed through the use of protoplasting techniques which eliminate the physical barrier of the plant cell wall. However, transport proteins are also ubiquitous in many of the membranes inside organisms and achieving access to these organelle membranes remains a challenge. Frequently, transport proteins are expressed exogenously into the plasma membrane of other organisms, however this comes with the caveat of removing the native membrane milieu with the possibility then of disrupting function and/or activity of the transporters. To characterize the function of the transporters, analytes are generally measured indirectly with uptake assays or through technically challenging patch-clamping methods.

While patch-clamping has been a great tool in measuring ion channels, proteins that are not sufficiently electrogenic and transporters have proven to be difficult or impossible to measure due to their slower transport. This means a vast number of biologically crucial transporting proteins cannot be measured directly. Despite their limitations, these techniques have collectively provided much of our initial understanding of transport proteins and the ways they function. Still, the multitude of challenges with current methodologies motivates the need for new approaches to answer the burgeoning questions in plant transport.

The design of a Plant membrane-on-Chip platform draws from the collective knowledge gained from prior works to develop a system which can provide *in vitro* and more facile means of directly measuring transporter function. Harnessing the capabilities of supported lipid bilayers (SLB) we can form biomimetic membranes using plasma native membrane material that naturally express transporters and recapitulate many of the properties of the native environments. This allows us to avoid many of the adverse effects of exogenous expression while also providing a more controlled environment for the interrogation of interactions and functions without the added complexity of *in vivo* methods. Additionally, we present how the incorporation of the native membrane SLB with biocompatible conductive surfaces allows us direct measurement of a plant copper transporter activity using traditional electrophysiological techniques.

The benefit to EIS and OECT potential step chronoamperometry is that they measure transporter function through the detection of impedance changes under analyte flux. This allows us to detect the function of slower transporters or electroneutral transporters that is nearly impossible with traditional patch-clamp. In summary, the work presented here represents the first steps towards a new era of flexible biomimetic devices that are amenable to directly characterizing a range of transporting proteins never before possible. For the plant domain, these advances open exciting possibilities to study transporter at the molecular scale

that has not been accessible to date but growing in importance as pressures mount for plants to respond to environment and climate stresses.

4.2 Future Directions

While the Plant Membrane-on-Chip platform can provide a needed tool for the study of plant transport proteins there are also a few outstanding challenges. We demonstrate here the use of a mesophyll plasma membrane SLB device, but the accessibility of internal membrane-localized proteins remains a challenge. Despite this, the future remains bright as through the development of organelle isolation and fractionation techniques, it may be possible to form organelle-derived SLBs. Access to the internal membranes, especially the tonoplasts and chloroplast membranes, would allow for the study of numerous other transport proteins. Some notable targets are AtCOPT5[4] and the AtPHT[96] and AtHMA[7] family of transporters that are proposed to be involved in organelle copper trafficking **[Fig. 1.1].** Due to the unique composition of organelle membranes, it may be necessary to design vesicle fusion strategies that may incorporate the use of different fusogenic liposomes, surface treatments and buffers. Crucially, it has been shown that SLBs can be formed from a wide range of organisms, plant species, tissues and preliminary work has shown SLB formation to be compatible with various buffers **[Fig 4.1].**[48,79,97]

One technical challenge is achieving the needed expression level of the transporter of interest in plants. Low protoplast transfection efficiencies of proteins can be a major bottleneck as proteins must first be expressed in planta, carried over during blebbing and finally incorporated in the SLB at a level high enough for electrical detection. Each of these steps lowers the available protein present, necessitating a high transfection rate. Incorporation of flow cytometry following transfections could largely eliminate this concern by providing a high throughput means to separate protoplasts expressing the protein of interest and

selectively blebbing them.

Though the Plant Membrane-on-chip platform is an *in-vitro* system it can also carry some of the challenges of *in-vivo* systems. As SLB largely recapitulates the native orientation of proteins the Plant membrane-on-Chip platform is currently limited to the measurement of influx carriers due to the geometry where ligands can only be added to the buffer above the SLB. The development of a SLB on a porous support would allow access to the luminal space and subsequently enable the measurement of efflux transporters. As another challenge, the nature of the native SLB system can act as a 'double-edged sword'. It is possible to recapitulate protein interactions, but care must be taken in selecting the appropriate cell background when attempting to isolate specific behaviors. In this work, we investigated the Cu oxidation state specificity of COPT mediated transport, however the likely presence of metalloreductases proved to be a confounding factor. To address this with our current system it would be ideal if we could obtain a plant line lacking expression of Cu plasma membrane metalloreductases such as FRO4/5 that also have minimal expression of copper transporters but the generation of such a line could prove difficult.[27] As an alternative, adding compounds that halt these enzyme's activity could be an alternative to developing a knockout. Further, the

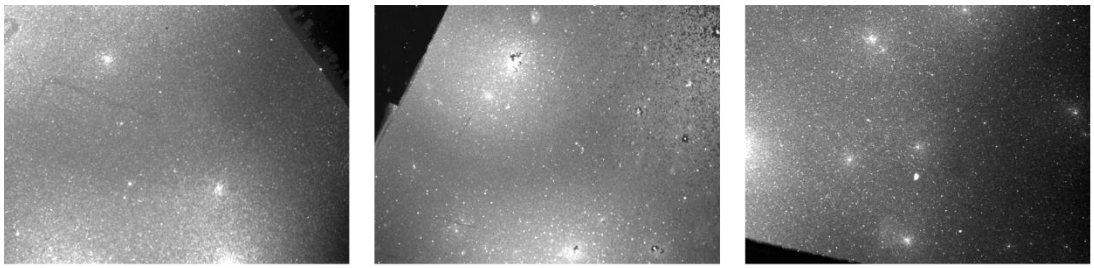

Figure 4.1: Root tissue derived *A. thaliana* Supported Lipid bilayers formed in various buffers.
Fluorescence images of R18 labeled supported lipid bilayers (SLBs) formed from derived A. thaliana root protoplast blebs with the multistep vesical fusion approach on PEDOT:PSS coated glass slides. SLBs were formed with 1:1 molar POPC:POPG fusiogenic liposomes on PAH treated PEDOT:PSS followed by addition of PEG8k. LEFT: D3 buffer, CENTER: PBS buffer. RIGHT: GPMV buffer with 5 mM magnesium chloride

use of a native SLB in combination with a cell-free expression or reconstituted protein SLB approach would allow one to design exactly what is present in the bilayer and allow experiments that could provide insight on protein behavior in their native environment and alone. While these approaches offer significant benefit, it also highlights that with biological systems there is no ‘one size fits all’ approach and to fully understanding the function and behavior of transporter proteins there will be a need for continued innovation.

REFERENCES

(1) Burkhead, J. L.; Gogolin Reynolds, K. A.; Abdel-Ghany, S. E.; Cohu, C. M.; Pilon, M. Copper Homeostasis. *New Phytologist* **2009**, *182* (4), 799–816. https://doi.org/10.1111/J.1469-8137.2009.02846.X.

(2) Ravet, K.; Pilon, M. Copper and Iron Homeostasis in Plants: The Challenges of Oxidative Stress. *Antioxid Redox Signal* **2013**, *19* (9), 919–932. https://doi.org/10.1089/ARS.2012.5084.

(3) Garcia-Molina, A.; Andrés-Colás, N.; Perea-García, A.; Neumann, U.; Dodani, S. C.; Huijser, P.; Peñarrubia, L.; Puig, S. The Arabidopsis COPT6 Transport Protein Functions in Copper Distribution under Copper-Deficient Conditions. *Plant Cell Physiol* **2013**, *54* (8), 1378–1390. https://doi.org/10.1093/PCP/PCT088.

(4) Ishka, M. R.; Chia, J. C.; Vatamaniuk, O. K. Advances in Understanding of Copper Function and Transport in Plants. In *Cation Transporters in Plants*; Elsevier, 2021; pp 205–226. https://doi.org/10.1016/B978-0-323-85790-1.00021-X.

(5) Andrés-Colás, N.; Perea-García, A.; Puig, S.; Peñarrubia, L. Deregulated Copper Transport Affects Arabidopsis Development Especially in the Absence of Environmental Cycles. *Plant Physiol* **2010**, *153* (1), 170–184. https://doi.org/10.1104/pp.110.153676.

(6) Seigneurin-Berny, D.; Gravot, A.; Auroy, P.; Mazard, C.; Kraut, A.; Finazzi, G.; Grunwald, D.; Rappaport, F.; Vavasseur, A.; Joyard, J.; Richaud, P.; Rolland, N. HMA1, a New Cu-ATPase of the Chloro Plast Envelope, Is Essential for Growth under Adverse Light Conditions*. *Journal of Biological Chemistry* **2006**, *281* (5), 2882–2892. https://doi.org/https://doi.org/10.1074/jbc.M508333200.

(7) Li, D.; Xu, X.; Hu, X.; Liu, Q.; Wang, Z.; Zhang, H.; Wang, H.; Wei, M.; Wang, H.; Liu, H.; Li, C. Genome-Wide Analysis and Heavy Metal-Induced Expression Profiling of the HMA Gene Family in Populus Trichocarpa. *Front Plant Sci* **2015**, *6*. https://doi.org/10.3389/fpls.2015.01149.

(8) Sancenón, V.; Puig, S.; Mira, H.; Thiele, D. J.; Peñarrubia, L. Identification of a Copper Transporter Family in Arabidopsis Thaliana. *Plant Mol Biol* **2003**, *51* (4), 577–587. https://doi.org/10.1023/A:1022345507112.

(9) Jung, H. Il; Gayomba, S. R.; Rutzke, M. A.; Craft, E.; Kochian, L. V.; Vatamaniuk, O. K. COPT6 Is a Plasma Membrane Transporter That Functions in Copper Homeostasis in Arabidopsis and Is a Novel Target of SQUAMOSA Promoter-Binding Protein-like 7. *Journal of Biological Chemistry* **2012**, *287*

(40), 33252–33267. https://doi.org/10.1074/JBC.M112.397810.

(10) Puig, S. Function and Regulation of the Plant COPT Family of High-Affinity Copper Transport Proteins. *Advances in Botany* **2014**, *2014*, 1–9. https://doi.org/10.1155/2014/476917.

(11) Sancenón, V.; Puig, S.; Mateu-Andrés, I.; Dorcey, E.; Thiele, D. J.; Peñarrubia, L. The Arabidopsis Copper Transporter COPT1 Functions in Root Elongation and Pollen Development. *Journal of Biological Chemistry* **2004**, *279* (15), 15348–15355. https://doi.org/10.1074/JBC.M313321200.

(12) Garcia-Molina, A.; Andrés-Colás, N.; Perea-García, A.; Del Valle-Tascõn, S.; Peñarrubia, L.; Puig, S. The Intracellular Arabidopsis COPT5 Transport Protein Is Required for Photosynthetic Electron Transport under Severe Copper Deficiency. *Plant Journal* **2011**, *65* (6), 848–860. https://doi.org/10.1111/j.1365-313X.2010.04472.x.

(13) Klaumann, S.; Nickolaus, S. D.; Fürst, S. H.; Starck, S.; Schneider, S.; Ekkehard Neuhaus, H.; Trentmann, O. The Tonoplast Copper Transporter COPT5 Acts as an Exporter and Is Required for Interorgan Allocation of Copper in Arabidopsis Thaliana. *New Phytologist* **2011**, *192* (2), 393–404. https://doi.org/10.1111/j.1469-8137.2011.03798.x.

(14) Lee, J.; Peña, M. M. O.; Nose, Y.; Thiele, D. J. Biochemical Characterization of the Human Copper Transporter Ctr1. *Journal of Biological Chemistry* **2002**, *277* (6), 4380–4387. https://doi.org/10.1074/JBC.M104728200.

(15) Eisses, J. F.; Kaplan, J. H. The Mechanism of Copper Uptake Mediated by Human CTR1: A Mutational Analysis. *Journal of Biological Chemistry* **2005**, *280* (44), 37159–37168. https://doi.org/10.1074/JBC.M508822200.

(16) Rees, E. M.; Lee, J.; Thiele, D. J. Mobilization of Intracellular Copper Stores by the Ctr2 Vacuolar Copper Transporter. *Journal of Biological Chemistry* **2004**, *279* (52), 54221–54229. https://doi.org/10.1074/JBC.M411669200.

(17) Sanz, A.; Pike, S.; Khan, M. A.; Carrió-Seguí, À.; Mendoza-Cózatl, D. G.; Peñarrubia, L.; Gassmann, W. Copper Uptake Mechanism of Arabidopsis Thaliana High-Affinity COPT Transporters. *Protoplasma* **2019**, *256* (1), 161–170. https://doi.org/10.1007/s00709-018-1286-1.

(18) De Feo, C. J.; Aller, S. G.; Unger, V. M. A Structural Perspective on Copper Uptake in Eukaryotes. *BioMetals* **2007**, *20* (3–4), 705–716. https://doi.org/10.1007/S10534-006-9054-7/FIGURES/7.

(19) Puig, S.; Lee, J.; Lau, M.; Thiele, D. J. Biochemical and Genetic Analyses of Yeast and Human High Affinity Copper Transporters Suggest a Conserved Mechanism for Copper Uptake*. *Journal of Biological Chemistry* **2002**, *277*

(29), 26021–26030. https://doi.org/https://doi.org/10.1074/jbc.M202547200.

(20) He, L.; Ma, H.; Song, W.; Zhou, Z.; Ma, C.; Zhang, H. Arabidopsis COPT1 Copper Transporter Uses a Single Histidine to Regulate Transport Activity and Protein Stability. *Int J Biol Macromol* **2023**, *241*, 124404. https://doi.org/https://doi.org/10.1016/j.ijbiomac.2023.124404.

(21) Yuan, M.; Li, X.; Xiao, J.; Wang, S. Molecular and Functional Analyses of COPT/Ctr-Type Copper Transporter-like Gene Family in Rice. *BMC Plant Biol* **2011**, *11* (1), 1–12. https://doi.org/10.1186/1471-2229-11-69/FIGURES/8.

(22) Zhou, H.; Thiele, D. J. Identification of a Novel High Affinity Copper Transport Complex in the Fission Yeast Schizosaccharomyces Pombe. *Journal of Biological Chemistry* **2001**, *276* (23), 20529–20535. https://doi.org/10.1074/JBC.M102004200.

(23) Yuan, M.; Wang, S.; Chu, Z.; Li, X.; Xu, C. The Bacterial Pathogen Xanthomonas Oryzae Overcomes Rice Defenses by Regulating Host Copper Redistribution. *Plant Cell* **2010**, *22* (9), 3164–3176. https://doi.org/10.1105/TPC.110.078022.

(24) Li, X.; Wang, Z.; Fu, Y.; Cheng, X.; Zhang, Y.; Fan, B.; Zhu, C.; Chen, Z. Two Ubiquitin-Associated ER Proteins Interact with COPT Copper Transporters and Modulate Their Accumulation. *Plant Physiol* **2021**, *187* (4), 2469–2484. https://doi.org/10.1093/plphys/kiab381.

(25) Gayomba, S. R.; Jung, H. Il; Yan, J.; Danku, J.; Rutzke, M. A.; Bernal, M.; Krämer, U.; Kochian, L. V.; Salt, D. E.; Vatamaniuk, O. K. The CTR/COPT-Dependent Copper Uptake and SPL7-Dependent Copper Deficiency Responses Are Required for Basal Cadmium Tolerance in A. Thaliana. *Metallomics* **2013**, *5* (9), 1262–1275. https://doi.org/10.1039/C3MT00111C.

(26) Ren, F.; Logeman, B. L.; Zhang, X.; Liu, Y.; Thiele, D. J.; Yuan, P. X-Ray Structures of the High-Affinity Copper Transporter Ctr1. *Nat Commun* **2019**, *10* (1), 1386. https://doi.org/10.1038/s41467-019-09376-7.

(27) Bernal, M.; Casero, D.; Singh, V.; Wilson, G. T.; Grande, A.; Yang, H.; Dodani, S. C.; Pellegrini, M.; Huijser, P.; Connolly, E. L.; Merchant, S. S.; Krämer, U. Transcriptome Sequencing Identifies SPL7-Regulated Copper Acquisition Genes FRO4/FRO5 and the Copper Dependence of Iron Homeostasis in Arabidopsis. *Plant Cell* **2012**, *24* (2), 738–761. https://doi.org/10.1105/TPC.111.090431.

(28) Magrì, A.; Tabbì, G.; Naletova, I.; Attanasio, F.; Arena, G.; Rizzarelli, E. A Deeper Insight in Metal Binding to the HCtr1 N-Terminus Fragment: Affinity, Speciation and Binding Mode of Binuclear Cu2+ and Mononuclear Ag+ Complex Species. *Int J Mol Sci* **2022**, *23* (6).

https://doi.org/10.3390/ijms23062929.

(29) Hedrichh, R.; Schroeder, J. I.; Fernandez, J. M. Patch-Clamp Studies on Higher Plant Cells: A Perspective. *Trends Biochem Sci* **1987**, *12*, 49–52. https://doi.org/https://doi.org/10.1016/0968-0004(87)90025-9.

(30) Janicka, M.; Wdowikowska, A.; Kłobus, G. Assay of Plasma Membrane H+-ATPase in Plant Tissues under Abiotic Stresses. In *Plant Membrane Proteomics: Methods and Protocols*; Mock, H.-P., Matros, A., Witzel, K., Eds.; Springer New York: New York, NY, 2018; pp 205–215. https://doi.org/10.1007/978-1-4939-7411-5_14.

(31) Kampfenkel, K.; Kushnir, S.; Babiychuk, E.; Inzé, D.; Van Montagu, M. Molecular Characterization of a Putative Arabidopsis Thaliana Copper Transporter and Its Yeast Homologue(*). *Journal of Biological Chemistry* **1995**, *270* (47), 28479–28486. https://doi.org/https://doi.org/10.1074/jbc.270.47.28479.

(32) Hamill, O. P.; Marty, A.; Neher, E.; Sakmann, B.; Sigworth, F. J. Improved Patch-Clamp Techniques for High-Resolution Current Recording from Cells and Cell-Free Membrane Patches. *Pflügers Archiv 1981 391:2* **1981**, *391* (2), 85–100. https://doi.org/10.1007/BF00656997.

(33) Margrie, T. W.; Brecht, M.; Sakmann, B. In Vivo, Low-Resistance, Whole-Cell Recordings from Neurons in the Anaesthetized and Awake Mammalian Brain. *Pflügers Archiv 2002 444:4* **2002**, *444* (4), 491–498. https://doi.org/10.1007/S00424-002-0831-Z.

(34) Kodandaramaiah, S. B.; Franzesi, G. T.; Chow, B. Y.; Boyden, E. S.; Forest, C. R. Automated Whole-Cell Patch-Clamp Electrophysiology of Neurons in Vivo. *Nature Methods 2012 9:6* **2012**, *9* (6), 585–587. https://doi.org/10.1038/nmeth.1993.

(35) NEHER, E.; SAKMANN, B. Single-Channel Currents Recorded from Membrane of Denervated Frog Muscle Fibres. *Nature* **1976**, *260* (5554), 799–802. https://doi.org/10.1038/260799a0.

(36) Lacerda, A. E.; Kramer, J.; Shen, K.-Z.; Thomas, D.; Brown, A. M. Comparison of Block among Cloned Cardiac Potassium Channels by Non-Antiarrhythmic Drugs. *European Heart Journal Supplements* **2001**, *3* (suppl_K), K23–K30. https://doi.org/10.1016/S1520-765X(01)90003-3.

(37) Elzenga, J. T. M.; Keller, C. P.; Van Volkenburgh, E. Patch Clamping Protoplasts from Vascular Plants 1: Method for the Quick Isolation of Protoplasts Having a High Success Rate of Gigaseal Formation. *Plant Physiol* **1991**, *97* (4), 1573–1575. https://doi.org/10.1104/pp.97.4.1573.

(38) Gamper, N.; Shapiro, M. S. Regulation of Ion Transport Proteins by Membrane Phosphoinositides. *Nature Reviews Neuroscience 2007 8:12* **2007**, *8* (12), 921–934. https://doi.org/10.1038/nrn2257.

(39) Simons, K.; Toomre, D. Lipid Rafts and Signal Transduction. *Nature Reviews Molecular Cell Biology 2000 1:1* **2000**, *1* (1), 31–39. https://doi.org/10.1038/35036052.

(40) Kholodenko, B. N. Cell-Signalling Dynamics in Time and Space. *Nature Reviews Molecular Cell Biology 2006 7:3* **2006**, *7* (3), 165–176. https://doi.org/10.1038/nrm1838.

(41) Diaz, A. J.; Albertorio, F.; Daniel, S.; Cremer, P. S. Double Cushions Preserve Transmembrane Protein Mobility in Supported Bilayer Systems. *Langmuir* **2008**, *24* (13), 6820. https://doi.org/10.1021/LA800018D.

(42) Ulmefors, H.; Nissa, J.; Pace, H.; Wahlsten, O.; Gunnarsson, A.; Simon, D. T.; Berggren, M.; Höök, F. Formation of Supported Lipid Bilayers Derived from Vesicles of Various Compositional Complexity on Conducting Polymer/Silica Substrates. *Langmuir* **2021**, *37* (18), 5494–5505. https://doi.org/10.1021/ACS.LANGMUIR.1C00175/ASSET/IMAGES/LARGE/LA1C00175_0007.JPEG.

(43) Pace, H.; Simonsson Nyström, L.; Gunnarsson, A.; Eck, E.; Monson, C.; Geschwindner, S.; Snijder, A.; Höök, F. Preserved Transmembrane Protein Mobility in Polymer-Supported Lipid Bilayers Derived from Cell Membranes. *Anal Chem* **2015**, *87* (18), 9194–9203. https://doi.org/10.1021/ACS.ANALCHEM.5B01449/ASSET/IMAGES/LARGE/AC-2015-014493_0006.JPEG.

(44) Roder, F.; Wilmes, S.; Richter, C. P.; Piehler, J. Rapid Transfer of Transmembrane Proteins for Single Molecule Dimerization Assays in Polymer-Supported Membranes. *ACS Chem Biol* **2014**, *9* (11), 2479–2484. https://doi.org/10.1021/CB5005806/SUPPL_FILE/CB5005806_SI_005.AVI.

(45) Kim, H.; Lee, K. Y.; Ryu, S. R.; Jung, K. H.; Ahn, T. K.; Lee, Y.; Kwon, O. S.; Park, S. J.; Parker, K. K.; Shin, K. Charge-Selective Membrane Protein Patterning with Proteoliposomes. *RSC Adv* **2015**, *5* (7), 5183–5191. https://doi.org/10.1039/c4ra12088d.

(46) Liu, H. Y.; Grant, H.; Hsu, H. L.; Sorkin, R.; Bošković, F.; Wuite, G.; Daniel, S. Supported Planar Mammalian Membranes as Models of in Vivo Cell Surface Architectures. *ACS Appl Mater Interfaces* **2017**, *9* (41), 35526–35538. https://doi.org/10.1021/ACSAMI.7B07500/ASSET/IMAGES/LARGE/AM-2017-075006_0011.JPEG.

(47) Suri, M.; Mohamed, Z.; Bint E Naser, S. F.; Mao, X.; Chen, P.; Daniel, S.;

Hanrath, T. Bioelectronic Platform to Investigate Charge Transfer between Photoexcited Quantum Dots and Microbial Outer Membranes. *ACS Appl Mater Interfaces* **2022**, *14* (13), 15799–15810. https://doi.org/10.1021/acsami.1c25032.

(48) Ghosh, S.; Mohamed, Z.; Shin, J. H.; Bint E Naser, S. F.; Bali, K.; Dörr, T.; Owens, R. M.; Salleo, A.; Daniel, S. Impedance Sensing of Antibiotic Interactions with a Pathogenic E. Coli Outer Membrane Supported Bilayer. *Biosens Bioelectron* **2022**, *204*. https://doi.org/10.1016/j.bios.2022.114045.

(49) Khan, M. S.; Dosoky, N. S.; Williams, J. D. Engineering Lipid Bilayer Membranes for Protein Studies. *International Journal of Molecular Sciences*. October 31, 2013, pp 21561–21597. https://doi.org/10.3390/ijms141121561.

(50) Grotz, N.; Fox, T.; Connolly, E.; Park, W.; Guerinot, M. Lou; Eide, D. Identification of a Family of Zinc Transporter Genes from Arabidopsis That Respond to Zinc Deficiency. *Proceedings of the National Academy of Sciences* **1998**, *95* (12), 7220–7224. https://doi.org/10.1073/pnas.95.12.7220.

(51) Liu, H. Y.; Chen, W. L.; Ober, C. K.; Daniel, S. Biologically Complex Planar Cell Plasma Membranes Supported on Polyelectrolyte Cushions Enhance Transmembrane Protein Mobility and Retain Native Orientation. *Langmuir* **2018**, *34* (3), 1061–1072. https://doi.org/10.1021/ACS.LANGMUIR.7B02945/SUPPL_FILE/LA7B02945_SI_003.AVI.

(52) Richards, M. J.; Hsia, C. Y.; Singh, R. R.; Haider, H.; Kumpf, J.; Kawate, T.; Daniel, S. Membrane Protein Mobility and Orientation Preserved in Supported Bilayers Created Directly from Cell Plasma Membrane Blebs. *Langmuir* **2016**, *32* (12), 2963–2974. https://doi.org/10.1021/ACS.LANGMUIR.5B03415/SUPPL_FILE/LA5B03415_SI_005.AVI.

(53) Quemeneur, F.; Sigurdsson, J. K.; Renner, M.; Atzberger, P. J.; Bassereau, P.; Lacoste, D. Shape Matters in Protein Mobility within Membranes. *Proc Natl Acad Sci U S A* **2014**, *111* (14), 5083–5087. https://doi.org/10.1073/PNAS.1321054111/SUPPL_FILE/SM02.MPG.

(54) Chao, Z.; Selivanovitch, E.; Kallitsis, K.; Lu, Z.; Pachaury, A.; Owens, R.; Daniel, S. Recreating the Biological Steps of Viral Infection on a Cell-Free Bioelectronic Platform to Profile Viral Variants of Concern. *Nat Commun* **2024**, *15* (1), 5606. https://doi.org/10.1038/s41467-024-49415-6.

(55) Nissa, J. *Interacting with Biological Membranes Using Organic Electronic Devices*.

(56) Nelson, P. H. A Permeation Theory for Single-File Ion Channels:

Corresponding Occupancy States Produce Michaelis–Menten Behavior. *J Chem Phys* **2002**, *117* (24), 11396–11403. https://doi.org/10.1063/1.1522709.

(57) Tunuguntla, R. H.; Henley, R. Y.; Yao, Y. C.; Pham, T. A.; Wanunu, M.; Noy, A. Enhanced Water Permeability and Tunable Ion Selectivity in Subnanometer Carbon Nanotube Porins. *Science (1979)* **2017**, *357* (6353), 792–796. https://doi.org/10.1126/SCIENCE.AAN2438.

(58) Su, H.; Liu, H. Y.; Pappa, A. M.; Hidalgo, T. C.; Cavassin, P.; Inal, S.; Owens, R. M.; Daniel, S. Facile Generation of Biomimetic-Supported Lipid Bilayers on Conducting Polymer Surfaces for Membrane Biosensing. *ACS Appl Mater Interfaces* **2019**, *11* (47), 43799–43810. https://doi.org/10.1021/acsami.9b10303.

(59) Pitsalidis, C.; Pappa, A. M.; Porel, M.; Artim, C. M.; Faria, G. C.; Duong, D. D.; Alabi, C. A.; Daniel, S.; Salleo, A.; Owens, R. M. Biomimetic Electronic Devices for Measuring Bacterial Membrane Disruption. *Advanced Materials* **2018**, *30* (39). https://doi.org/10.1002/adma.201803130.

(60) Zhang, S.; Kumar, P.; Nouas, A. S.; Fontaine, L.; Tang, H.; Cicoira, F. Solvent-Induced Changes in PEDOT:PSS Films for Organic Electrochemical Transistors. *APL Mater* **2015**, *3* (1). https://doi.org/10.1063/1.4905154.

(61) Zhang, Y.; Inal, S.; Hsia, C. Y.; Ferro, M.; Ferro, M.; Daniel, S.; Owens, R. M. Supported Lipid Bilayer Assembly on PEDOT:PSS Films and Transistors. *Adv Funct Mater* **2016**, *26* (40), 7304–7313. https://doi.org/10.1002/adfm.201602123.

(62) Strakosas, X.; Wei, B.; Martin, D. C.; Owens, R. M. Biofunctionalization of Polydioxythiophene Derivatives for Biomedical Applications. *Journal of Materials Chemistry B*. Royal Society of Chemistry 2016, pp 4952–4968. https://doi.org/10.1039/c6tb00852f.

(63) Bernards, D. A.; Malliaras, G. G. Steady-State and Transient Behavior of Organic Electrochemical Transistors. *Adv Funct Mater* **2007**, *17* (17), 3538–3544. https://doi.org/10.1002/adfm.200601239.

(64) Khodagholy, D.; Rivnay, J.; Sessolo, M.; Gurfinkel, M.; Leleux, P.; Jimison, L. H.; Stavrinidou, E.; Herve, T.; Sanaur, S.; Owens, R. M.; Malliaras, G. G. High Transconductance Organic Electrochemical Transistors. *Nat Commun* **2013**, *4*. https://doi.org/10.1038/ncomms3133.

(65) Guidelli, R.; Becucci, L. 4 Electrochemistry of Biomimetic Membranes; 2012; pp 147–266. https://doi.org/10.1007/978-1-4614-2137-5_4.

(66) Koutsouras, D. A.; Gkoupidenis, P.; Stolz, C.; Subramanian, V.; Malliaras, G. G.; Martin, D. C. Impedance Spectroscopy of Spin-Cast and Electrochemically

Deposited PEDOT:PSS Films on Microfabricated Electrodes with Various Areas. *ChemElectroChem* **2017**, *4* (9), 2321–2327. https://doi.org/https://doi.org/10.1002/celc.201700297.

(67) Chang, B. Y.; Park, S. M. Electrochemical Impedance Spectroscopy. *Annual Review of Analytical Chemistry* **2010**, *3* (1), 207–229. https://doi.org/10.1146/annurev.anchem.012809.102211.

(68) Valincius, G.; Meškauskas, T.; Ivanauskas, F. Electrochemical Impedance Spectroscopy of Tethered Bilayer Membranes. *Langmuir* **2012**, *28* (1), 977–990. https://doi.org/10.1021/la204054g.

(69) Proctor, C. M.; Rivnay, J.; Malliaras, G. G. Understanding Volumetric Capacitance in Conducting Polymers. *J Polym Sci B Polym Phys* **2016**, *54* (15), 1433–1436. https://doi.org/https://doi.org/10.1002/polb.24038.

(70) DalCorso, G.; Manara, A.; Piasentin, S.; Furini, A. Nutrient Metal Elements in Plants. *Metallomics* **2014**, *6* (10), 1770–1788. https://doi.org/10.1039/c4mt00173g.

(71) Binder, B. M.; Rodríguez, F. I.; Bleecker, A. B. The Copper Transporter RAN1 Is Essential for Biogenesis of Ethylene Receptors in Arabidopsis*. *Journal of Biological Chemistry* **2010**, *285* (48), 37263–37270. https://doi.org/https://doi.org/10.1074/jbc.M110.170027.

(72) Hirayama, T.; Kieber, J. J.; Hirayama, N.; Kogan, M.; Guzman, P.; Nourizadeh, S.; Alonso, J. M.; Dailey, W. P.; Dancis, A.; Ecker, J. R. RESPONSIVE-TO-ANTAGONIST1, a Menkes/Wilson Disease–Related Copper Transporter, Is Required for Ethylene Signaling in Arabidopsis. *Cell* **1999**, *97* (3), 383–393. https://doi.org/https://doi.org/10.1016/S0092-8674(00)80747-3.

(73) Rahmati Ishka, M.; Vatamaniuk, O. K. Copper Deficiency Alters Shoot Architecture and Reduces Fertility of Both Gynoecium and Androecium in Arabidopsis Thaliana. *Plant Direct* **2020**, *4* (11). https://doi.org/10.1002/pld3.288.

(74) Yao, S.; Kang, J.; Guo, G.; Yang, Z.; Huang, Y.; Lan, Y.; Zhou, T.; Wang, L.; Wei, C.; Xu, Z.; Li, Y. The Key Micronutrient Copper Orchestrates Broad-Spectrum Virus Resistance in Rice. *Sci Adv* **2024**, *8* (26), eabm0660. https://doi.org/10.1126/sciadv.abm0660.

(75) Chai, L.-X.; Dong, K.; Liu, S.-Y.; Zhang, Z.; Zhang, X.-P.; Tong, X.; Zhu, F.-F.; Zou, J.-Z.; Wang, X.-B. A Putative Nuclear Copper Chaperone Promotes Plant Immunity in Arabidopsis. *J Exp Bot* **2020**, *71* (20), 6684–6696. https://doi.org/10.1093/jxb/eraa401.

(76) Zhang, C.; Lu, W.; Yang, Y.; Shen, Z.; Ma, J. F.; Zheng, L. OsYSL16 Is

Required for Preferential Cu Distribution to Floral Organs in Rice. *Plant Cell Physiol* **2018**, *59* (10), 2039–2051. https://doi.org/10.1093/pcp/pcy124.

(77) Puig, S.; Andrés-Colás, N.; García-Molina, A.; Peñarrubia, L. Copper and Iron Homeostasis in Arabidopsis: Responses to Metal Deficiencies, Interactions and Biotechnological Applications. *Plant Cell Environ* **2007**, *30* (3), 271–290. https://doi.org/10.1111/J.1365-3040.2007.01642.X.

(78) De Feo, C. J.; Aller, S. G.; Siluvai, G. S.; Blackburn, N. J.; Unger, V. M. Three-Dimensional Structure of the Human Copper Transporter HCTR1. *Proc Natl Acad Sci U S A* **2009**, *106* (11), 4237–4242. https://doi.org/10.1073/PNAS.0810286106/SUPPL_FILE/0810286106SI.PDF.

(79) Stuebler, M.; Manzer, Z. A.; Liu, H.-Y.; Miller, J.; Richter, A.; Krishnan, S.; Selivanovitch, E.; Banuna, B.; Jander, G.; Reimhult, E.; Zipfel, W. R.; Roeder, A. H. K.; Piñeros, M. A.; Daniel, S. Plant Membrane-On-A-Chip: A Platform for Studying Plant Membrane Proteins and Lipids. *ACS Appl Mater Interfaces* **2024**, *16* (16), 20092–20104. https://doi.org/10.1021/acsami.3c18562.

(80) Yamasaki, H.; Hayashi, M.; Fukazawa, M.; Kobayashi, Y.; Shikanai, T. SQUAMOSA Promoter Binding Protein–Like7 Is a Central Regulator for Copper Homeostasis in Arabidopsis . *Plant Cell* **2009**, *21* (1), 347–361. https://doi.org/10.1105/tpc.108.060137.

(81) Harayama, T.; Riezman, H. Understanding the Diversity of Membrane Lipid Composition. *Nature Reviews Molecular Cell Biology*. Nature Publishing Group May 1, 2018, pp 281–296. https://doi.org/10.1038/nrm.2017.138.

(82) Furt, F.; Simon-Plas, F.; Mongrand, S. Lipids of the Plant Plasma Membrane. In *The Plant Plasma Membrane*; Murphy, A. S., Schulz, B., Peer, W., Eds.; Springer Berlin Heidelberg: Berlin, Heidelberg, 2011; pp 3–30. https://doi.org/10.1007/978-3-642-13431-9_1.

(83) Reszczyńska, E.; Hanaka, A. Lipids Composition in Plant Membranes. *Cell Biochem Biophys* **2020**, *78* (4), 401–414. https://doi.org/10.1007/s12013-020-00947-w.

(84) Letelier, M. E.; Lepe, A. M.; Faúndez, M.; Salazar, J.; Marín, R.; Aracena, P.; Speisky, H. Possible Mechanisms Underlying Copper-Induced Damage in Biological Membranes Leading to Cellular Toxicity. *Chem Biol Interact* **2005**, *151* (2), 71–82. https://doi.org/https://doi.org/10.1016/j.cbi.2004.12.004.

(85) Espírito, S. C.; Wen, L. E.; G, E. C.; Davide, Q.; W, D. D.; J, C. C.; Gregor, G. Bacterial Killing by Dry Metallic Copper Surfaces. *Appl Environ Microbiol* **2011**, *77* (3), 794–802. https://doi.org/10.1128/AEM.01599-10.

(86) Karlsson, H. L.; Cronholm, P.; Hedberg, Y.; Tornberg, M.; De Battice, L.;

Svedhem, S.; Wallinder, I. O. Cell Membrane Damage and Protein Interaction Induced by Copper Containing Nanoparticles—Importance of the Metal Release Process. *Toxicology* **2013**, *313* (1), 59–69. https://doi.org/https://doi.org/10.1016/j.tox.2013.07.012.

(87) Dancis, A.; Yuan, D. S.; Haile, D.; Askwith, C.; Eide, D.; Moehle, C.; Kaplan, J.; Klausner', R. D. *Molecular Characterization of a Copper Transport Protein in S. Cerevisiae: An Unexpected Role for Copper in Iron Transport*; 1994; Vol. 76.

(88) Binder, H.; Arnold, K.; Ulrich, A. S.; Zschörnig, O. Interaction of Zn2+ with Phospholipid Membranes. *Biophys Chem* **2001**, *90* (1), 57–74. https://doi.org/https://doi.org/10.1016/S0301-4622(01)00130-2.

(89) Lu, Y.-P.; Li, Z.-S.; Rea, P. A. AtMRP1 Gene of Arabidopsis Encodes a Glutathione S-Conjugate Pump: Isolation and Functional Definition of a Plant ATP-Binding Cassette Transporter Gene. *Proceedings of the National Academy of Sciences* **1997**, *94* (15), 8243–8248. https://doi.org/10.1073/pnas.94.15.8243.

(90) Dancis, A.; Haile, D.; Yuan, D. S.; Klausner, R. D. The Saccharomyces Cerevisiae Copper Transport Protein (Ctr1p). Biochemical Characterization, Regulation by Copper, and Physiologic Role in Copper Uptake. *Journal of Biological Chemistry* **1994**, *269* (41), 25660–25667. https://doi.org/10.1016/S0021-9258(18)47300-0.

(91) Zhai, Z.; Jung, H. Il; Vatamaniuk, O. K. Isolation of Protoplasts from Tissues of 14-Day-Old Seedlings of Arabidopsis Thaliana. *Journal of Visualized Experiments* **2009**, No. 30. https://doi.org/10.3791/1149.

(92) Jung, H.; Zhai, Z.; Vatamaniuk, O. K. Direct Transfer of Synthetic Double-Stranded RNA into Protoplasts of Arabidopsis Thaliana. In *RNAi and Plant Gene Function Analysis: Methods and Protocols*; Kodama, H., Komamine, A., Eds.; Humana Press: Totowa, NJ, 2011; pp 109–127. https://doi.org/10.1007/978-1-61779-123-9_8.

(93) Zhai, Z.; Sooksa-nguan, T.; Vatamaniuk, O. K. Establishing RNA Interference as a Reverse-Genetic Approach for Gene Functional Analysis in Protoplasts. *Plant Physiol* **2009**, *149* (2), 642–652. https://doi.org/10.1104/pp.108.130260.

(94) Soumpasis, D. M. Theoretical Analysis of Fluorescence Photobleaching Recovery Experiments. *Biophys J* **1983**, *41* (1), 95–97. https://doi.org/10.1016/S0006-3495(83)84410-5.

(95) Lu, Z.; van Niekerk, D.; Savva, A.; Kallitsis, K.; Thiburce, Q.; Salleo, A.; Pappa, A. M.; Owens, R. M. Understanding Electrochemical Properties of Supported Lipid Bilayers Interfaced with Organic Electronic Devices. *J Mater*

Chem C Mater **2022**, *10* (20), 8050–8060. https://doi.org/10.1039/d2tc00826b.

(96) Wan, Y.; Wang, Z.; Xia, J.; Shen, S.; Guan, M.; Zhu, M.; Qiao, C.; Sun, F.; Liang, Y.; Li, J.; Lu, K.; Qu, C. Genome-Wide Analysis of Phosphorus Transporter Genes in Brassica and Their Roles in Heavy Metal Stress Tolerance. *Int J Mol Sci* **2020**, *21* (6). https://doi.org/10.3390/ijms21062209.

(97) Liu, H. Y.; Pappa, A. M.; Pavia, A.; Pitsalidis, C.; Thiburce, Q.; Salleo, A.; Owens, R. M.; Daniel, S. Self-Assembly of Mammalian-Cell Membranes on Bioelectronic Devices with Functional Transmembrane Proteins. *Langmuir* **2020**, *36* (26), 7325–7331. https://doi.org/10.1021/acs.langmuir.0c00804.